POLITECNICO DI TORINO

I Facoltà di Ingegneria
Corso di Laurea in Ingegneria Meccanica

Tesi di Laurea Magistrale

Numerical and experimental tools for NVH characterization of a steering-column

Relatori:
Prof. Mauro Velardocchia
Prof. Elvio Bonisoli

Candidato:
Stefano Averame

Luglio 2020

Ringraziamenti

Ringrazio il gruppo di ricerca di Meccanica del Veicolo, per avermi generosamente accolto e supportato per questo lavoro di tesi.
Ringrazio i Dottori e gli Ingegneri di Iveco, per l’opportunità e la disponibilità concessa.
Ringrazio la mia fidanzata Alessia, per aver condiviso ogni momento e per l’impareggiabile appoggio nei periodi più duri.
Ringrazio soprattutto la mia famiglia, per l’enorme sostegno e l’incessante incoraggiamento, che mi ha permesso di concludere questo importante percorso.

Index

Abstract

This document resumes the Master Thesis work: the creation of a suitable and accurate finite element model of a steering-wheel for NVH studies and the further preliminary evaluations for the experimental tests of both steering-wheel and steering-column. A punctual description of each phase is reported, including the results of numerical modal analysis run by two different softwares of the steering-wheel models. The final steps, regarding the future experimental tests, useful for correlating the FE models to the real object, include the bench building and setting up.

Introduction

Nowadays, the possibility, provided by technology, to predict the mechanical behaviours of a structure is crucial: the decreasing need of prototypes for evaluating performances permits to focus the available resources on deeper aspects of the research and development area. The trucks constructor Iveco requested an NVH predictive model of their new top truck steering-column, in order to have the possibility to virtually manage and run comfort analysis and studies of the vehicle. The Finite Element Method is the main tool available for analysing a mechanical component or assembly, under many different points of view. For this purpose, a finite element model for modal analysis is the most suitable solution. The entire work is divided in three phases: for first, a reliable and easily manageable finite element model has to be created, then an experimental test has to be executed, in order to verify the numerical model and to provide the necessary data for the last phase, the correlation of the finite element model to the real object. This document resumes the modelling phase and the preliminary steps to the experimental analysis, from the bench setting up to the sensors positioning.
According to the following equation:

$$\mathbf{M}\ddot{\mathbf{x}} + \mathbf{K}\mathbf{x} = \mathbf{0}$$

the mass matrix **M** and the stiffness matrix **K** have to be evaluated, in order to run the analysis. It is clearly an approximation of the physical properties of the structure, as only mass and stiffness are considered, while the damping effects are totally neglected. For simple material such as steel, stiffness is quite a linear property and the damping is very low, so the solution of the equation accurately represents the physical behaviour; on the other hand, considering rubber, the stiffness strongly changes with the load and the deformation the structure is subjected to and the damping is the most influencing property, so the solution of the equation can be just a vague idea of the actual behaviour. An automotive steering-wheel, that is the critical component of the whole steering-column, is heavily covered by a rubber layer, that damps the vibrations of the metallic frame. In order to reach a good numerical representation, the finite element model has to be built allowing further tunings, after the experimental test. In the first two chapters, the steering-column and wheel models provided by the constructor are described; then, Chapters 3 and 4 resume the creation of two new wheel models and their modal analysis by Optistruct; in Chapters 5 and 6 the two models are further modified, reducing their complexity, and analysed by Optistruct and Lupos. The results obtained are then compared in Chapter 7. Finally, the last three Chapters resume the experimental setup: the definition of the test rigs, the FE model of the steering-column test bench and its modal analysis, the sensors positioning.

1. Constructor steering-column finite element model

The constructor provided a finite element model, in .bdf MSC Nastran file format, and the related modal analysis results, in .op2 file format, of the steering-column. For first, both the files have been deeply analysed and many issues has come out. Initially, the model provided should have been the starting point of the correlation phase, but the modelling problems pointed out in Paragraph 1.2 and in Chapter 2 led to the building of a new one.

1.1 Model characteristics

The provided finite element model has been analysed in detail, pointing out both geometrical and physical properties, with particular attention to the used finite element modelling techniques.

1.1.1 Geometry properties

The provided FE model has the geometrical properties reported in the Table 1.1.1.1. As it is visible, many second order elements have been used: in Table 1.1.1.1 TRIA6 (second order shells) and TETRA10 (second order tetrahedral solids). This technique ensures high accuracy, but turns in a very high number of nodes. It is a very fast way of modelling a structure from a CAD file, as even a complex geometry can be precisely represented thanks to the high number of nodes. Nevertheless, such a model is very hardly manageable, considering both the tuning and the numerical analysis execution.

Table 1.1.1.1 – Model properties.

	Quantity
Nodes	328361
Elements	240023
TRIA3	2262
TRIA6	52336
QUAD4	3139
TETRA4	2515
TETRA10	179488
RBE2	279
RBE3	2
CONM2	2

The two-dimensional elements are usually used for modelling components with two dimensions much larger than the third, while three-dimensional elements are used for thicker components. The rigid body elements RBE2 and RBE3 are respectively used for connecting components to each other and for imposing a kinematic relationship. In this case, the RBE3s are used for connecting the lumped masses CONM2s to the structure; in this way, the mass represented by the CONM2 is considered in the mass matrix only.
Shells' thicknesses are reported, in metres, in Table 1.1.1.2.

Table 1.1.1.2 – Shells thickness.

ID shell	Thickness [m]
1	1e-4
2	3.5e-3
3	3.5e-3
4	5.0e-3
5	5.0e-3
6	5.0e-3
7	3.0e-3
8	1e-4

1.1.2 Materials

The materials used in the definition of the model are reported in Table 1.1.2.1. The units system used is ton-mm-N. Redundant materials are present, probably due to an inaccurate composition of the model from the CAD files. A deeper analysis is reported in Paragraph 1.2. Mostly, the materials represented seem to be steel (MAT1_5, MAT1_9 and MAT1_22), aluminium (MAT1_7, MAT1_8, MAT1_19 and MAT1_20) and rubber (MAT1_23).

Table 1.1.2.1 – Materials and their properties

Material	Density [kg/m^3]	Young module [Pa]	Poisson coefficient [-]
MAT1_5	7.8e3	2.05e11	0.3
MAT1_7	2.7e3	6.83e10	0.33
MAT1_8	2.7e3	7e10	0.3
MAT1_9	7.8e3	2e11	0.3
MAT1_19	2.7e3	7e10	0.3
MAT1_20	1.6e4	7e10	0.3
MAT1_22	1.0e4	2e11	0.3
MAT1_23	10	7e10	0.3

1.1.3 Mass matrix

The mass matrix M0 of the model is reported, from the .f06 file, in Table 1.1.3.1.

Table 1.1.3.1 – Model mass matrix.

1.667e-02	-1.888e-20	-4.515e-20	4.436e-17	9.280	1.224e01
-1.888e-20	1.667e-02	-2.437e-21	-9.280	-1.193e-17	-1.478e01
-4.515e-20	-2.437e-21	1.667e-02	-1.224e01	1.478e01	-3.243e-17
4.436e-17	-9.280	-1.224e01	1.503e04	-1.084e04	7.627e03
9.280	-1.193e-17	1.478e01	-1.084e04	1.967e04	6.814e03
1.224e01	-1.478e01	-3.243e-17	7.627e03	6.814e03	2.295e04

The first 3x3 sub-matrix can be seen as a diagonal matrix, because elements that are out the diagonal are machine zero. The mass and the barycentre position of the model are reported:

$$m_{tot} = 166.7 \text{ kg} \tag{1.1.3.1}$$

$$\mathbf{G} = \begin{bmatrix} -0.8864 \\ -0.7341 \\ 0.5567 \end{bmatrix} \text{ m} \tag{1.1.3.2}$$

The translational and rotational properties, barycentric and with respect to the global coordinate system, result:

$$\mathbf{J}_{xyz} = \begin{bmatrix} 0.875 & -0.00289 & 0.599 \\ -0.00289 & 1.41 & -0.00149 \\ 0.599 & -0.00149 & 0.871 \end{bmatrix} \text{ kg m}^2 \tag{1.1.3.3}$$

$$\mathbf{J}_{G,\bar{x}\bar{y}\bar{z}} = \begin{bmatrix} 1.406 & 0 & 0 \\ 0 & 0.2739 & 0 \\ 0 & 0 & 1.472 \end{bmatrix} \text{ kg m}^2 \tag{1.1.3.4}$$

1.2 Issues

The model has shown several details that are not clear. A detailed evaluation is reported in the two following paragraphs.

1.2.1 Geometry

There are several missing parts in the FEM:

- the model does not include the steering shaft and its bottom support; they are thought to be important elements for the analysis. They are reported in the STEP model, but they are not present in the FEM one, as shown by Figure 1.2.1.1 and Figure 1.2.1.2. These parts will not be experimentally analysed, however their presence is thought to be important, at least as concerns the masses. The shaft is telescopic, so it is free to move along its axis and should not influence the modal behaviour;

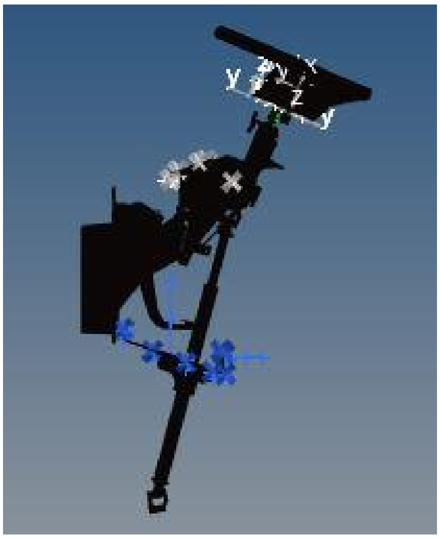

Figure 1.2.1.1 – STEP model.

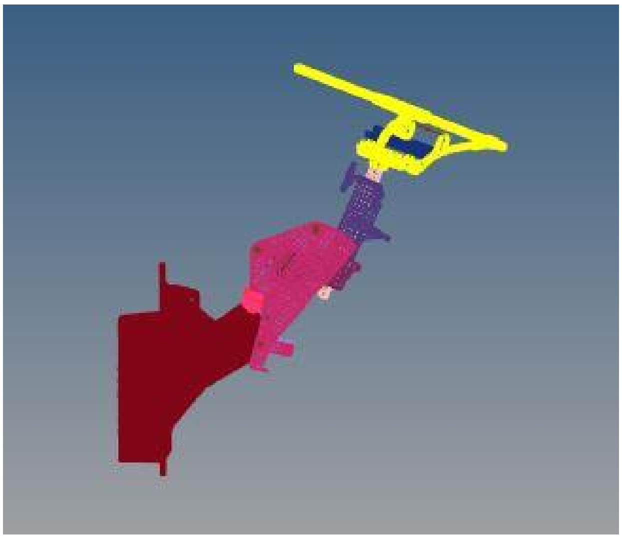

Figure 1.2.1.2 – FEM model.

- the FE model does not include the upper bearing, just under the wheel; it is reported only in the STEP. This missing certainly detaches the model from the real component. Probably it is an involuntary missing, the lower bearing has been modelled by a star of RBE2. Figure 1.2.1.3 and Figure 1.2.1.4 show the lower bearing FEM and the upper one absence;

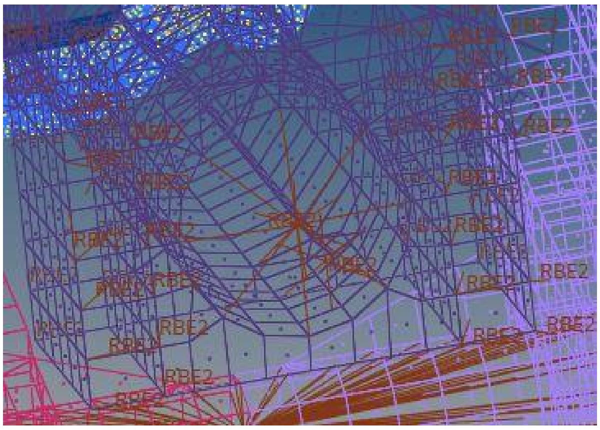

Figure 1.2.1.3 – Lower bearing FEM.

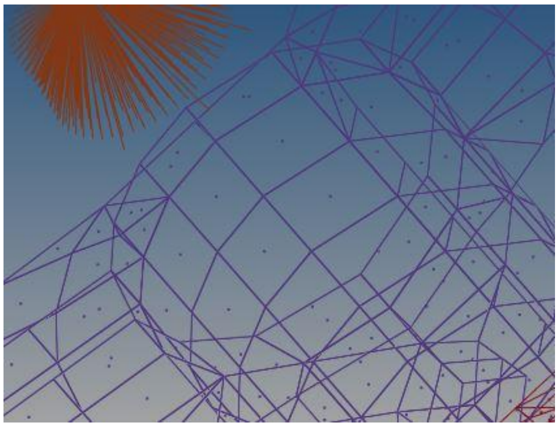

Figure 1.2.1.4 – Upper bearing missing.

- the FE model does not include the little cylinder shown in Figure 1.2.1.5; it could be for safety reasons or it could be due to real eigenvalue analysis;

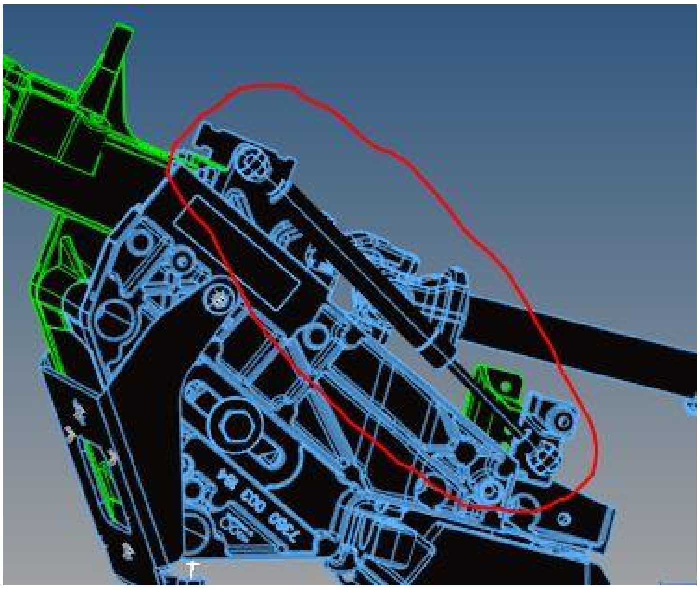

Figure 1.2.1.5 – Missing cylinder.

- the FE model does not include the component highlighted in Figure 1.2.1.6; it seems to be a link to the chassis, so its absence has high importance on the modal analysis. However, if the experimental analysis will be done without this component, as the same as the following correlation, the model could be modified properly adding the relating constraints and the results should be correct.

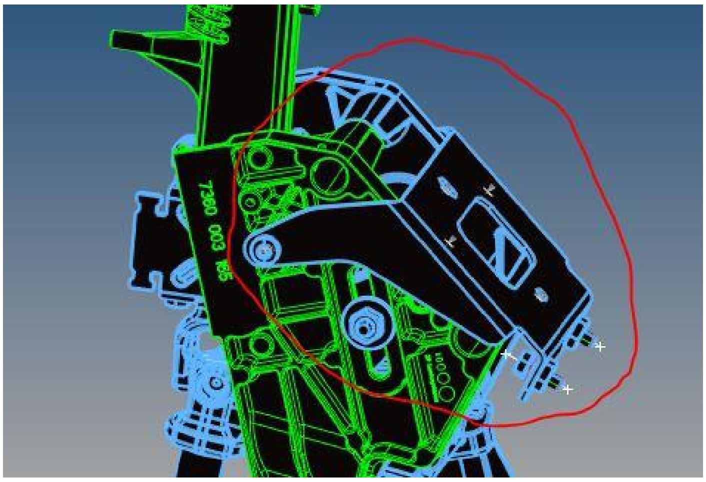

Figure 1.2.1.6 – Missing component.

1.2.2 Materials

Homogeneous isotropic materials are assumed in the model. The materials characteristics are reported in Table 1.2.2.1. As already noticed, many redundancies are present (in red), indicating the need of an accurate check and resetting of the whole model. Table 1.2.2.1 shows, in blue, unusual combinations of density and Young module: very high density for MAT1_20 and MAT1_22, while they are supposed to be, according to their Young modules, respectively aluminium and steel; MAT1_23 has a too low density, as it is supposed to be aluminium. These materials are used for modelling the wheel and these unusual physical properties values are supposed to simulate the actual vibrational behaviour. Anyway, this kind of unphysical settings has to be evaluated after an accurate analysis of the experimental test data.

Table 1.2.2.1 – Properties of materials.

Material	Density [kg/m^3]	Young module [Pa]	Poisson coefficient [-]
MAT1_5	7.8e3	2.05e11	0.3
MAT1_7	2.7e3	6.83e10	0.33
MAT1_8	2.7e3	7e10	0.3
MAT1_9	7.8e3	2e11	0.3
MAT1_19	2.7e3	7e10	0.3
MAT1_20	1.6e4	7e10	0.3
MAT1_22	1.0e4	2e11	0.3
MAT1_23	10	7e10	0.3

1.3. Modal analysis

The modal analysis, run by MSC Nastran, on the model given by Iveco leads to the results reported in Table 1.3.1. Only modes with frequencies up to 70 Hz have been evaluated.

Table 1.3.1 – Natural frequencies and qualitative description.

# Mode	Frequency [Hz]	Description
1	15.03	First bend on XZ
2	17.16	First bend on YZ
3	21.76	First torsional around Z
4	27.21	First bend of the wheel on XZ
5	47.06	Second bend of the wheel
6	47.31	
7	55.98	Second bend on YZ
8	56.48	Second bend on XZ

From Figure 1.3.1 to Figure 1.3.8 an illustration of the first 8 modes are reported. These results are not probably correct, but they can provide an overview of the numerical results.

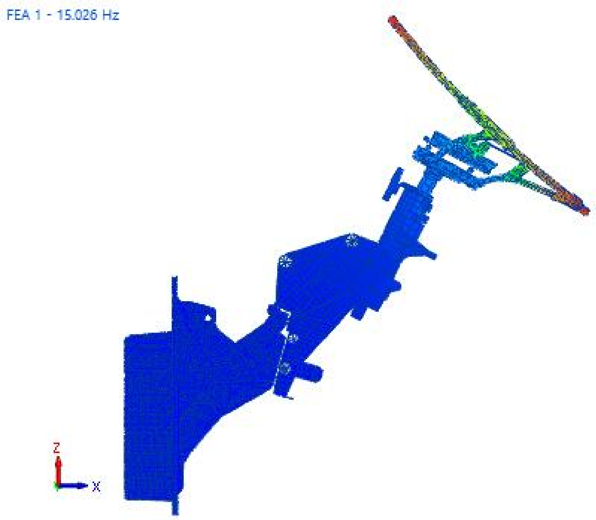

Figure 1.3.1 – First mode at 15.03 Hz.

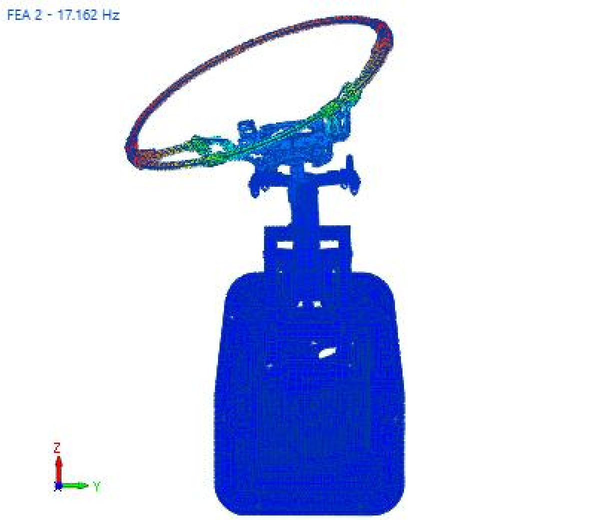

Figure 1.3.2 – Second mode at 17.16 Hz.

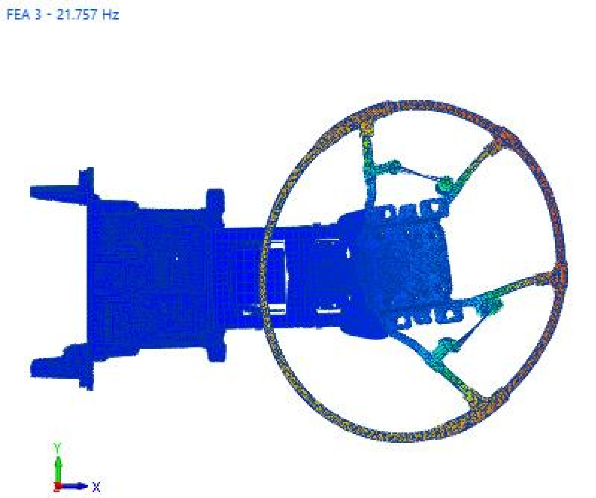

Figure 1.3.3 – Third mode at 21.76 Hz.

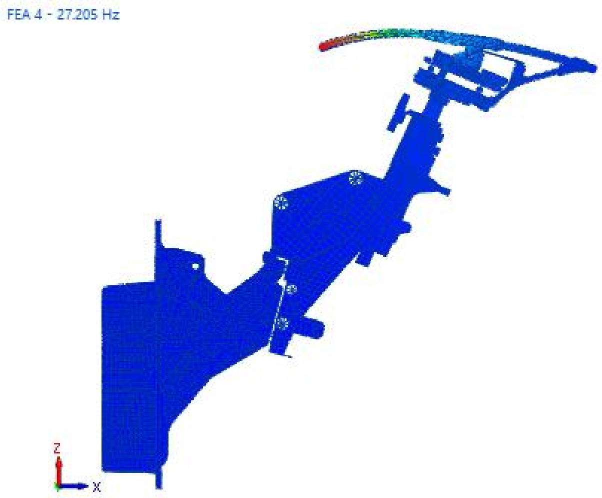

Figure 1.3.4 – Fourth mode at 27.21 Hz.

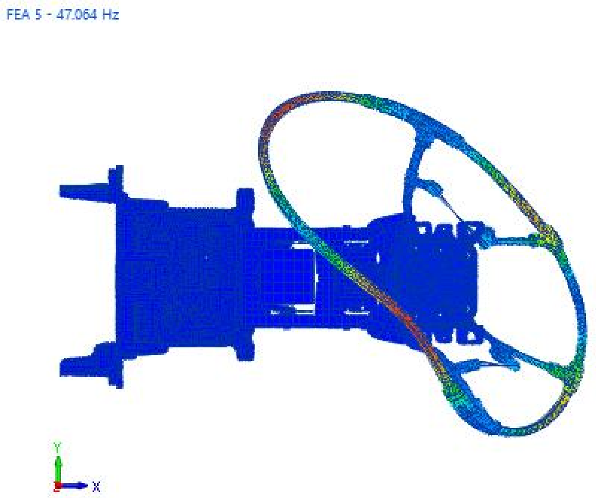

Figure 1.3.5 – Fifth mode at 47.06 Hz.

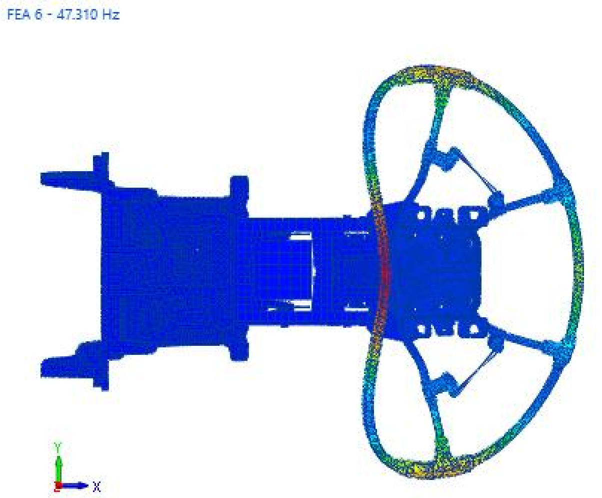

Figure 1.3.6 – Sixth mode at 47.31 Hz.

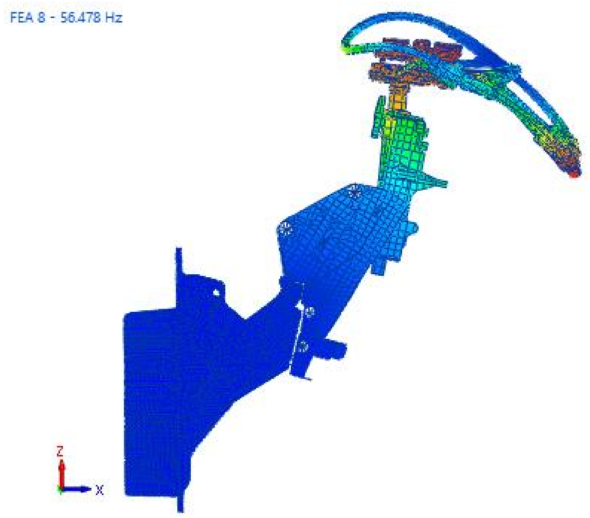

Figure 1.3.7 – Seventh mode at 55.98 Hz.

Figure 1.3.8 – Eighth mode at 56.48 Hz.

Because of the absence of the upper bearing, these results are thought to underestimate the real natural modes frequencies. A punctual analysis and correction of the issues highlighted in the previous paragraph is required in order to obtain reliable results. The first component that will be examined is the wheel, as it is the most complex in the whole structure and the one requiring the highest attention, as it is the main physical interface with the user.

2. Constructor steering-wheel finite element model

The steering-wheel has been deeply analysed. It is composed mostly of three materials: steel for the frame, aluminium for the connectors of the frame and the central part and rubber, for the covering. There are several plastic parts and few electronic components, but they are not supposed to influence the vibrational behaviour, so they will not be considered.
The frame is formed by steel rods, connected by tubular elements obtained by aluminium fusions. The internal rods are inserted in proper cavities in the central part, that hosts the steel seating for the steering shaft. A steel plate, mounted on the central part, acts as a support for many plastic objects and covers; it will not be considered. The rubber covers everything, except the zone around the shaft seating in the central part. The wheel has a diameter of about 470 mm and a weight of 3.966 kg, excluded the plastics and the electronics: it will be tested without these parts.

2.1 Constructor finite elements model

The discretization process is simply executed by CAE softwares such as Solidworks in a completely automated way; the number of nodes cannot be punctually controlled by the user, but it can be selected a finer or a coarser tetrahedral mesh. FEM softwares such as Hypermesh allow to choose elements type and a much better control in the mesh creation. The constructor chose the faster way, modelling the system in a quite automated way and resulting in a very high number of nodes. Second order elements have been used. A brief description of every part model is reported below. Figure 2.1.1 shows the whole model.

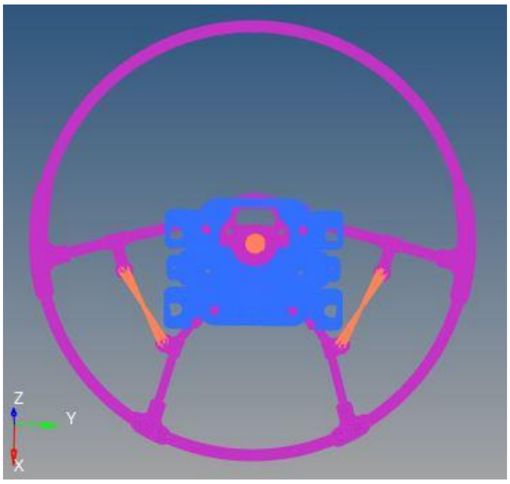

Figure 2.1.1 – Constructor model.

2.1.1 Wheel frame

The wheel frame has been modelled using 61074 tetrahedral elements and so 98414 nodes. This part is composed by steel rods with circular section, linked by tubular aluminium connectors; the technique used provides an accurate representation of the real vibrational behaviour, but the simple geometry of the part suggests the use of much less elements. T-connectors are linked to the other parts by RBE2s. Figure 2.1.1.1 reports the part, Figure 2.1.1.2 shows the detail of a T-connector.

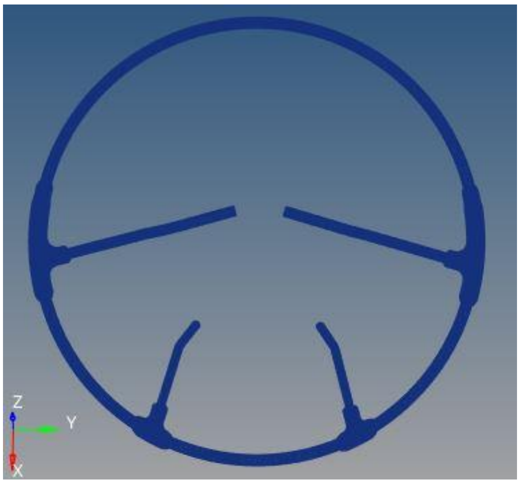

Figure 2.1.1.1 – Wheel frame model.

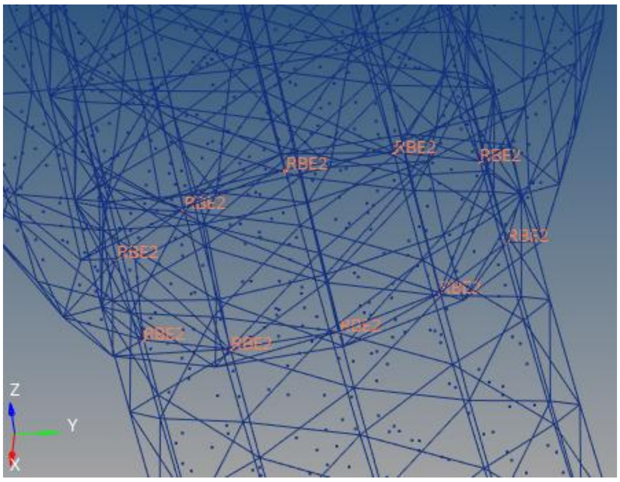

Figure 2.1.1.2 – T-connector detail, RBE2 links.

2.1.2 Central plate

The central plate is a 2 mm thick steel plate. It has been modelled by 17668 second order tetrahedral elements, resulting in 37002 nodes. This choice is not good, as the thin geometry suggests the use of first order shell elements, much less heavy for computing. Figure 2.1.2.1 shows the part.

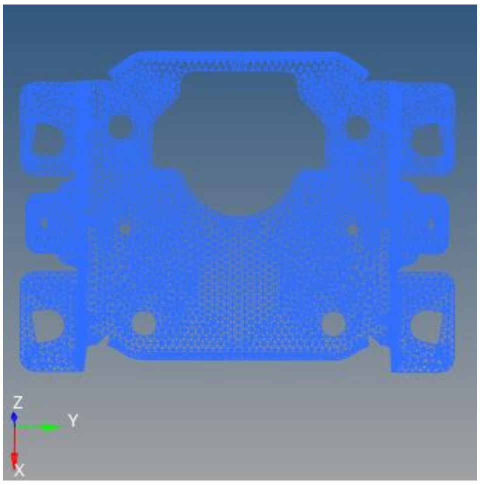

Figure 2.1.2.1 – Central plate.

2.1.3 Central part

The central part has been modelled using 37272 tetrahedral elements, resulting in 62823 nodes. This part is a quite thick aluminium fusion, so the kind of element chosen is reasonable. However, the number of elements is very high and there is not the need of a second order mesh. This model probably represents accurately the real behaviour of the object, but the computational effort is high. The same results could be obtained using first order bigger elements. Figure 2.1.3.1 shows a view of the part.

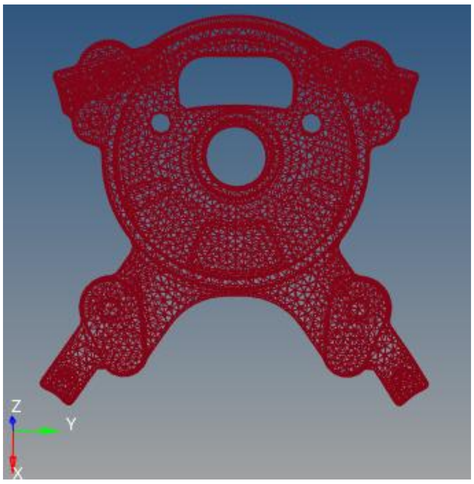

Figure 2.1.3.1 – Central part.

2.1.4 Supports

The supports that link the frame with the upper plastic parts of the wheel have been modelled by 13056 second order tetrahedral elements, resulting in 23924 nodes. The number of elements is obviously high with respect to the quite small dimensions of the parts, while the type of element is reasonable. The plastic parts are modelled by concentrated masses, linked to the connectors using RBE3s, that are specific links for connecting taking in to account of inertial properties only. Figure 2.1.4.1 shows the described parts.

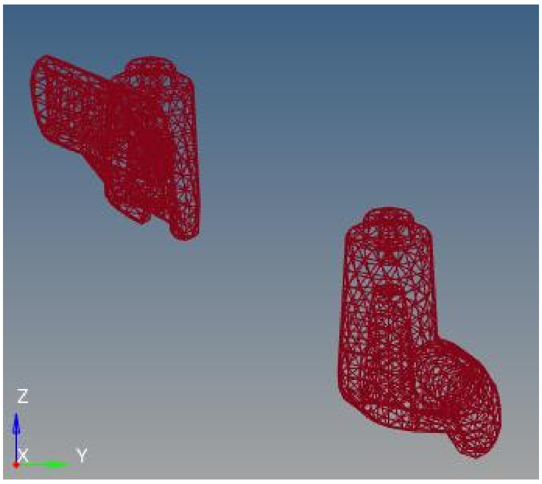

Figure 2.1.4.1 – One of the two supports couples.

2.1.5 Rubber layer

The rubber thin layer that covers the wheel has been modelled with 52336 two order triangular shell elements, resulting in 91490 nodes. The thickness assigned is 0.1 mm, clearly not a real value. The physical properties, included density and Young module, given to the elements are not real: they try to simulate the complex behaviour of the rubber layer wrapping the wheel. The mesh is coincident with the meshes of the other parts, as a skin. Figure 2.1.5.1 represents the model.

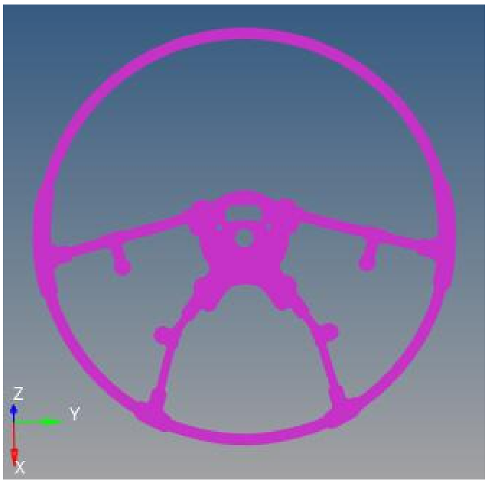

Figure 2.1.5.1 – Rubber layer.

2.1.6 Elements properties

An important aspect of every model is the set of physical characteristics assigned to the elements. In Hypermesh, Property and Material cards allow to define the physical behaviour of elements, through density, Young module, Poisson coefficient and every morphological quantity that can help the definition of an element. Table 2.1.6.1 resumes how the constructor defined the components in the model, reporting the Material and Property cards used.

Table 2.1.6.1 – Property and Material cards for each component.

Component	**Property**		**Material**			
	Type	Thickness [m]	Type	Density [kg/m^3]	Young module [GPa]	Poisson module [-]
Wheel frame	PSOLID	-	MAT1	16000	70	0.3
Central part & Supports	PSOLID	-	MAT1	2790	70	0.3
Central plate	PSHELL	0.0001	MAT1	10000	200	0.3
Rubber layer	PSOLID	-	MAT1	10	70	0.3

It is evident the unusual values assigned to the Material cards of Wheel frame and Rubber layer, probably to simulate the complex vibrational behaviour of the assembly, due to the rubber physical properties.

3. New models creation

The given model resulted to be not optimized for a modal analysis, so this chapter describes the building of two new models. However, the finite element model provided by the constructor resulted to be incoherent with the physical model, as it referred to an old CAD, so it has been necessary the construction of an updated model.
The creation of the new models began with the import of CAD geometry in Hypermesh. Both the models share the same structural parts, modelled in nearly the same way. The most important difference is given by the rubber part: the first model has been built as the lightest, so only the inertial characteristics of non-structural parts have been taken into account. The second model, as the given one, includes a dedicated mesh for the rubber part. The two models are described in the following Paragraph 3.1 and Paragraph 3.2.

3.1 First model

This first attempt is shown in Figure 3.1.1; Figure 3.1.2 shows the real dimensions of 1D elements. The building process started with the wheel internal frame, as it is the most important. Then, a long time has been spent on the central part meshing and as last supports for upper, non-structural parts. The rubber part, in order to keep a low number of nodes, has been modelled with only non-structural masses. The following chapters report the whole creation process.

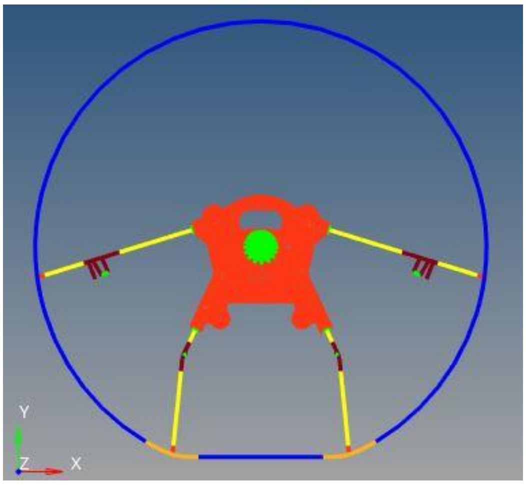

Figure 3.1.1 – First model.

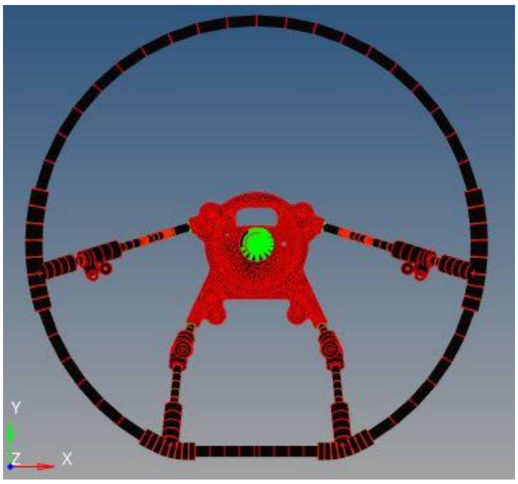

Figure 3.1.2 –1D elements dimensions.

3.1.1 Wheel frame

The frame of the wheel has been modelled using 1D beam with circular section. This solution reduced drastically the number of nodes and elements: 251 elements and 259 nodes. Connectors have been modelled by tubular beam, linked to arms by 84 rigid joints, that provide a strong cinematic relation between the nodes. Figure 3.1.1.1 reports the part, Figure 3.1.1.2 shows the detail of a connector. In order to have a well-manageable model, nodes with the same coordinates, such as the external parts and their connectors, have not been collapsed, but they have been linked using rigid joints, blocking all six degrees of freedom. A detailed explanation of the procedure is reported in Appendix A. In case of modifications, this solution allows to delete nodes from a component

without modifying the other. The T-connection has been realized connecting the three elements in the same node.
Hypermesh allows to quickly design sections to be assigned to beam elements, through a simple software that starts from the selection of the type (bar, rod, tube, etc...) and ends with the definition of dimensions (thickness, diameters, length of sides for bars, etc...); then the software calculates the properties of the section (area, moments of inertia).

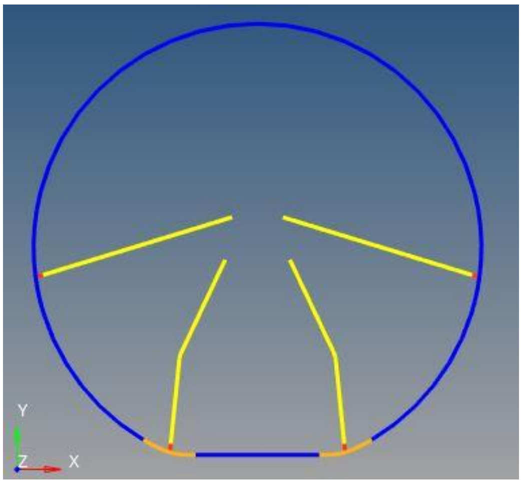

Figure 3.1.1.1 – Wheel internal frame.

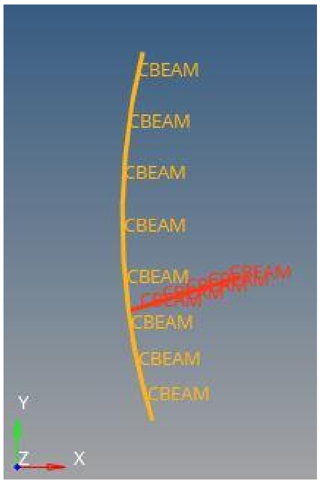

Figure 3.1.1.2 – Connector detail.

3.1.2 Central part

As in the given model, this part has been represented by a tetrahedral mesh, using 53271 first order elements, resulting in 12064 nodes. Figure 3.1.2.1 shows the new mesh. The detailed and complex geometry took a quite long time to be analyzed and meshed, particular attention has been given to zones of contact and link with other bodies, ignoring fillets and small details, as their importance in the global stiffness and mass matrices is thought to be negligible.

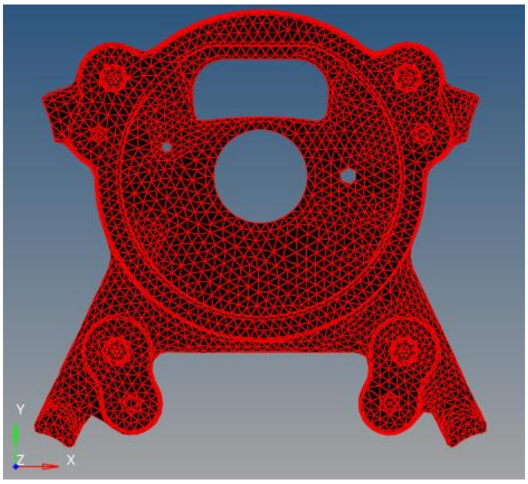

Figure 3.1.2.1 – Central plate mesh.

3.1.3 Central plate

The central plate has been ignored in the new model, as it has not any structural importance. In the experimental phase it will be removed.

3.1.4 Supports

The supports have been modelled using 64 tubular and bar 1D beam elements, resulting in 70 nodes. Unlike the provided model, the upper plastic components, such as buttons and covers, have not been modelled, because every part has been dismantled from the frame for the experimental tests, in order to reduce mismatches. Figure 3.1.4.1 shows the finite element model of a couple of supports. It is composed by different types of elements, in order to get a model similar to the real object, avoiding the complexity of a solid mesh. The vertical elements have tubular section, while horizontal ones are bars.

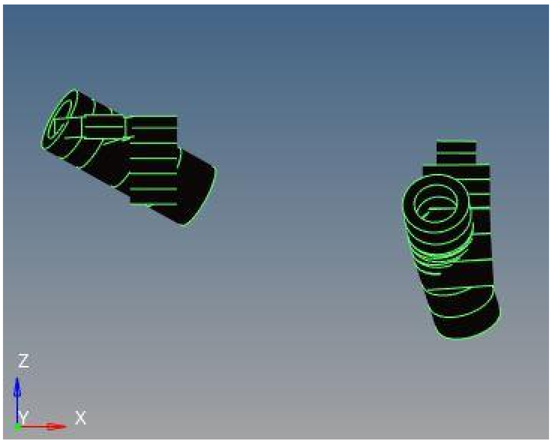

Figure 3.1.4.1 – Supports, real dimensions view.

3.1.5 Rubber layer

The rubber layer has not been explicitly modelled: in order to achieve a light model, only its inertial characteristics have been taken into account, as the low stiffness properties of the rubber should not be so relevant. Hypermesh allows to add non-structural masses, expressed as mass for unit of length, on many element types, such as CBEAM, while it is not allowed for solid elements. A first attempt has been done valuating volume from CAD of pieces of rubber and relating them with the model volume, as the same as with mass. Simple calculations and trials led to a total mass equal to the real object's. The non-structural mass is added as a parameter in Property cards, so new cards have been created for components with a corresponding variable rubber thickness, in order to have a mass distribution similar to the real one. Table 3.1.5.1 briefly reports the non-structural mass values along the elements. Hypermesh do not permit the non-structural mass to be set on solid elements, used for the central part mesh: the non-structural mass distribution has been made taking into account this fact, increasing the value on the frame beams near those zones. Figure 3.1.5.1 and following define the position of components described in Table 3.1.5.1. Surely, the distribution proposed is not completely correct, but it is a starting point for further tunings, after the experimental data will be acquired and analysed.

Table 3.1.5.1 – Non-structural mass distribution.

Component	Non-structural mass [kg/m]
Wheel external frame	0.339
Wheel external frame thicker layer	0.568
Wheel internal frame	0.568
Wheel internal frame thicker layer	1.25
T-connectors internal side & Supports	0.300

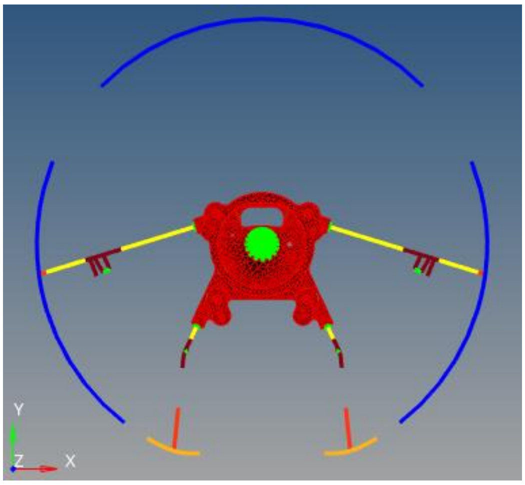

Figure 3.1.5.1 – Blue lines show Wheel external frame, yellow lines show Wheel internal frame thicker layer.

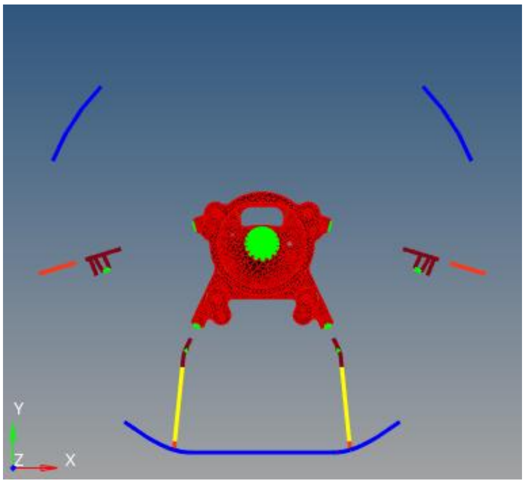

Figure 3.1.5.2 – Blue lines show Wheel external frame thicker layer, yellow lines show Wheel internal frame.

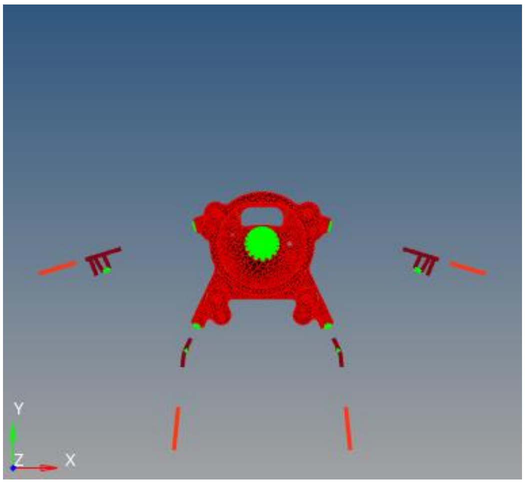

Figure 3.1.5.3 – Red lines show T-connectors internal side.

3.1.6 Shaft seating

The central part is connected to the shaft through a steel grooved collet, that has been modelled by a set of 6 coaxial beams with different tubular sections. The grooves, that characterize the joint with the shaft, have been neglected, as their influence is very low. The shaft will be modelled as a 6 dofs constraint acting directly on its seating. Figure 3.1.6.1 shows the real dimension view of the part.

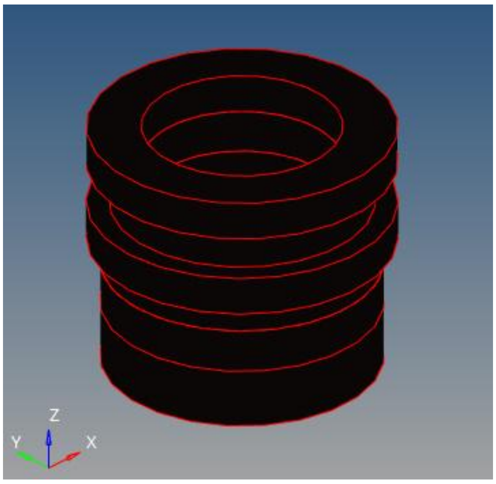

Figure 3.1.6.1 – Shaft seating.

3.1.7 Elements properties

As already done for the constructor model, the Property and Material cards are resumed in Table 3.1.7.1. In order to have a complete description of the model, the details of beam elements are reported in Table 3.1.7.2, indicating for each case the type of section and its dimensions.

Table 3.1.7.1 – Property and Material cards details.

Component	Property	Material			
	Type	Type	Density [kg/m^3]	Young module [GPa]	Poisson coefficient [-]
Wheel external frame	PBEAML	MAT1	7800	210	0.3
Wheel internal frame	PBEAML	MAT1	7800	210	0.3
T-connectors external side	PBEAML	MAT1	2790	75	0.3
T-connectors internal side	PBEAML	MAT1	2790	75	0.3
Supports	PBEAML	MAT1	2790	75	0.3
Central part	PSOLID	MAT1	2790	75	0.3
Shaft seating	PBEAML	MAT1	7800	210	0.3

Table 3.1.7.2 – Beam elements details.

Component	Section		
	Type	External diameter [m] (BAR Dimension 1 [m])	Internal diameter [m] (BAR Dimension 2 [m])
Wheel external frame	ROD	0.011	-
Wheel internal frame	ROD	0.008	-
	ROD	0.010	-
T-connectors external side	TUBE	0.017	0.011
T-connectors internal side	TUBE	0.017	0.010
	TUBE	0.014	0.008
Supports	TUBE	0.010	0.004
	TUBE	0.014	0.008
	TUBE	0.017	0.004
	ROD	0.017	-
	TUBE	0.016	0.010
	TUBE	0.012	0.004
	TUBE	0.010	0.006
	BAR	0.012	0.005
	BAR	0.005	0.005
Shaft seating	TUBE	0.031	0.026
	TUBE	0.031	0.024
	TUBE	0.031	0.022
	TUBE	0.034	0.022
	TUBE	0.029	0.022

3.2 Second model

The second model is based on the first one, differences on structural parts are due to modifications after testing the model running several modal analysis. However, central part and connectors have not been modified, so they are not reported. Figure 3.2.1 shows a view of the model.

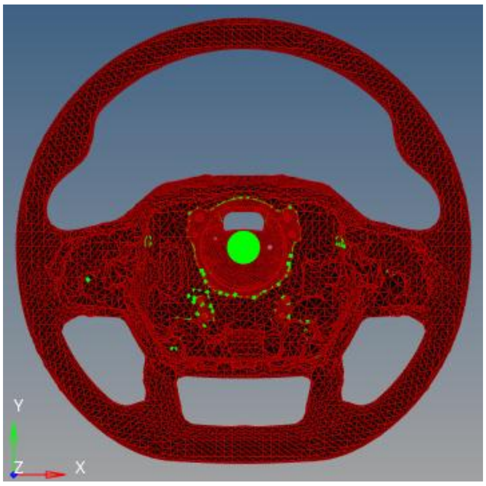

Figure 3.2.1 – Model with Rubber.

3.2.1 Wheel frame

As in the first model, the frame has been modelled by 1D beam elements. Because of bad results in modal analysis, the number of nodes has been increased to 291 and elements to 283. A detailed explanation is reported in Paragraph 3.2.2, while describing the rubber discretization.

3.2.2 Rubber layer

The rubber layer has been modelled using 76568 first order tetrahedrons, resulting in 17538 nodes. In order to simplify the process, the rubber has been meshed neglecting the hollow shape of the real part. Particular attention has been given to the meshing process and linking, because of the different nature of the tetrahedral mesh of the rubber and the beam elements of the frame. In a first attempt, the rubber mesh was forced to include the frame nodes. In order to evaluate the behaviour of the model, a modal analysis was run. Figure 3.2.2.1 reports the issue noticed: an improbable torsion in rubber at 429.45 Hz, due to the low stiffness of the material, between the common nodes with the frame. Therefore, a second attempt has been made doubling the number of frame nodes in critical zones. Moreover, a different technique has been used: in order to obtain a more flexible and modifiable model, the links with the other components have been realized by rigid elements RBE2s, through the use of a simple script that connected nodes of different components with a distance smaller than 5 millimetres, for the Central part, and 8 millimetres for the Wheel frame; a better detailed explanation is reported in Appendix A. The difference in distances taken as linking limit is due to the need of locking, through a single node of the beams composing the frame, the degrees of freedom of many solid elements.
As a first attempt, the material density has been calculated dividing the difference in mass between the real object and the model by the volume of the mesh, in order to reach the real total mass. The differences in volume between real and model, due to the hollow real shape, have been neglected,

so the resulting density is a bit smaller than real one. Table 3.2.2.1 resumes the physical characteristics assigned to the rubber.

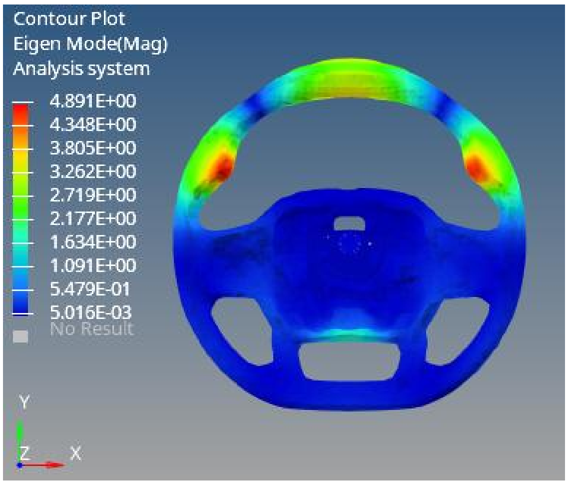

Figure 3.2.2.1 – Rubber mode at 429.45 Hz, showing unnatural torsion in rubber part.

Table 3.2.2.1 – Rubber physical properties.

Density [kg/m^3]	434
Young module [MPa]	5
Poisson coefficient	0.49

These values are just a first attempt to represent the behaviour of the real system, they will be adjusted after an accurate analysis of experimental data.

3.3 Models renumbering

Every time a node, an element or every other entity of a model is created, Hypermesh assigns it an identification number. This process follows the natural sequence of the numbers, regardless the position or the properties of the entity created. So, at the end of the analysis of a geometry and the further creation of a model, maybe after iterative processes and many trials, the user has a list of nodes, elements, components and properties with insensible identification numbers. The readability of the model results very low and, in case of need, the work with id numbers becomes very hard. In order to solve this issue, a renumbering process is required. Table 3.3.1 and Table 3.3.2 report the renumbering done for the new models; it is clear the logic behind the assignments done.

Table 3.3.1 – New models nodes renumbering.

Components	**Model w/out rubber**		**Model with rubber**	
	From:	To:	From:	To:
External wheel frame	100	172	100	204
Internal wheel frame	300	429	300	429
Connectors	500	557	500	557
Supports	600	669	600	669
Shaft seating	700	706	700	706
Central part	800	12863	800	12863
Rubber layer	-	-	15000	32537

Table 3.3.2 – New models elements renumbering.

Components	**Model w/out rubber**		**Model with rubber**	
	From:	To:	From:	To:
External wheel frame	100	172	100	204
Internal wheel frame	300	425	300	425
Connectors	500	551	500	551
Supports	600	663	600	663
Shaft seating	700	705	700	705
Central part	800	54070	800	54070
Rubber layer	-	-	55000	131567

4. Comparison of the three models

The three models are now compared, Table 4.1 places beside the main characteristics:

Table 4.1 – Main finite elements models characteristics.

		Old	**New – w/out rubber**	**New – with rubber**
Central part	Type of elements	Tetrahedrons	Tetrahedrons	Tetrahedrons
	Number of elements	37272	53271	53271
	Number of nodes	62823	12064	12064
Internal frame	Type of elements	Tetrahedrons	Beams	Beams
	Number of elements	61074	251	283
	Number of nodes	98414	259	291
Central plate	Type of elements	Tetrahedrons	-	-
	Number of elements	17668	-	-
	Number of nodes	37002	-	-
Supports	Type of elements	Tetrahedrons	Beams	Beams
	Number of elements	13056	64	64
	Number of nodes	23924	70	70
Rubber layer	Type of elements	Triangles	-	Tetrahedrons
	Number of elements	52336	-	76568
	Number of nodes	91490	-	17538
Rigid links	Number of elements	218	127	696
Total	Number of elements	181624	53719	130888
	Number of nodes	224632	12400	29970

The differences in the used modelling techniques are clearly visible: the numbers of nodes and elements have been drastically reduced, making the model even better adjustable. The effect of the low number of nodes has been evident running the modal analysis, in the difference of calculation time. The next paragraph reports the results obtain by Optistruct analysis. Figure 4.1 compares the three models.

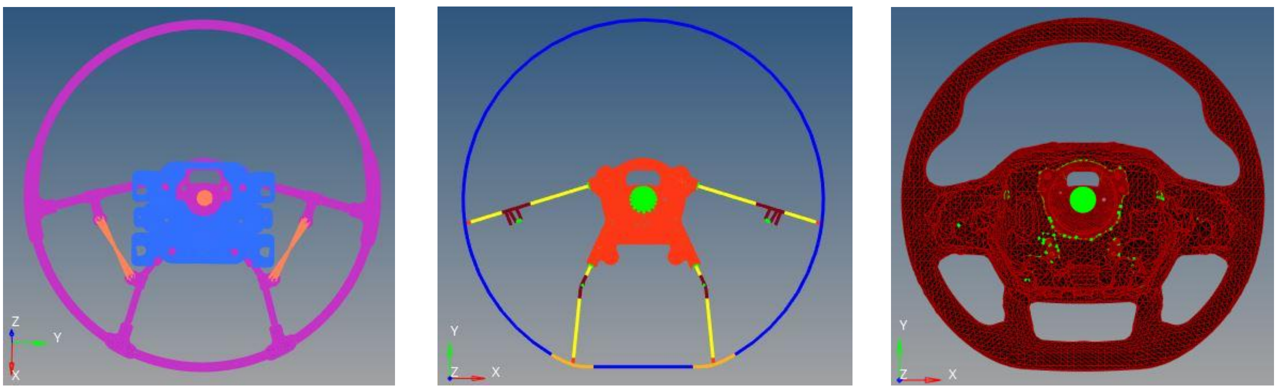

Figure 4.1 – Visual comparison of the three wheel models, the Constructor's, the first and the second models respectively.

4.1 Modal analysis by Optistruct

A preliminary analysis has been run in Optistruct, in order to evaluate the normal modes and to have an idea of the vibrational behaviour of the system. For first, the constructor's model has been tested, even if the geometry is not correct, just for a comparison of the different methods. A complete constrain has been imposed to the models, as they were mounted on a blocked steering system. Table 4.1.1 reports the first ten normal modes frequencies for the three models.

Table 4.1.1 – First ten frequencies of normal modes analysis comparison.

	Frequencies [Hz]		
Mode	Constructor's model	Model with NSM	Model with rubber
1	19.67	44.87	44.46
2	20.35	46.22	46.90
3	27.46	67.57	68.67
4	30.61	68.02	70.73
5	47.17	109.0	109.7
6	47.59	114.9	113.1
7	82.33	150.4	149.4
-	-	-	149.9
-	-	-	210.6
-	-	-	221.8
-	-	-	226.0
-	-	-	238.7
-	-	-	253.3
8	124.5	277.0	272.3
9	134.5	281.2	279.8
-	-	-	286.6
-	-	-	288.9
10	149.7	296.8	291.1

The following figures show a representation of the ten modes. As it can be noticed from Table 4.1.1 and from Figure 4.1.1 to Figure 4.1.10, the first seven modes found by the analysis of the two new models are quite similar, as the main structural component, the wheel frame, has been modelled in the same way. Modes from 8 to 10 show the influence of the rubber; however, it has not to be forgotten that this type of analysis do not consider the damping effect, that obviously represents the most important property, and role, of the rubber in these systems. Besides, the rubber has a particular elastic behaviour, and its Young module is not constant through deformation: the model includes only a value, 5 MPa, thought to be reliable for a first approach. Experimental data will provide a solid base on which a more precise analysis of rubber influence could be done.
Table 4.1.2 reports the time taken by the software to run the analysis for the three models. As expected, the model without the rubber has taken much less time than the others.

Table 4.1.2 – Time for running modal analysis by Optistruct.

Model	**Time [mm:ss]**
Old	17:53
New – without rubber	00:32
New – with rubber	01:41

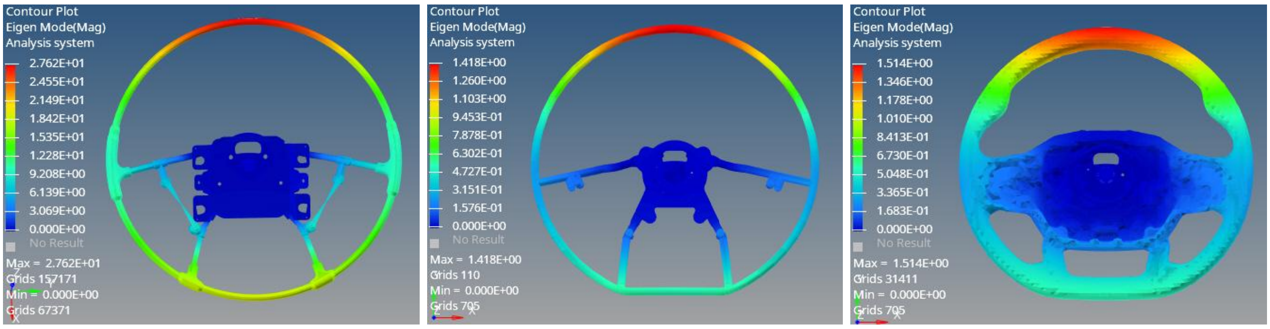

Figure 4.1.1 – First mode, respectively at 19.67 Hz, 44.87 Hz and 44.46 Hz.

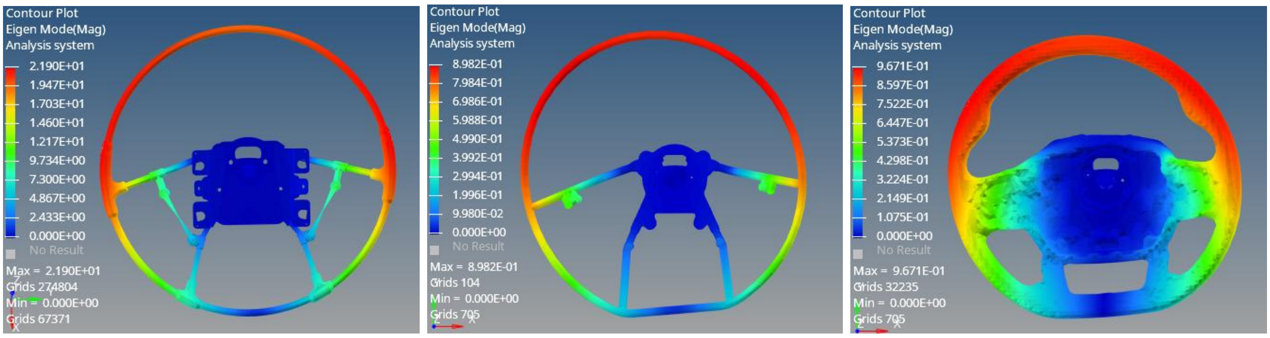

Figure 4.1.2 – Second mode, respectively at 20.35 Hz, 46.22 Hz and 46.90 Hz.

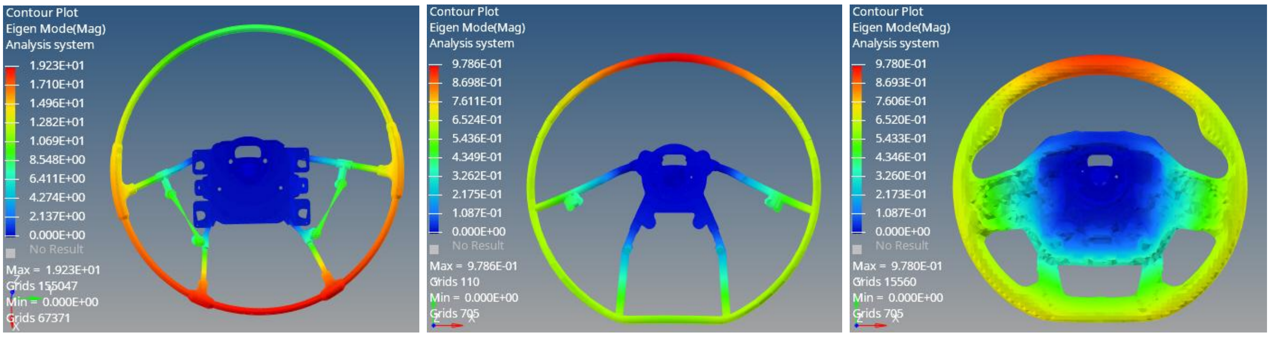

Figure 4.1.3 – Third mode, respectively at 27.46 Hz, 67.57 Hz and 68.67 Hz.

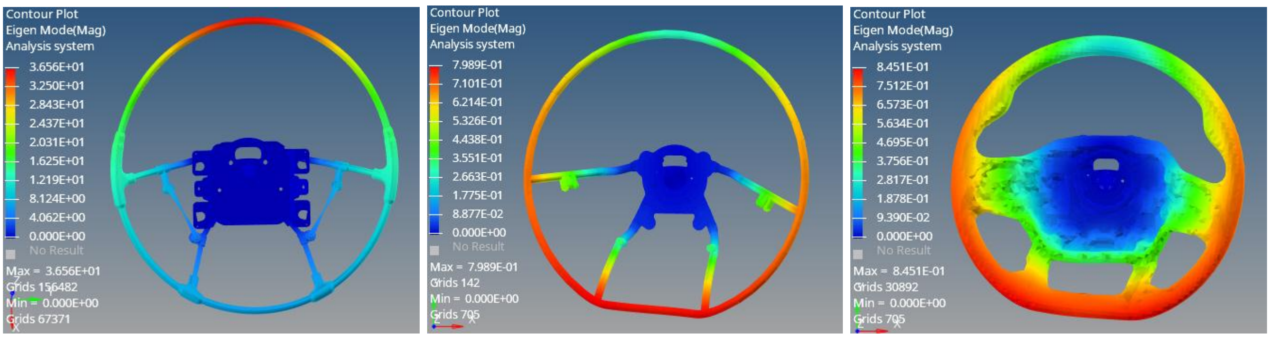

Figure 4.1.4 – Fourth mode, respectively at 30.61 Hz, 68.02 Hz and 70.73 Hz.

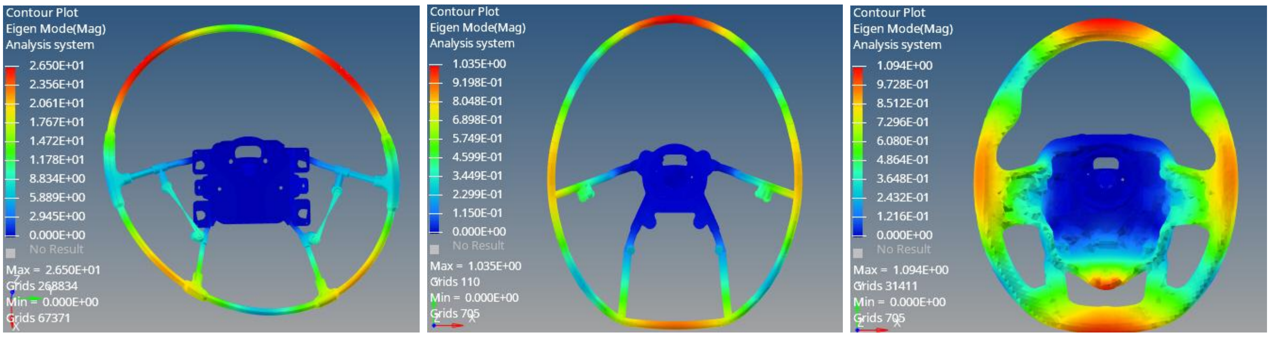

Figure 4.1.5 – Fifth mode, respectively at 47.17 Hz, 109.0 Hz and 109.7 Hz.

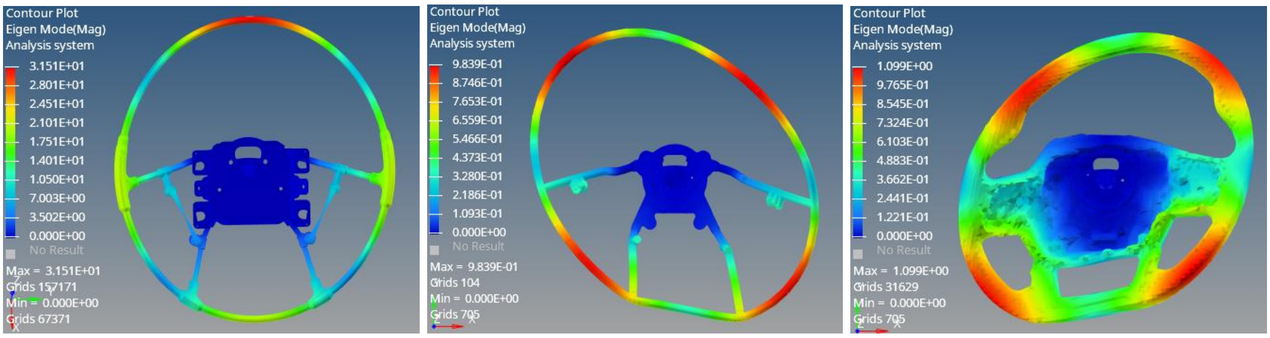

Figure 4.1.6 – Sixth mode, respectively at 47.59 Hz, 114.9 Hz and 113.1 Hz.

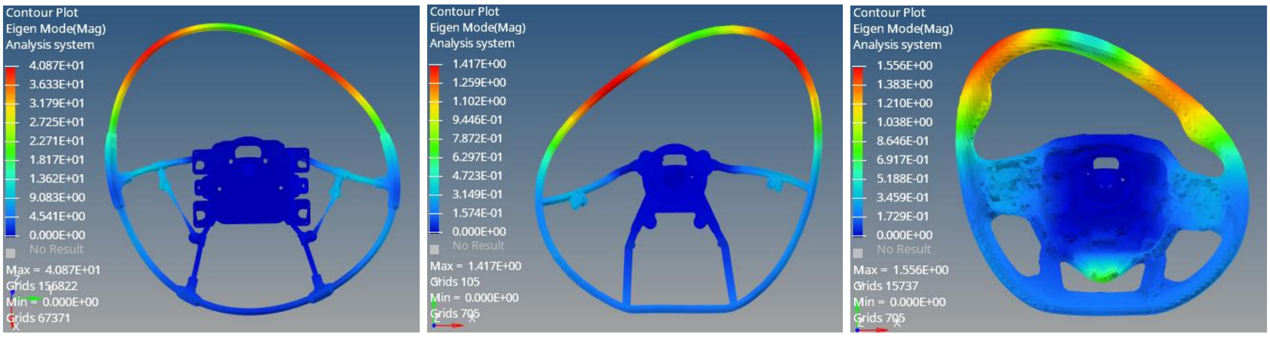

Figure 4.1.7 – Seventh mode, respectively at 82.33 Hz, 150.4 Hz and 149.4 Hz.

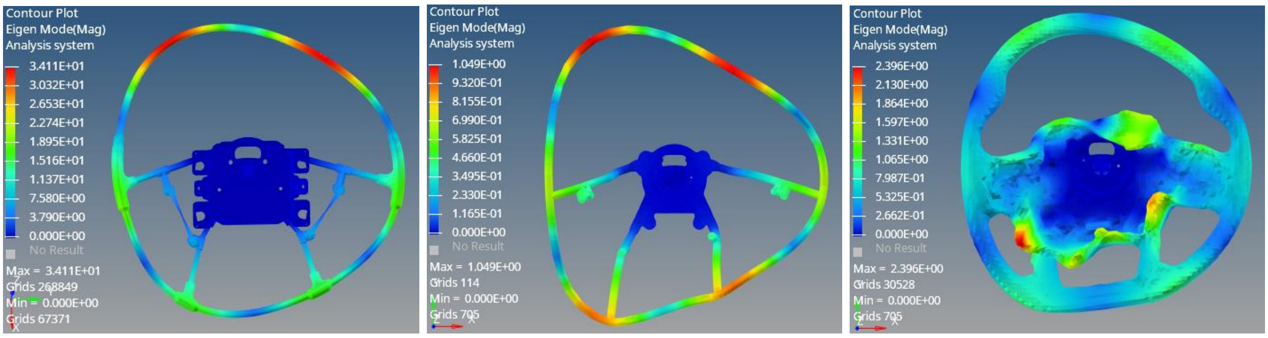

Figure 4.1.8 – Eighth mode, respectively at 124.5 Hz, 277.0 Hz and 272.3 Hz.

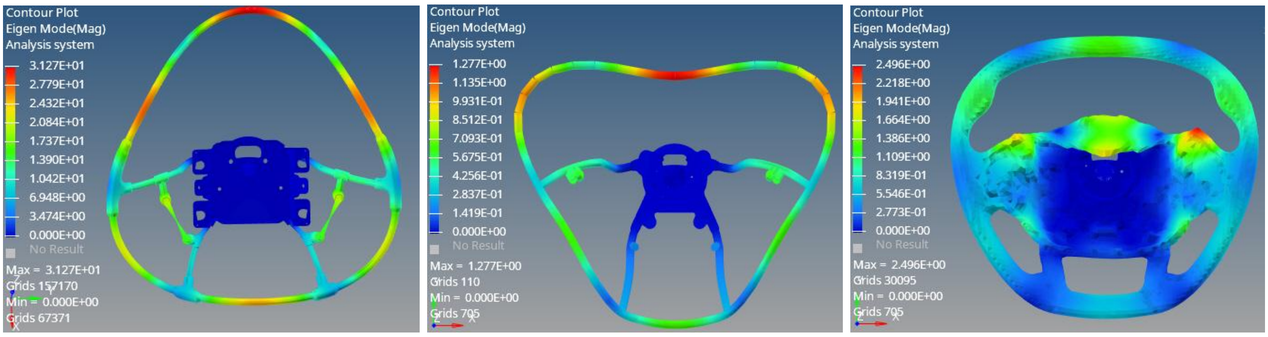

Figure 4.1.9 – Ninth mode, respectively at 134.5 Hz, 281.2 Hz and 279.8 Hz.

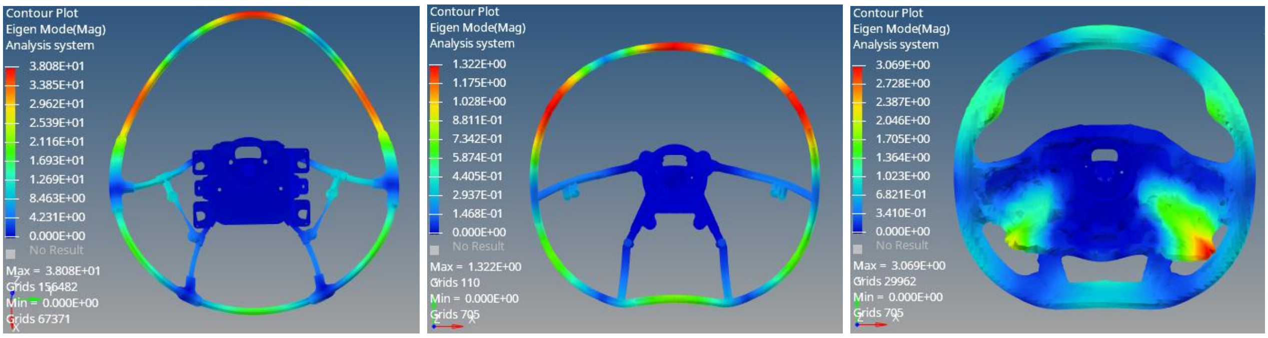

Figure 4.1.10 – Tenth mode, respectively at 149.7 Hz, 296.8 Hz and 221.8 Hz.

From Figure 4.1.11 to Figure 4.1.13 the modes due to the presence of the rubber are reported. They are not structural, they are just the result of numerical calculation, their physical importance is negligible.

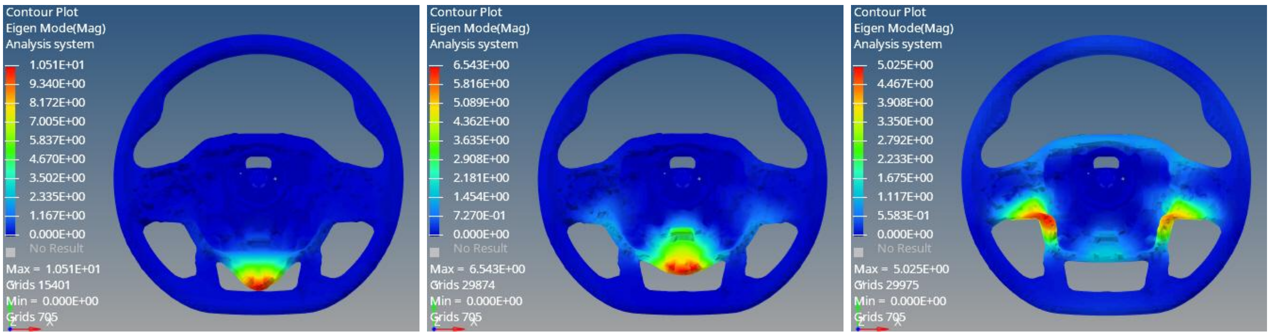

Figure 4.1.11 – First three rubber modes, respectively at 149.9 Hz, 210.6 Hz and 221.8 Hz.

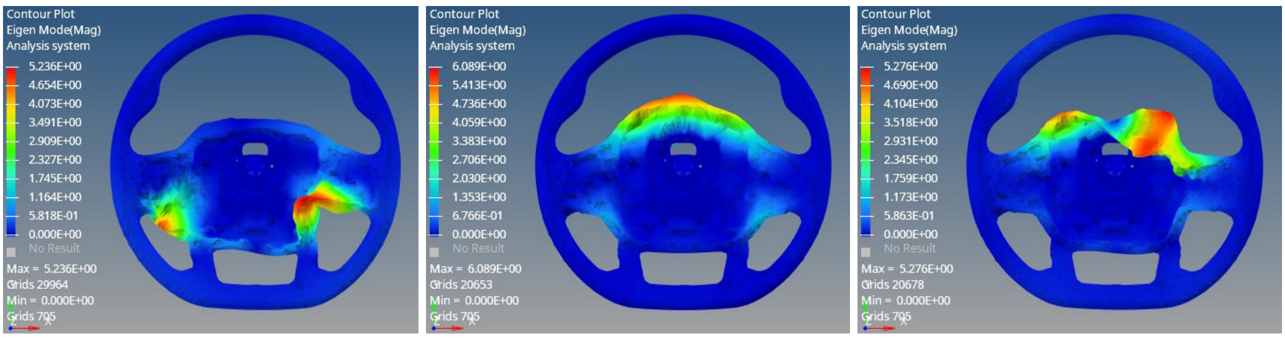

Figure 4.1.12 – Fourth, fifth and sixth rubber mode,
respectively at 226.0 Hz, 238.7 Hz and 253.3 Hz.

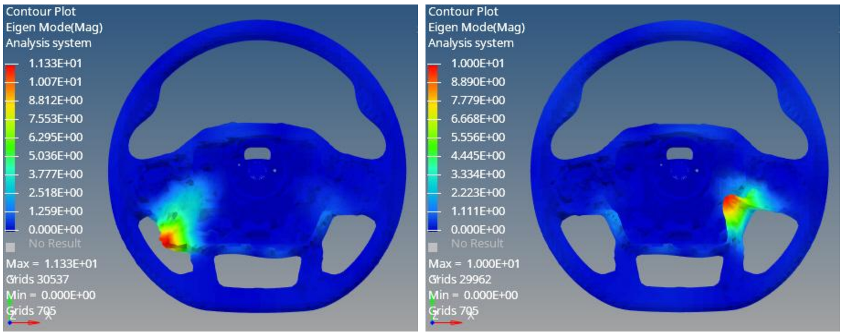

Figure 4.1.13 – Seventh and eighth rubber mode, respectively at 286.6 Hz and 288.9 Hz.

The study of numerical models suggests that modelling by a low number of nodes could be a good technique, as demonstrated by the time taken by the modal analysis by Optistruct for the three models. Besides, a lighter model can be managed much more easily, requiring a lower computing power. However, experimental data will be decisive for better understanding the pros and cons of the different methods.

5. The Minecraft Project applied to the wheel models

The creation of a new typology of model came from two necessities: firstly, in order to keep on searching a deeper reduction and simplification of the model, and then the possibility to use an alternative software, Lupos, that at the moment cannot run tetrahedral elements analysis.
The new models maintains the same structure as the old ones, the only changes concern the solid meshed parts. The idea is to drastically simplify the solid mesh by the use of the simplest solid figure: the cube. The whole process is run in Matlab and uses Lupos format files for its evaluations. For first, the model parts that have to be substituted are exported from Hypermesh in Nastran Bulk Data File format, in order to be easily translated in Lupos format. Then a Matlab program creates a parallelepiped that includes the whole part and subsequently it is divided in cubes of an user imposed dimension, originating a new solid mesh. Comparing the position of old and new mesh nodes, a reduction process is run and deletes every new node whose distance is over a certain value, imposed by the user. The result is a sort of approximation of the old mesh. Obviously, the level of detail is determined by the dimension of the new hexahedral elements; considering a model for modal analysis, there is no need of an high level of detail, resulting in a quite good reduction in number of nodes and simplification in the calculation process, being a regular hexahedrons mesh. The resulting mesh has been imported in Hypermesh by a TCL script for further modifications and adjustments.

5.1 Central part rebuilding

The first component to be remodelled is the central part. Previously, this part was modelled by a tetrahedral mesh, using 3 mm elements. This value is just the mean of the effective dimensions of every tetrahedron composing the mesh. The dimension of hexahedrons for the new mesh has been set to 5 mm, in order to have a good reduction. Having a finer starting mesh is important, because it ensure a good approximation of the real geometry of the object.
The result is reported by Figure 5.1.1; Figure 5.1.2 shows the old mesh. The reduction is evident: the number of nodes passed from 12064 to 3168 and the number of elements from 53271 to 1988. However, this strong reduction caused a large number of details to be neglected: Figure 5.1.3 and Figure 5.1.4 show the different representation of the cavities hosting the internal rods of the frame. This issue causes the mass of the part to rise, so to maintain a good correlation with the real object, its density has been set to 1853 kg/m^3, in order to get the same mass as the previous model, which is supposed to be very similar to the actual piece.

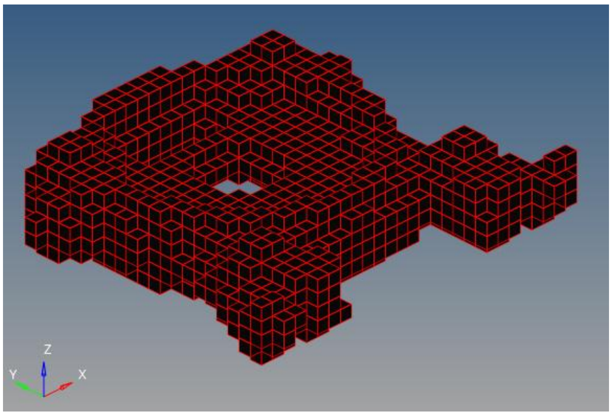

Figure 5.1.1 – New mesh.

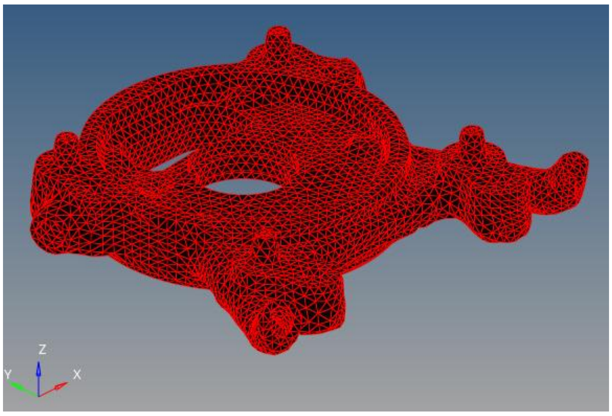

Figure 5.1.2 – Old mesh.

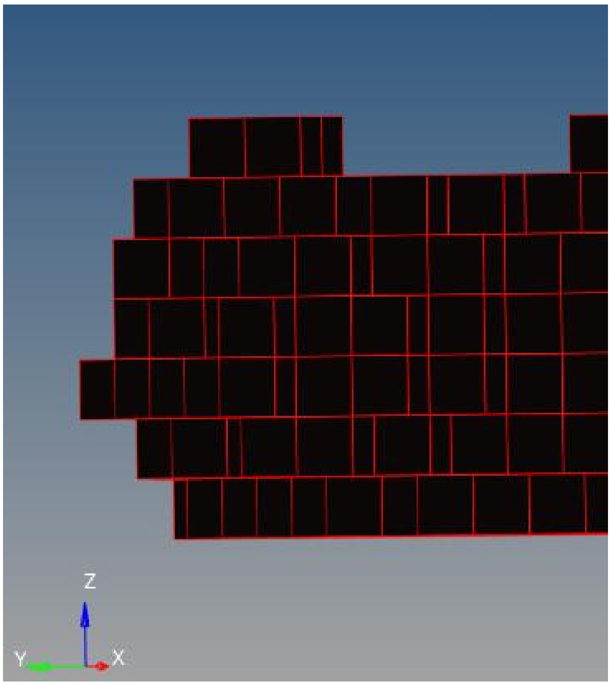

Figure 5.1.3 – Absence of cavities.

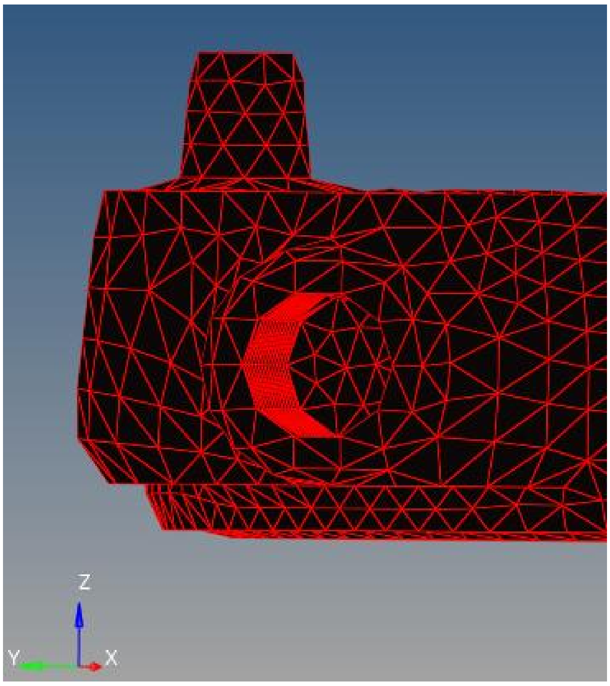

Figure 5.1.4 – Cavity hosting internal frames.

5.2 Rubber layer rebuilding

The Rubber layer has been remodelled using 8 mm hexahedrons. The dimension of the elements has been kept the same as the starting model, nevertheless a good reduction in the number of nodes and elements has been achieved: they passed from 17538 nodes and 76568 elements to respectively 13727 and 8915. Again, this process has caused the loss of details and cavities, so a new value of density has been set, in order to reach the real mass, to 353.5 kg/m^3. Figure 5.2.1 reports the new mesh and Figure 5.2.2 the old one.

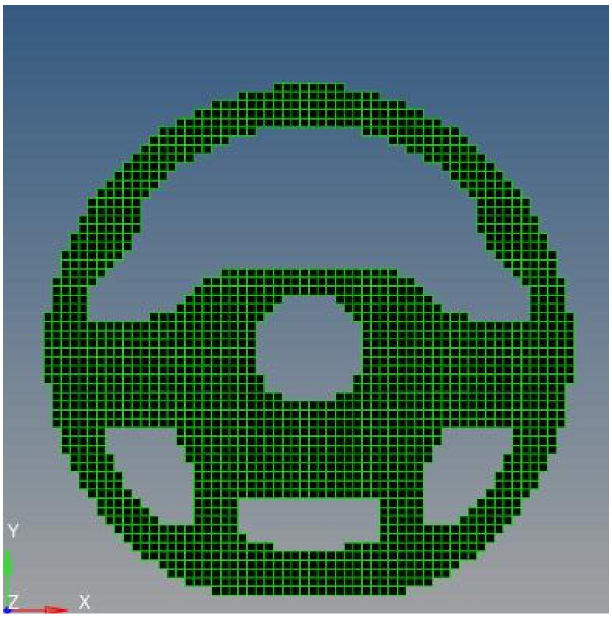

Figure 5.2.1 – New mesh.

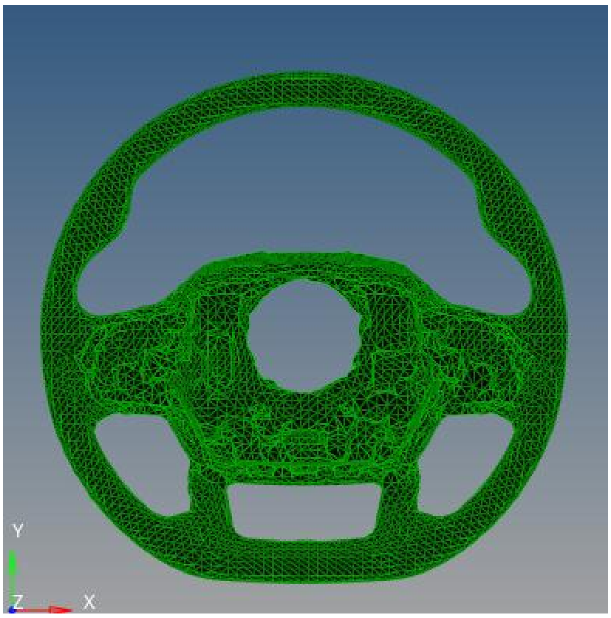

Figure 5.2.2 – Old mesh.

5.3 New model without Rubber layer

As done before, a model without the Rubber layer has been created, starting from the previous one. The whole Frame has been maintained the same, including the Supports; the central part has been substituted with the new one and all the rigid elements connecting it to the Frame have been deleted. Then, through the TCL script developed for connecting the Rubber to the Frame, the Central part has been linked to the Frame. The distance set as tolerance is 5 mm, the dimension of an hexahedral element. The connection between Central part nodes and the Shaft seating has been remodelled too, by RBE2s, created using the same TCL script as before and setting a tolerance of 16 mm. Figure 5.3.1 reports the new model. Table 5.3.1 resumes the main characteristic of the new part of the model.

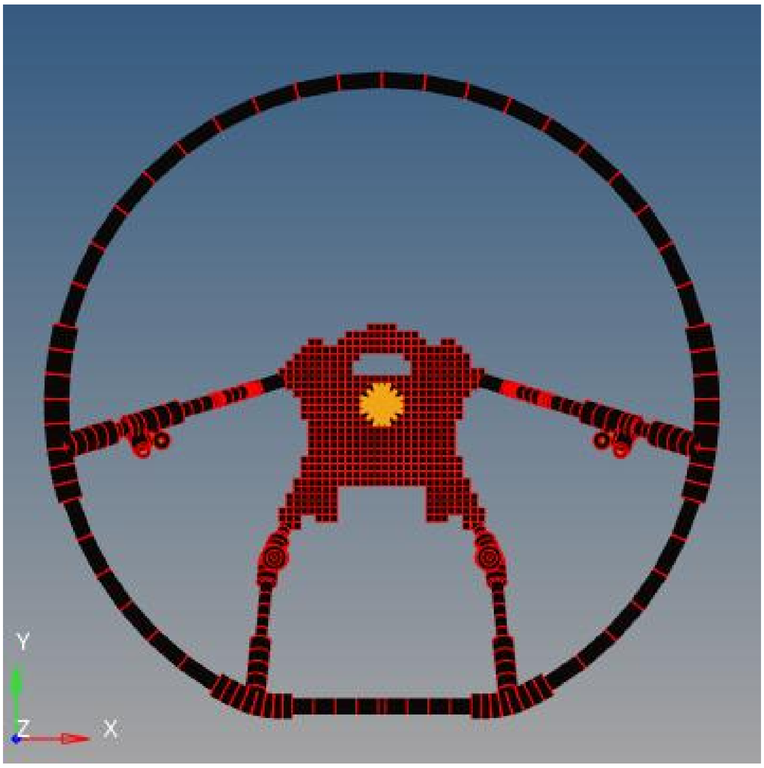

Figure 5.3.1 – New model without Rubber, real 1D elements dimensions view.

Table 5.3.1 – New model main characteristics changes.

	Old Central part	New Central part
Number of nodes	12064	3168
Number of elements	53271	1988
Real density [kg/m^3]	2790	2790
Real weight [kg]	0.460	0.693
Adjusted density [kg/m^3]	-	1853
New weight [kg]	-	0.460

5.4 New model with Rubber layer

The new model has been built starting from the old one. For first, the Central part and the Rubber layer have been deleted with their rigid elements. Then, the new parts have been imported. The linking process has been done in two times: for first, the Central part has been connected to the frame by RBE2s elements with a tolerance of 5 mm; successively the Rubber has been connected to the Frame, the Supports and the Central part by RBE2s elements with a tolerance of 8 mm. In the end, a dependency check has been run, in order to avoid multiple master relationships between nodes, as the TCL script does not consider any relation between nodes that existed before its run. Figure 5.4.1 shows the new model. Table 5.4.1 resumes the main characteristics of the new parts.

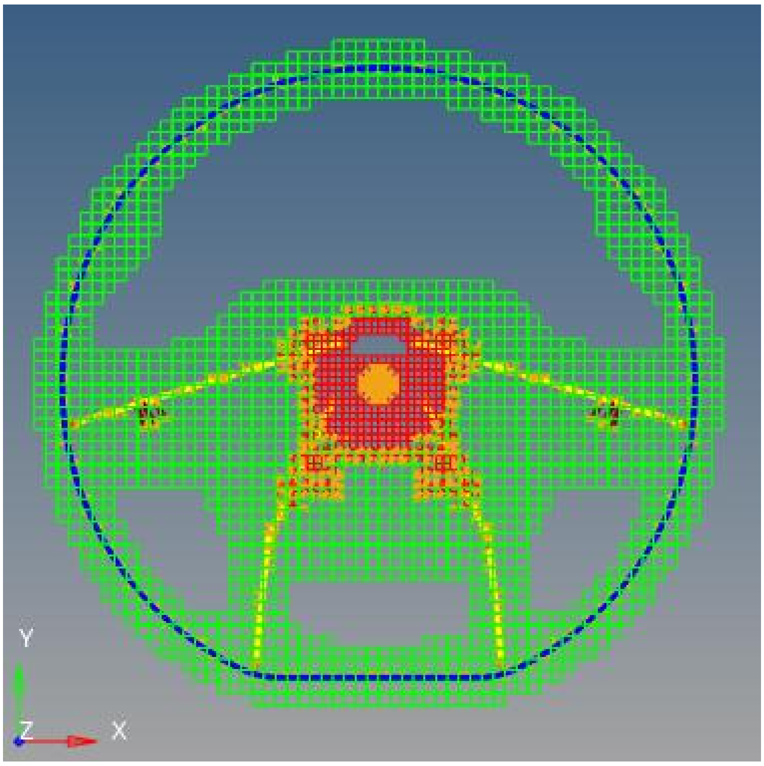

Figure 5.4.1 – New model with Rubber.

Table 5.4.1 – New parts main characteristics.

	Old Central part	**New Central part**	**Old Rubber layer**	**New Rubber layer**
Number of nodes	12064	3168	17538	13727
Number of elements	53271	1988	76568	8915
Real density [kg/m^3]	2790	2790	434	434
Real weight [kg]	0.460	0.693	1.614	1.981
Adjusted density [kg/m^3]	-	1853	-	353.5
New weight [kg]	-	0.460	-	1.614

5.5 Models comparison

The four models are now compared. The number of nodes, elements and degrees of freedom are reported in Table 5.5.1. The strong reduction introduced with the new meshing technique is evident:

the number of nodes has reached a decrement of 62% for the model without the Rubber, while the number of elements has been reduced of about 95%; for the model with Rubber the decrement has been lower in both nodes and elements, just 43% and 90% respectively. The effects due to this strong reduction are visible in Table 5.5.2, that resumes the times taken by the machine to run a modal analysis by Optistruct.

Table 5.5.1 – Main characteristic of models.

	Tetrahedral w/out Rubber	**Tetrahedral with Rubber**	**Hexahedral w/out Rubber**	**Hexahedral with Rubber**
# of nodes	12400	29970	3504	17263
# of elements	53719	131489	2573	13317
# of dofs	39420	96645	12042	60174

Table 5.5.2 – Computational time of the four models comparison.

	Tetrahedral w/out Rubber	**Tetrahedral with Rubber**	**Hexahedral w/out Rubber**	**Hexahedral with Rubber**
Time [mm:ss]	00:32	01:41	00:08	01:14

The computational time results strongly lowered for the new models: a reduction of 75% has been achieved for the model without Rubber, making the analysis immediate.

6. Modal analysis

A modal analysis has been run in Optistruct and Lupos. This choice has the double purpose of checking the models and verifying the reliability of Lupos updates. The results are reported in the following paragraphs, putting beside the new models described in the previous chapter with the two models characterized by tetrahedral mesh. Reporting both frequencies and shapes, an accurate comparison is done, pointing out differences and similarities.

6.1 Modal analysis by Optistruct

The modal analysis run for this models are meant to evaluate the first ten structural modes. Although the frequencies under investigation for the whole column are lower, it is important, in order to have a good correlation of the model, to study a quite large number of modes, at least for the wheel, as it is the interface with the user.

6.1.1 Model without Rubber

For first, the model without Rubber has been analyzed. Table 6.1.1.1 resumes the results obtained for both the models without Rubber, comparing the effect of the different mesh solid elements. Only the first ten modes are reported.

Table 6.1.1.1 – Optistruct modal analysis results for models without Rubber.

Tetrahedral mesh model		**Hexahedral mesh model**	
Mode #	Frequency [Hz]	Mode #	Frequency [Hz]
1	44.87	1	45.80
2	46.22	2	46.22
3	67.57	3	68.30
4	68.02	4	69.98
5	109.0	5	109.4
6	114.9	6	116.4
7	150.4	7	150.3
8	277.0	8	278.2
9	281.2	9	280.0
10	296.8	10	296.7

It is important to notice that the modes reported in Table 6.1.1.1 are very similar for the two models, despite the great difference in number of nodes and degrees of freedom. These results, that obviously have to be compared with the experimental data, open a view on how a strong simplification is possible for modal analysis. From Figure 6.1.1.1 to Figure 6.1.1.10, the first ten modes representation of the two models without the Rubber layer are put aside.

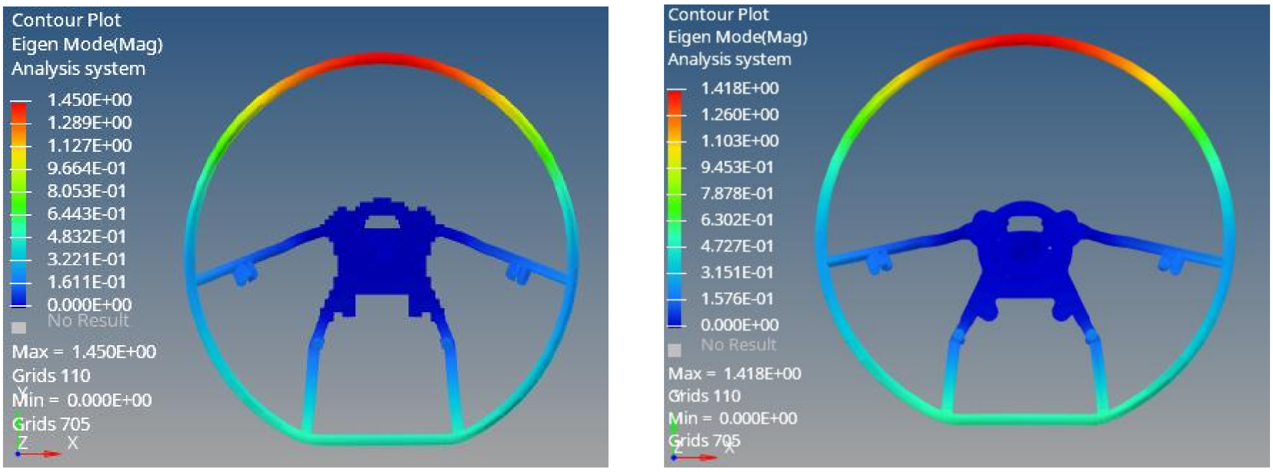

Figure 6.1.1.1 – Models without Rubber, first mode at 45.80 Hz and 44.87 Hz respectively.

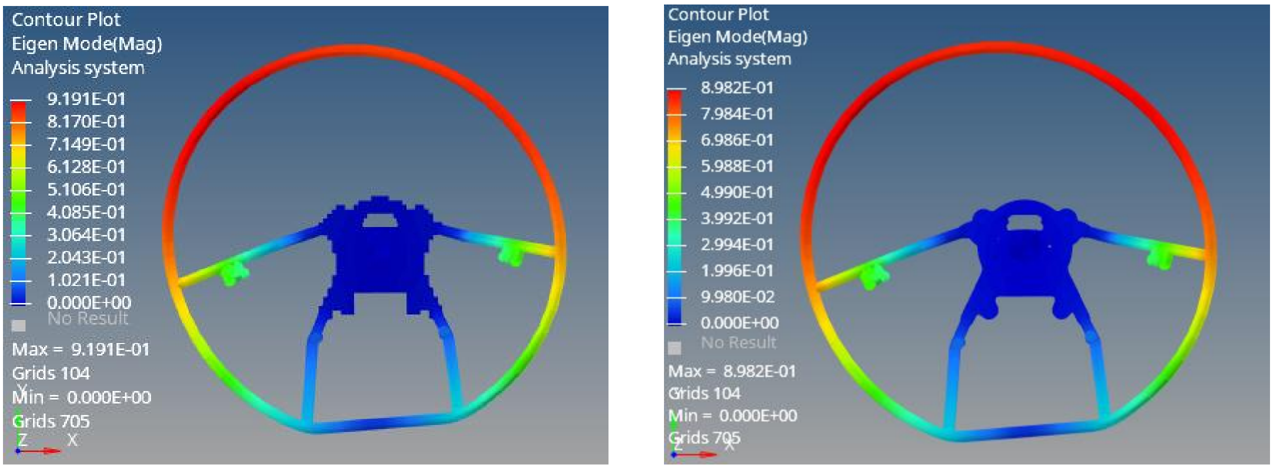

Figure 6.1.1.2 – Models without Rubber, second mode at 46.22 Hz both.

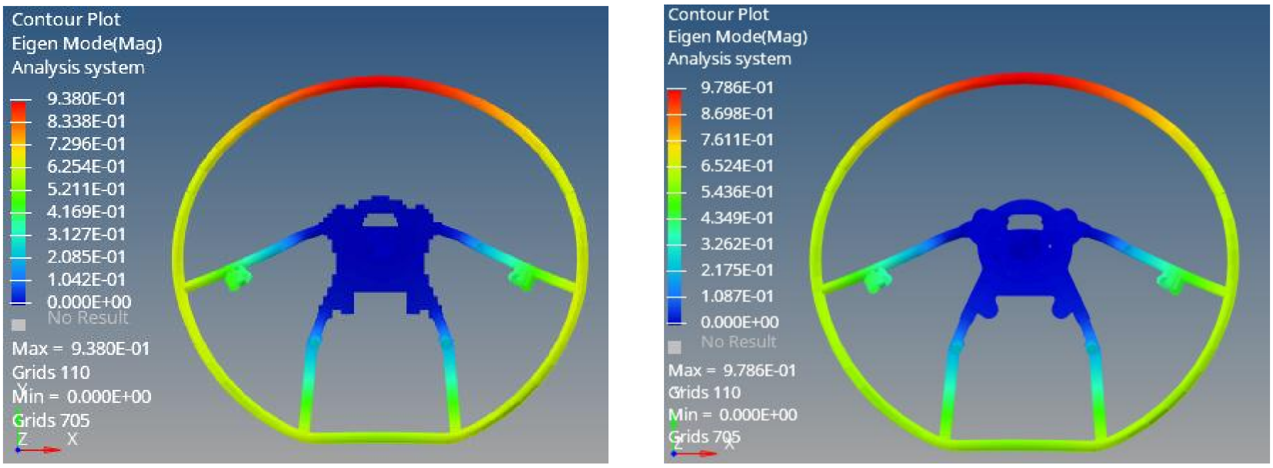

Figure 6.1.1.3 – Models without Rubber, third mode at 68.30 Hz and 67.57 Hz respectively.

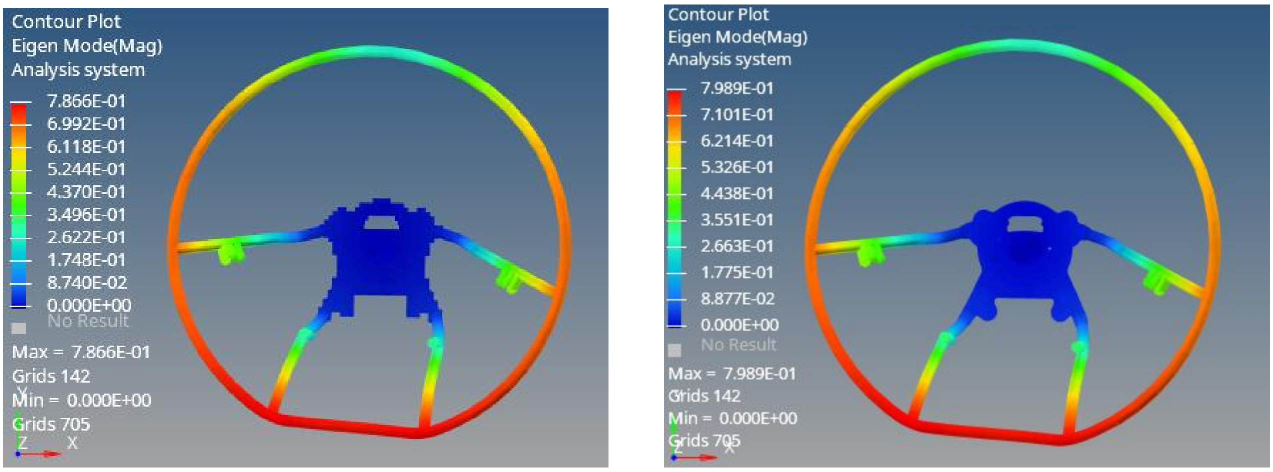

Figure 6.1.1.4 – Models without Rubber, fourth mode at 69.98 Hz and 68.02 Hz respectively.

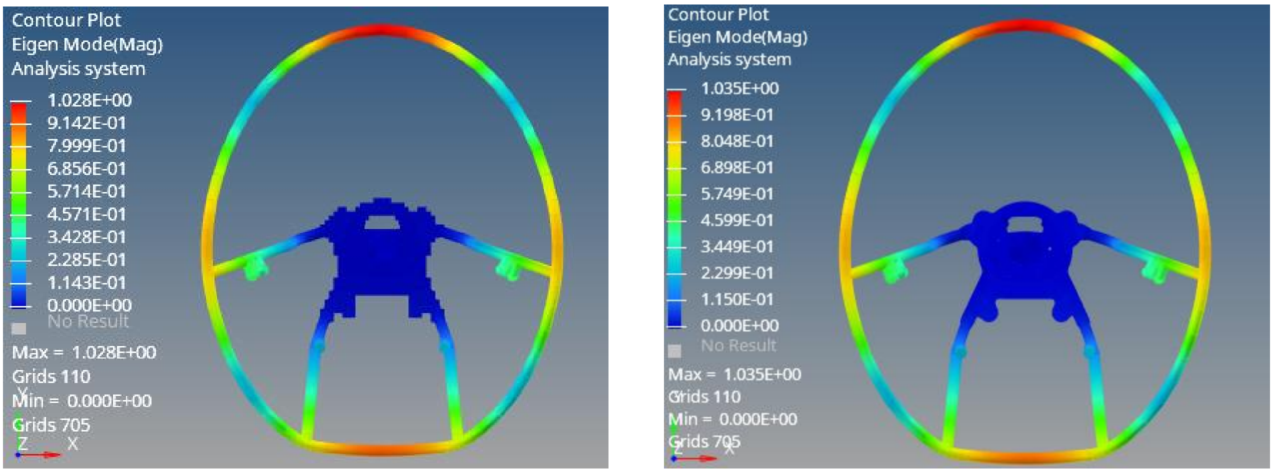

Figure 6.1.1.5 – Models without Rubber, fifth mode at 109.4 Hz and 109.0 Hz respectively.

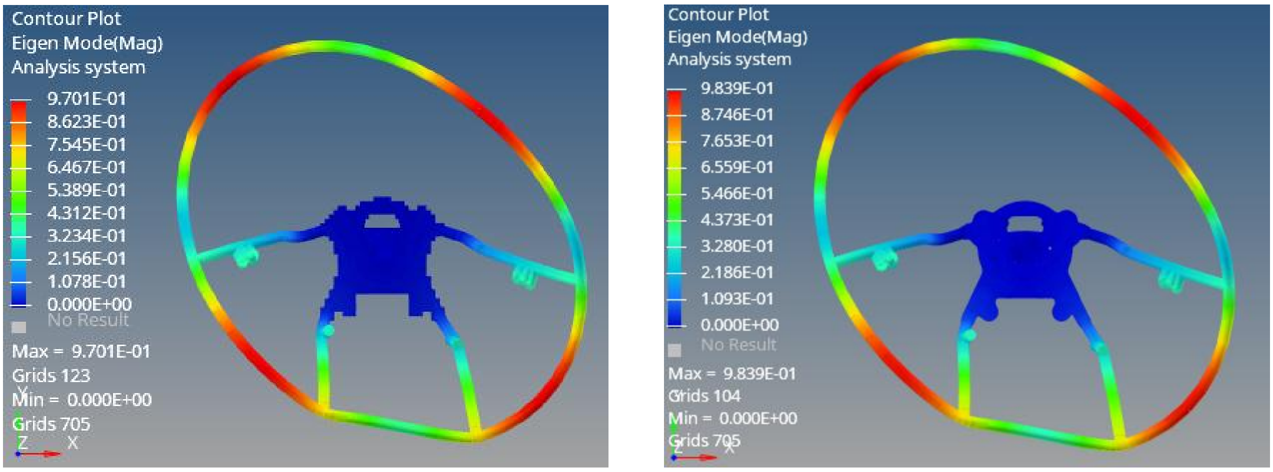

Figure 6.1.1.6 – Models without Rubber, sixth mode at 116.4 Hz and 114.9 Hz respectively.

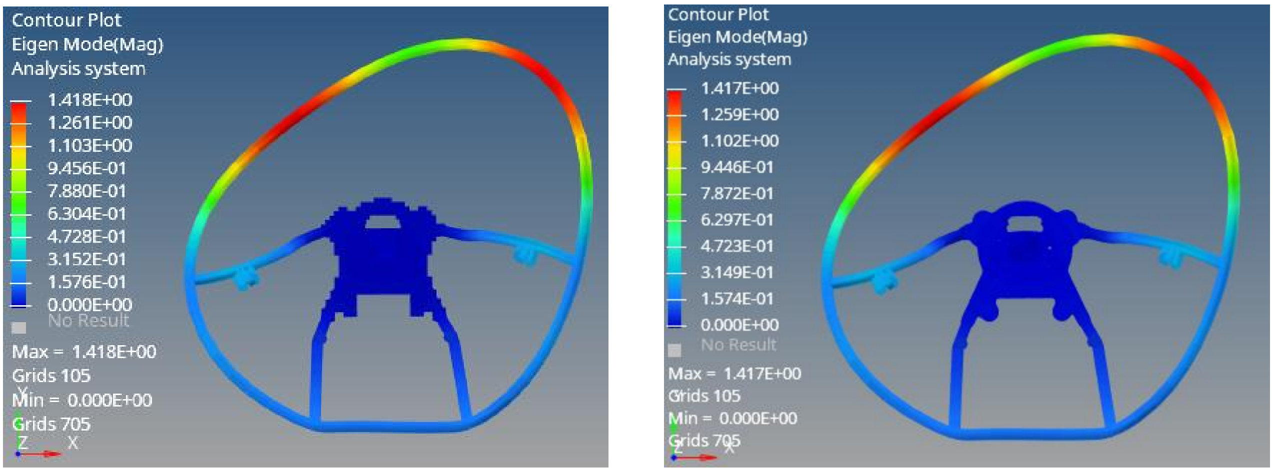

Figure 6.1.1.7 – Models without Rubber, seventh mode at 150.3 Hz and 150.4 Hz respectively.

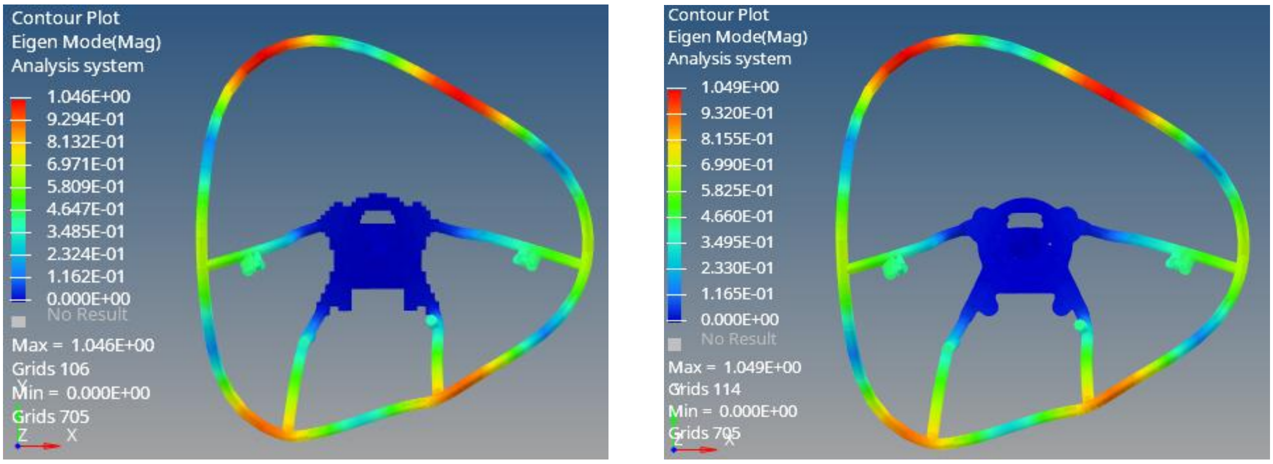

Figure 6.1.1.8 – Models without Rubber, eighth mode at 278.2 Hz and 277.0 Hz respectively.

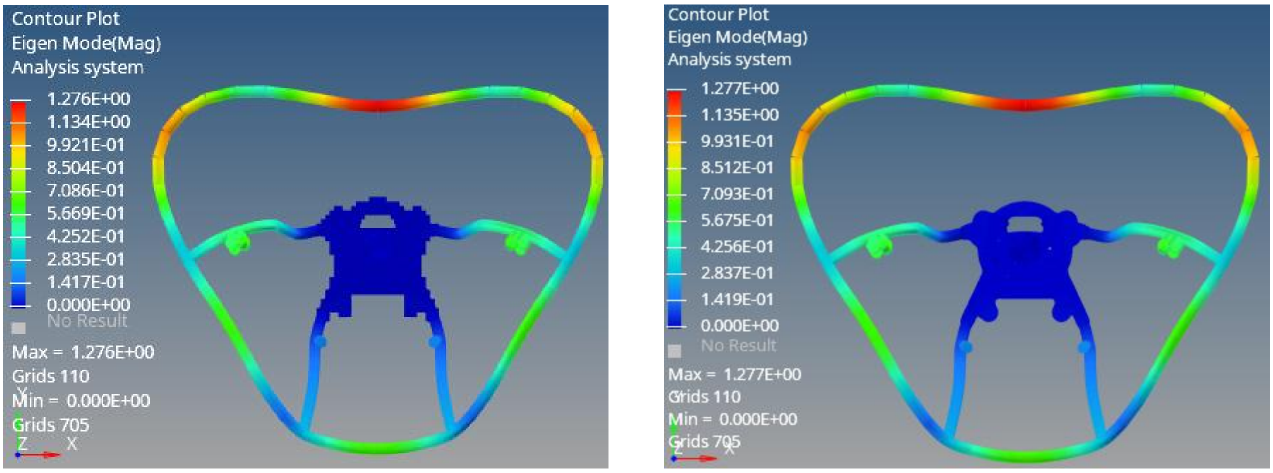

Figure 6.1.1.9 – Models without Rubber, ninth mode at 280.0 Hz and 281.2 Hz respectively.

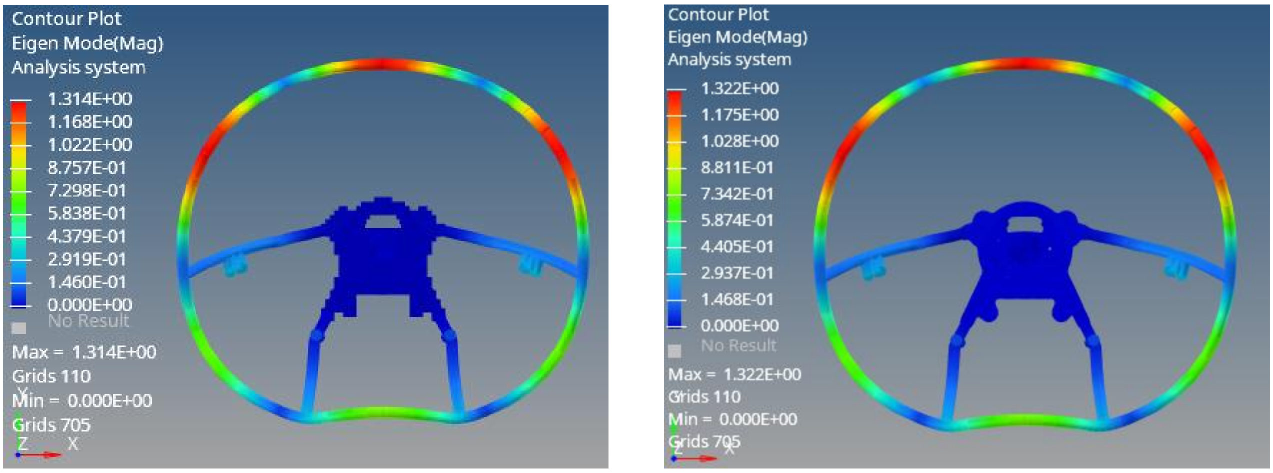

Figure 6.1.1.10 – Models without Rubber, tenth mode at 296.7 Hz and 296.8 Hz respectively.

6.1.2 Model with Rubber

Table 6.1.2.1 resumes the results obtained for the two models with the Rubber; the first ten structural modes are reported, including Rubber modes just by the way. The values of frequency are quite similar, at least for the structural modes; this is just expected, as the structural components and the total masses are the same. Differences are visible for Rubber modes (in Table 6.1.2.1 are reported with a "-" instead of an identification number), as the mesh is quite different in degrees of freedom number and shape.

Table 6.1.2.1 – Optistruct modal analysis results for models with Rubber.

Tetrahedral mesh model		**Hexahedral mesh model**	
Mode #	Frequency [Hz]	Mode #	Frequency [Hz]
1	44.55	1	45.45
2	46.90	2	47.11
3	68.67	3	69.96
4	70.73	4	73.30
5	109.7	5	110.0
6	113.1	6	115.3
7	149.4	-	142.9
-	149.9	7	149.7
-	210.6	-	214.1
-	221.8	-	226.7
-	226.0	-	231.2
-	238.7	-	249.0
-	253.3	-	252.4
8	272.3	8	272.9
9	279.8	9	280.4
-	286.6	-	281.0
-	288.9	-	285.5
10	291.1	10	289.3

As for the previous model, these results show the possibility to simplify the discretization and reduce the number of nodes, leading to shorter computational time, as reported in Table 5.5.2.

Figure 6.1.2.1 to Figure 6.1.2.10 represent the first ten structural modes of the models with the Rubber. They result to be very similar in frequency and shape.

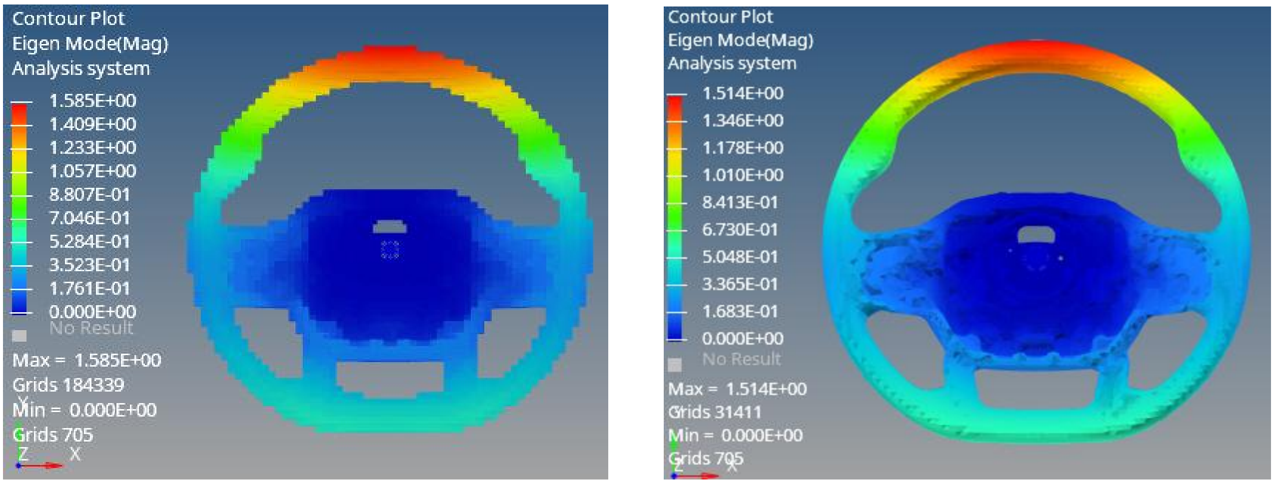

Figure 6.1.2.1 – Models with Rubber, first structural mode at 45.45 Hz and 44.55 Hz respectively.

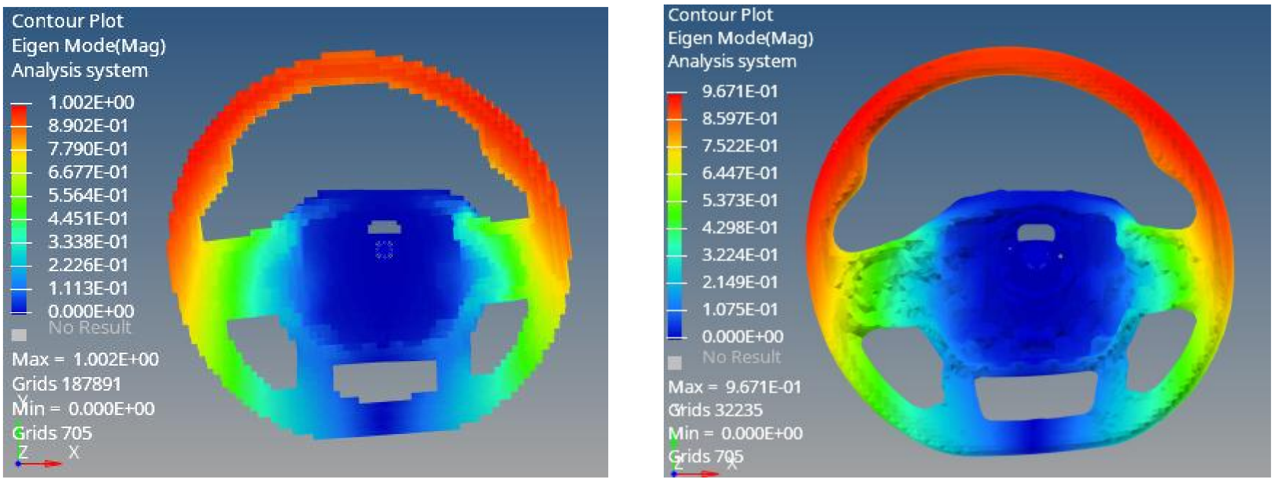

Figure 6.1.2.2 – Models with Rubber, second structural mode at 47.11 Hz and 46.90 Hz respectively.

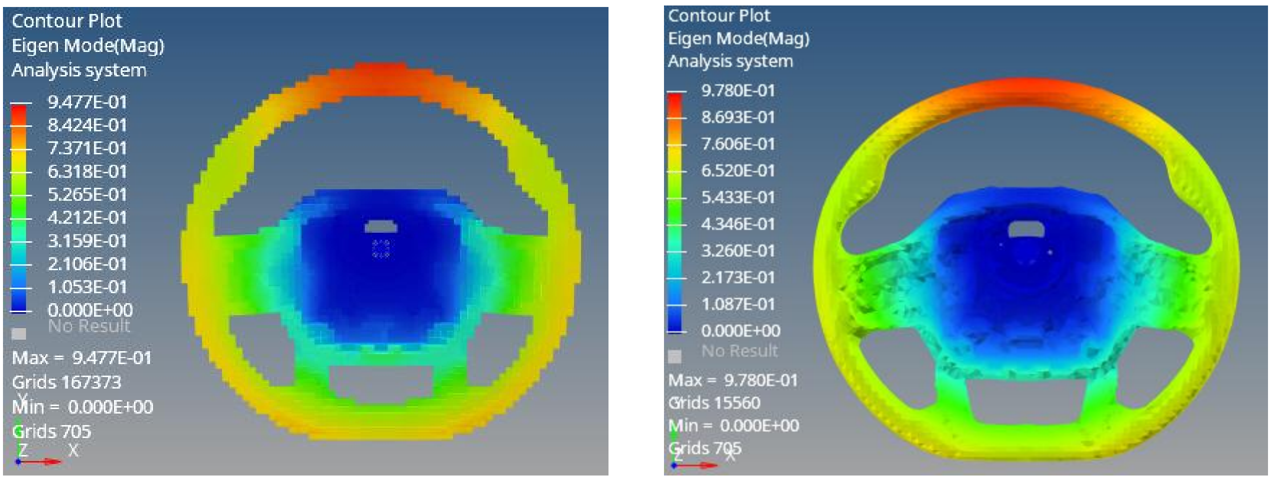

Figure 6.1.2.3 – Models with Rubber, third structural mode at 69.96 Hz and 68.67 Hz respectively.

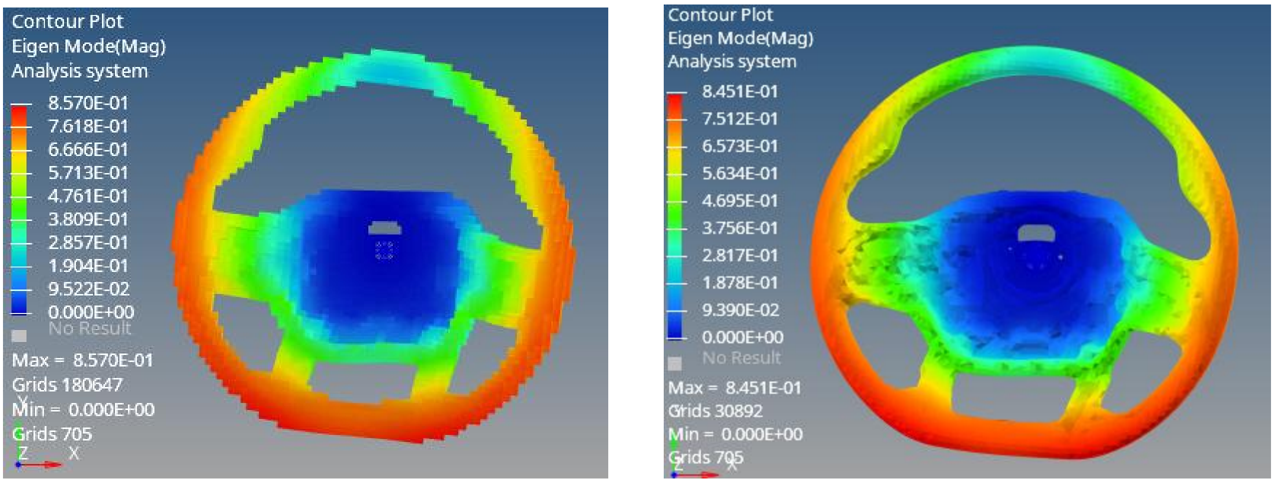

Figure 6.1.2. 4 – Models with Rubber, fourth structural mode at 73.30 Hz and 70.73 Hz respectively.

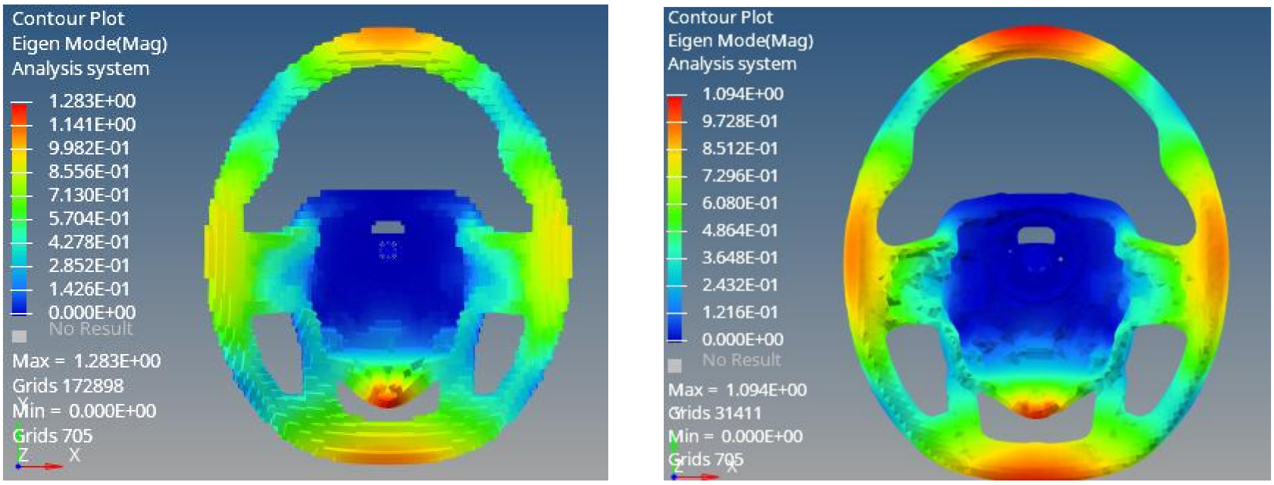

Figure 6.1.2.5 – Models with Rubber, fifth structural mode at 110.0 Hz and 109.7 Hz respectively.

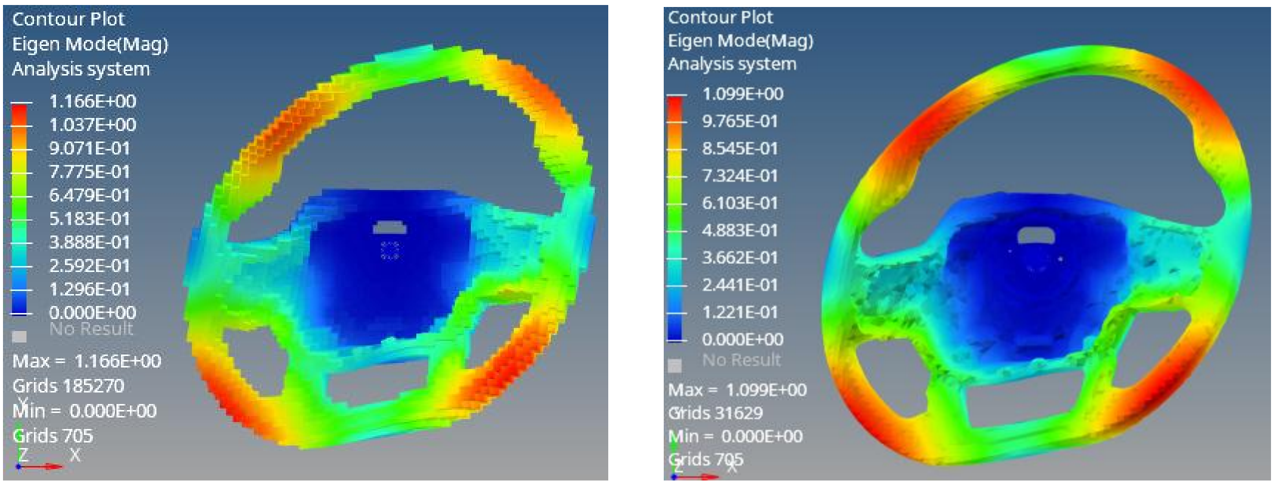

Figure 6.1.2.6 – Models with Rubber, sixth structural mode at 115.3 Hz and 113.1 Hz respectively.

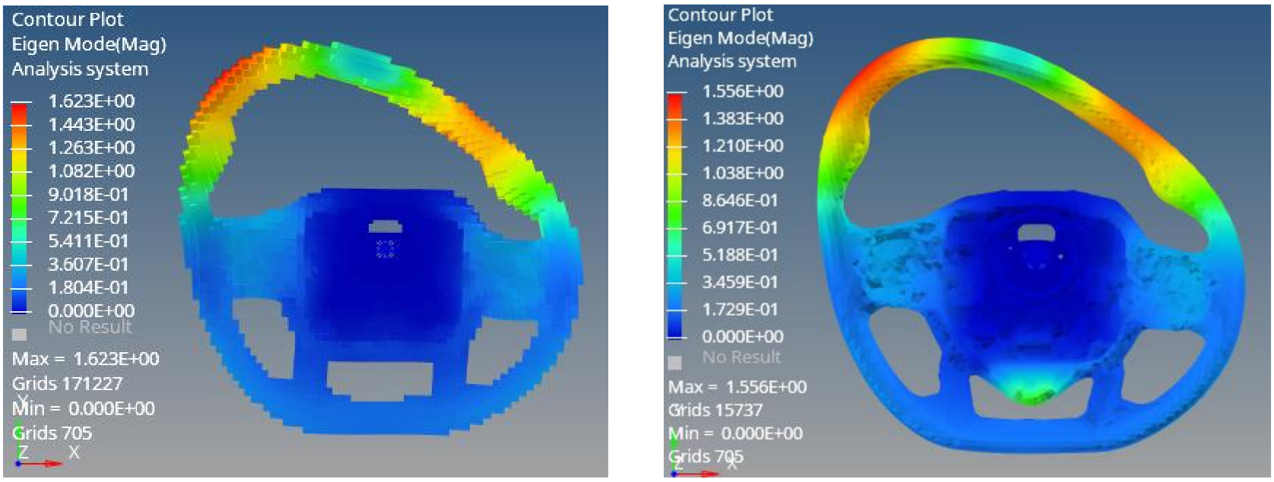

Figure 6.1.2.7 – Models with Rubber, seventh structural mode at 149.7 Hz and 149.4 Hz respectively.

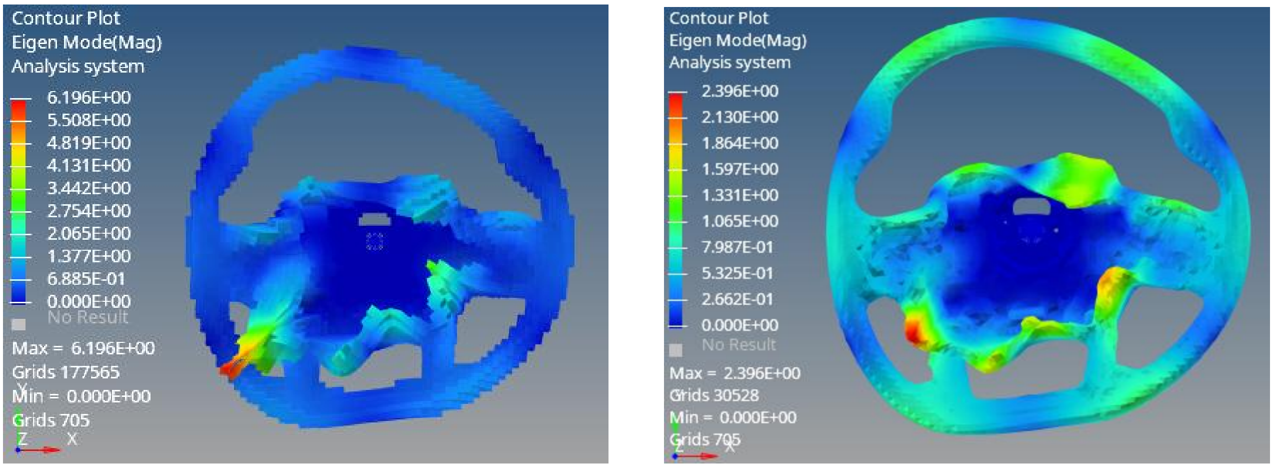

Figure 6.1.2.8 – Models with Rubber, eighth structural mode at 272.9 Hz and 272.3 Hz respectively.

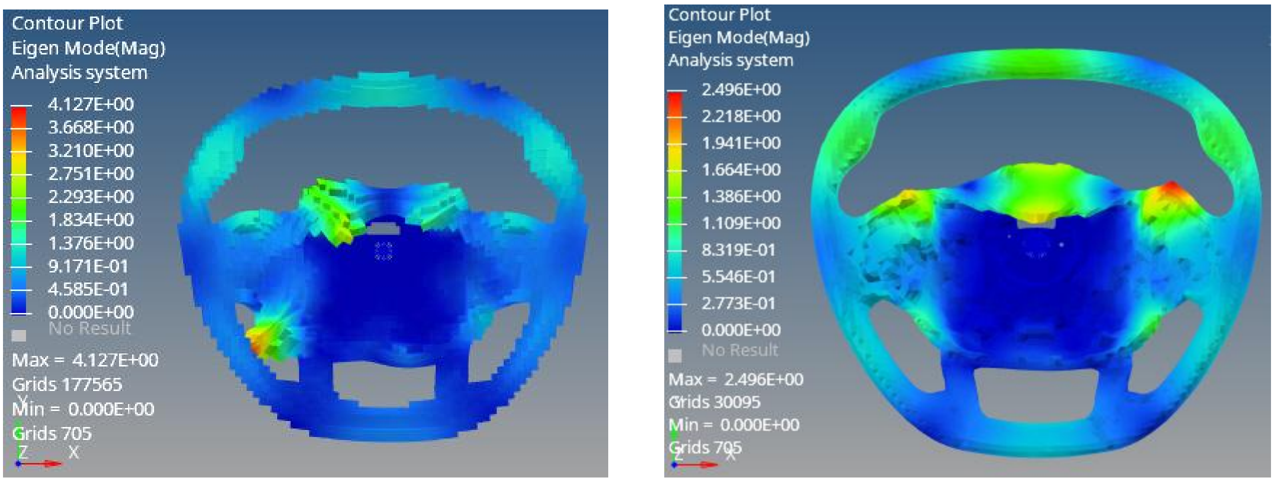

Figure 6.1.2.9 – Models with Rubber, ninth structural mode at 280.4 Hz and 279.8 Hz respectively.

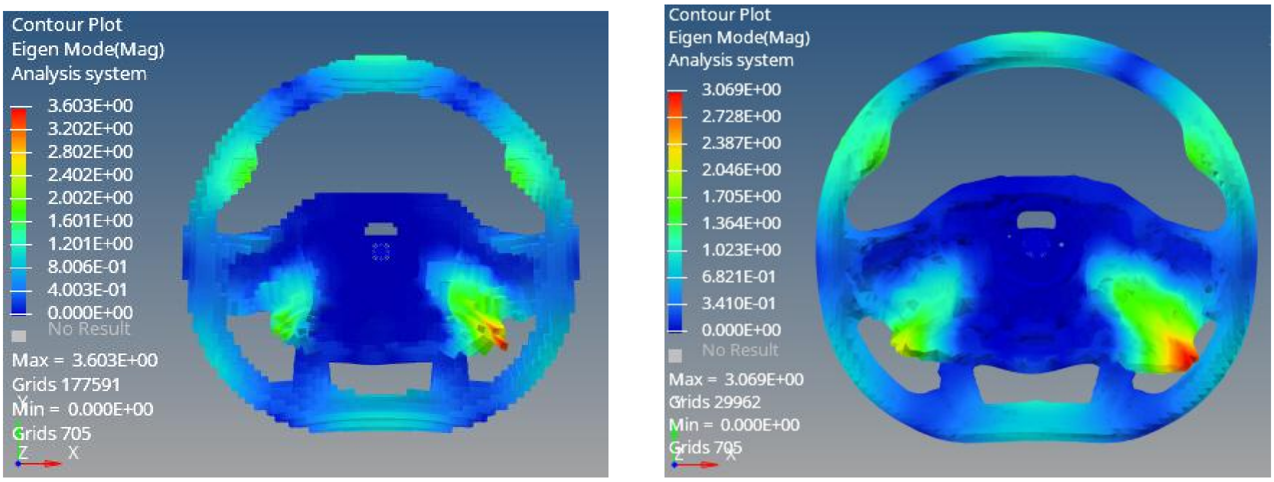

Figure 6.1.2.10 – Models with Rubber, tenth structural mode at 289.3 Hz and 291.1 Hz respectively.

Non-structural modes have not been reported, as they are just the result of numerical calculation and do not have any physical sense, because of the rubber dissipation properties that have not been considered in these analysis. In fact, as the experimental tests will show, these modes cannot be easily visible on the real object, because the rubber layer is very hard to be excited by the test hammer.

6.2 Modal analysis by Lupos

LUPOS [1] is a LUmped Parameters Open Source FEM code written completely in Matlab. It includes a list of useful tools for finite elements numerical analysis, in addition to a solver for several types of analysis. It requires, as input, a Nastran format bulk data file, that is translated to a simpler format. At the moment, this software can run modal analysis of many types of elements, but the only 3D element supported is the hexahedron, so only hexahedral meshed models have been analyzed. Table 6.2.1 reports the time taken by the machine to run the two modal analysis.

Table 6.2.1 – Computational time for modal analysis by Lupos.

	Model without Rubber	**Model with Rubber**
Time [mm:ss]	00:40	07:22

6.2.1 Model without Rubber

For first, the simplest model has been analysed. LUPOS does not support non-structural mass property yet, so in order to keep into account of the mass of the Rubber, the density of each beam element has been modified, adding the previously indicated non-structural mass and reaching a distribution the most similar to the actual one. Table 6.2.1.1 reports the frequencies of modes evaluated during the modal analysis.

Table 6.2.1.1 – Lupos modal analysis results for model without Rubber.

Mode #	Frequency [Hz]
1	43.56
2	50.24
3	67.31
4	70.08
5	109.4
6	114.7
7	148.9
8	266.1
9	278.3
10	296.8

6.2.2 Model with Rubber

The model including a solid mesh modelling the Rubber has been analysed by Lupos. The frequencies obtained as results are reported in Table 6.2.2.1.

Table 6.2.2.1 – Lupos modal analysis results for model with Rubber.

Mode #	Frequency [Hz]
1	49.60
2	56.59
3	72.65
4	80.99
5	117.6
6	122.1
-	142.3
7	151.8
-	219.6
-	229.3
-	233.0
-	256.5
-	259.7
-	277.0
8	277.5
-	285.3
-	290.3
9	292.4

7. Optistruct vs Lupos: results comparison

A comparison of the frequencies and shapes is reported, as follow, pointing out the differences between them.

7.1 Model without Rubber

The results obtained by the two solvers are put aside in Table 7.1.1, which reports the frequencies of the first ten modes.

Table 7.1.1 – Model without Rubber, frequencies comparison.

Optistruct		Lupos	
Mode #	**Frequency [Hz]**	**Mode #**	**Frequency [Hz]**
1	45.80	1	43.56
2	46.22	2	50.24
3	68.30	3	67.31
4	69.98	4	70.08
5	109.4	5	109.4
6	116.4	6	114.7
7	150.3	7	148.9
8	278.2	9	278.3
9	280.0	8	266.1
10	296.7	10	296.8

From Figure 7.1.1 to Figure 7.1.10 the first ten modes representations are reported, for the two softwares solutions comparison.

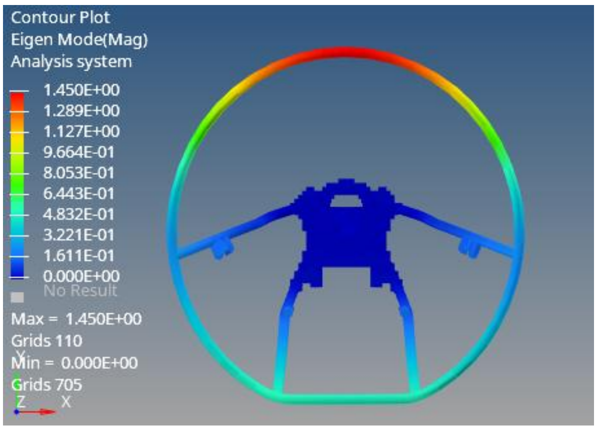

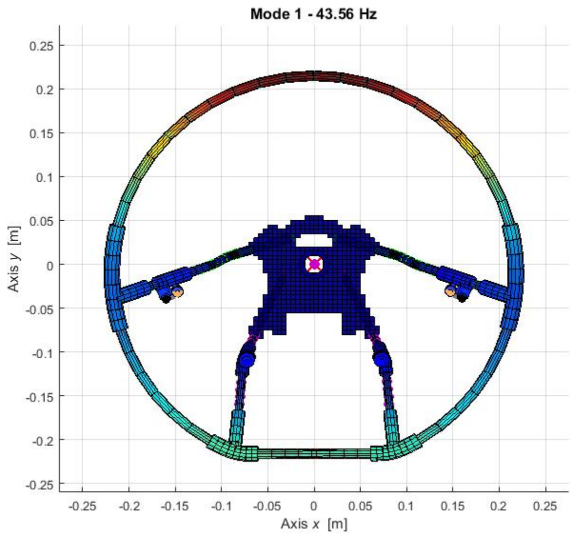

Figure 7.1.1 – Model without Rubber, first mode at 45.80 Hz and 43.56 Hz respectively.

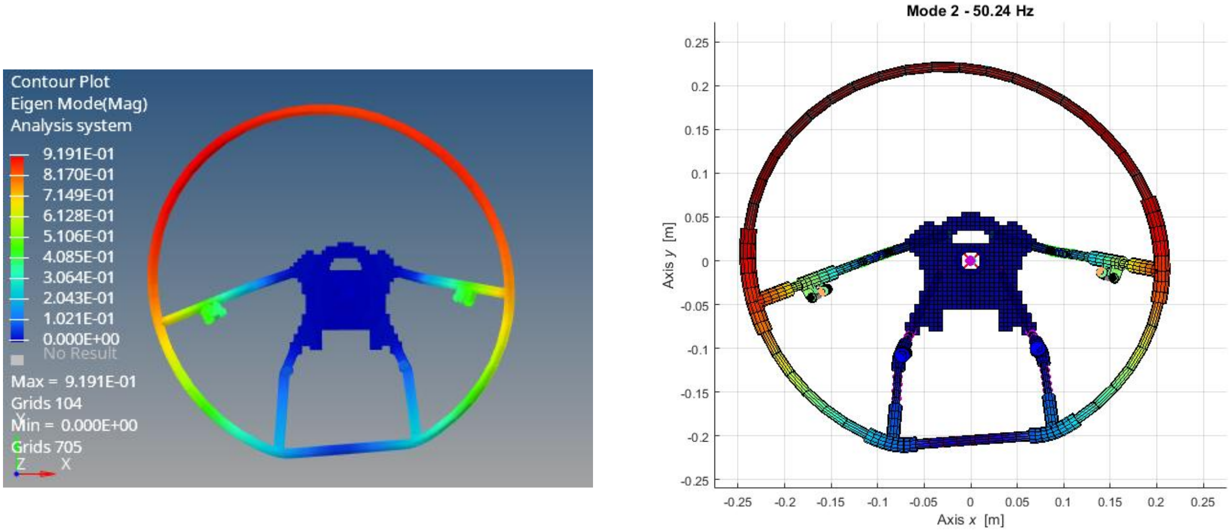

Figure 7.1.2 – Model without Rubber, second mode at 46.22 and 50.24 Hz respectively.

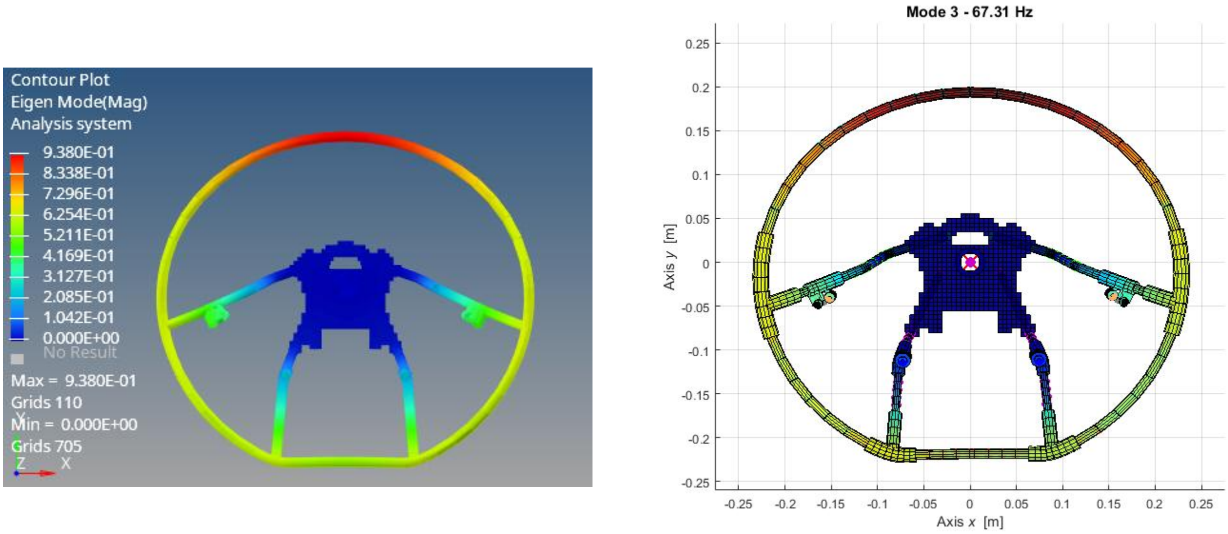

Figure 7.1.3 – Model without Rubber, third mode at 68.30 Hz and 67.31 Hz respectively.

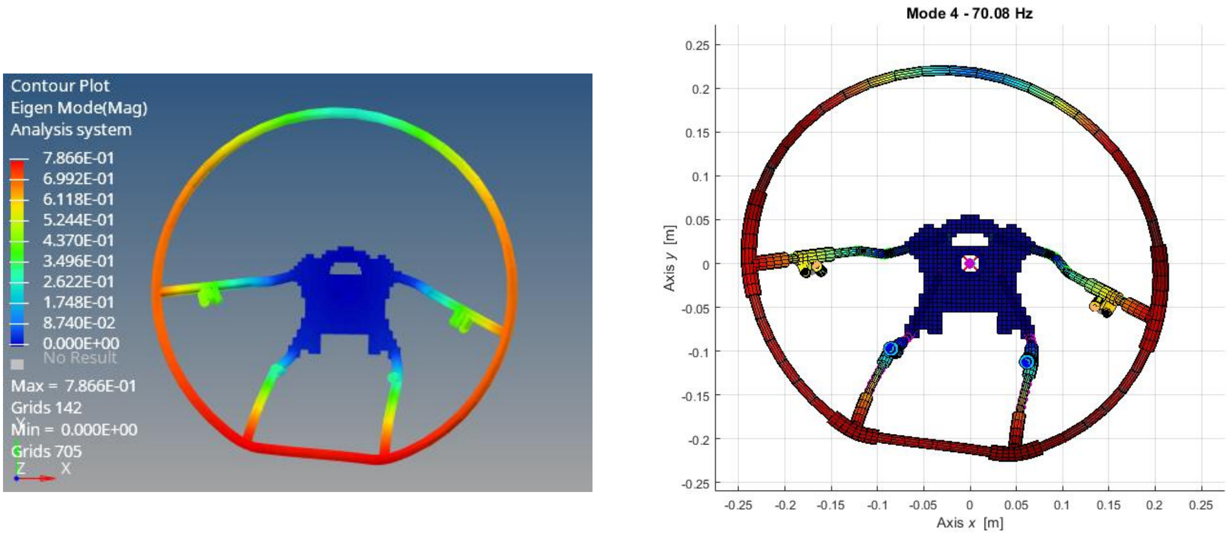

Figure 7.1.4 – Model without Rubber, fourth mode at 69.98 and 70.08 Hz respectively.

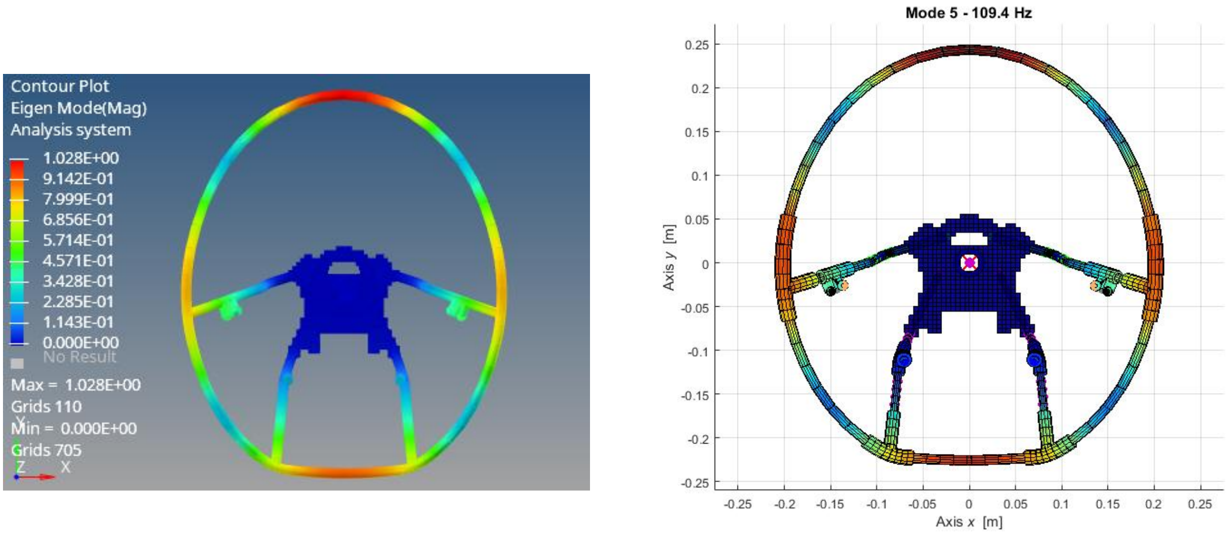

Figure 7.1.5 – Model without Rubber, fifth mode at 109.4 Hz both.

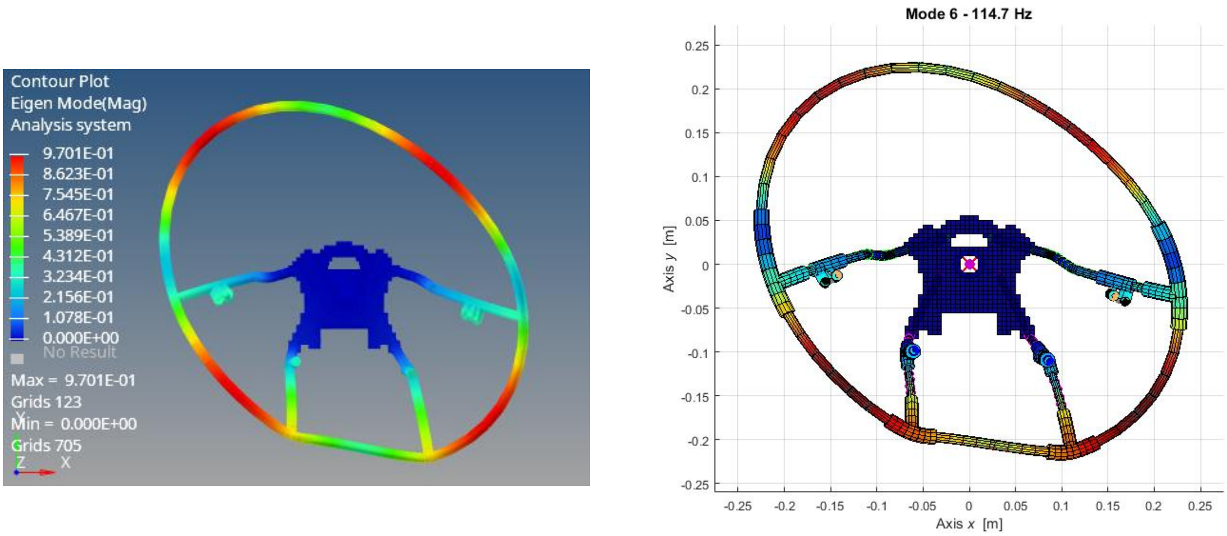

Figure 7.1.6 – Model without Rubber, sixth mode at 116.4 Hz and 114.7 Hz respectively.

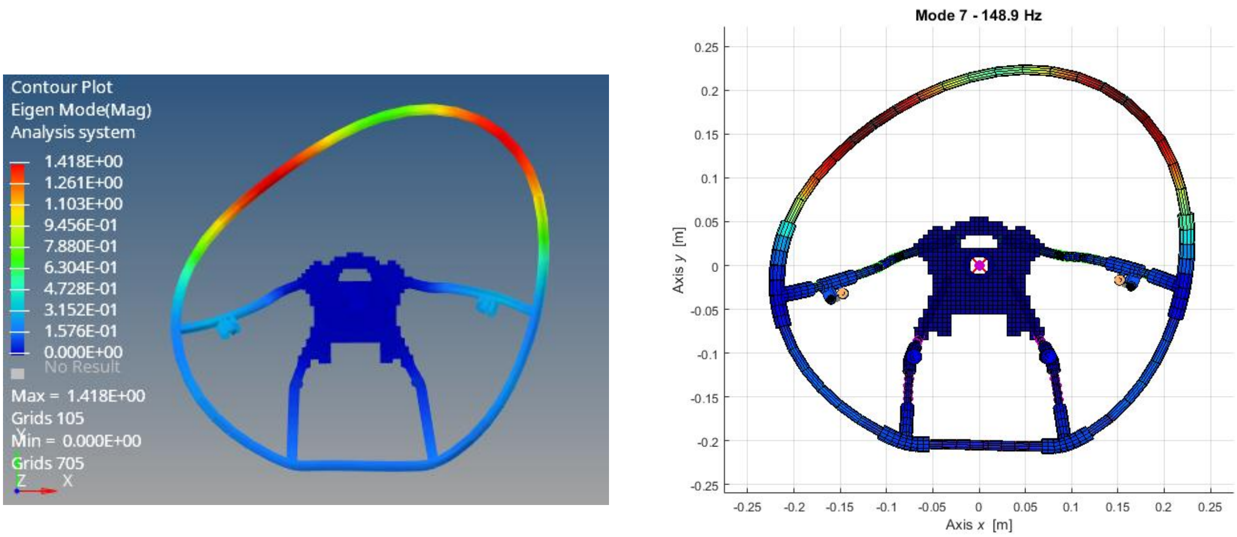

Figure 7.1.7 – Model without Rubber, seventh mode at 150.3 Hz and 148.9 Hz respectively.

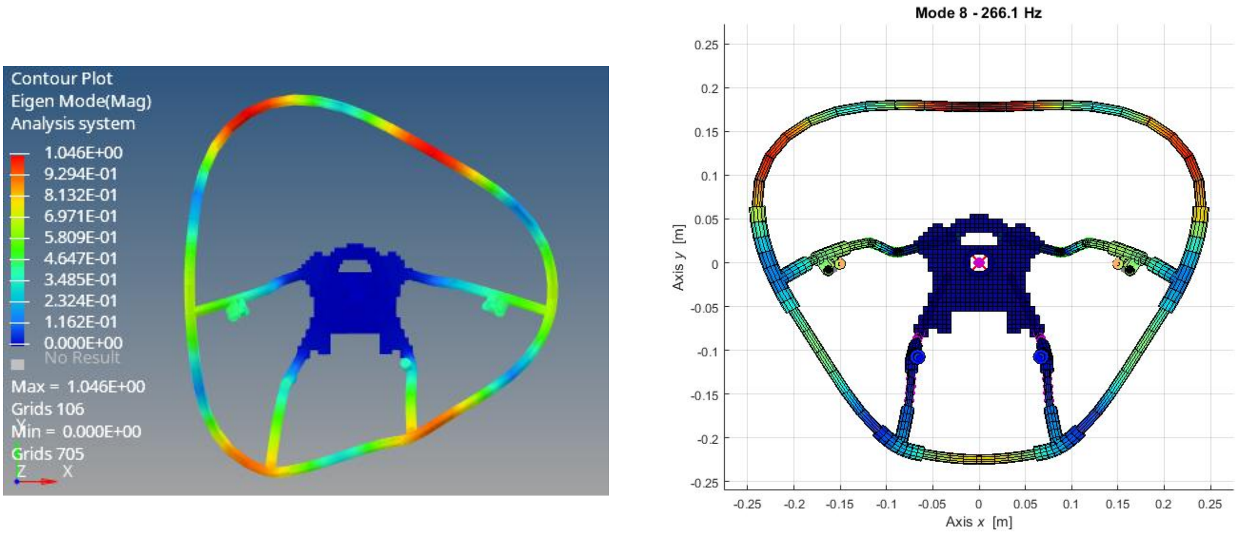

Figure 7.1.8 – Model without Rubber, eighth mode at 278.2 Hz and 266.1 Hz respectively.

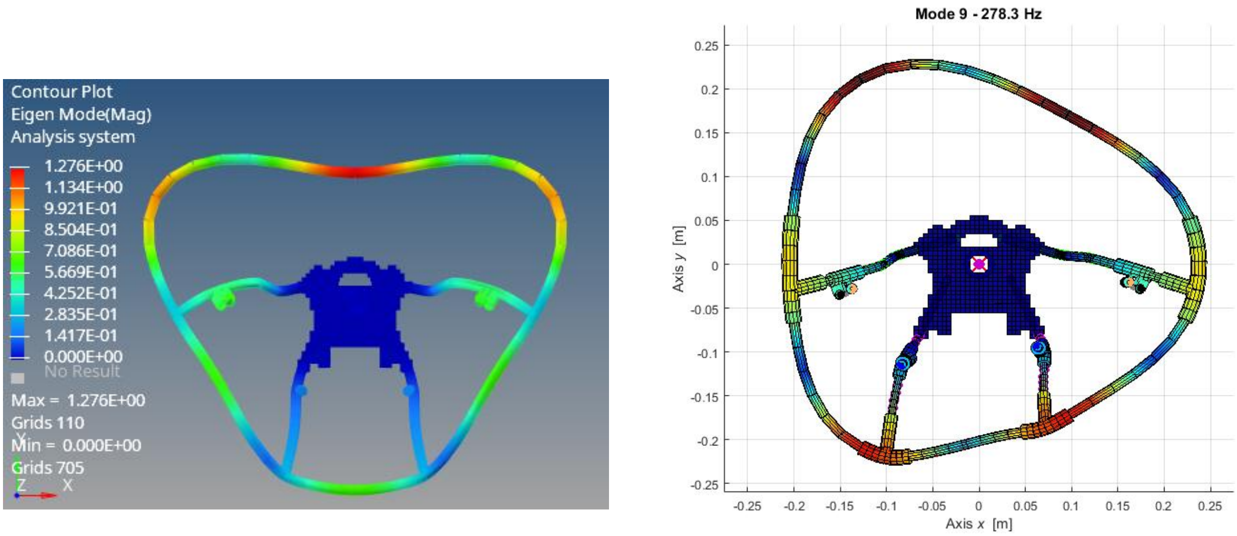

Figure°7.1.9 – Model without Rubber, ninth mode at 280.0 Hz and 278.3 Hz respectively.

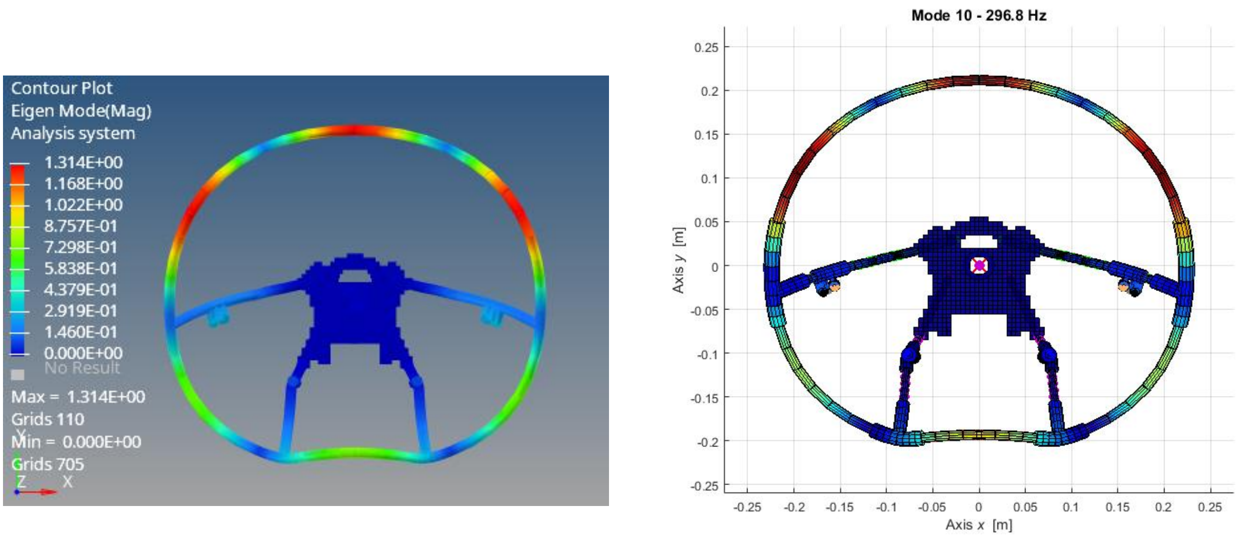

Figure 7.1.10 – Model without Rubber, tenth mode at 296.7 Hz and 296.8 Hz respectively.

As reported in Figure 7.1.8 and Figure 7.1.9 the eighth mode by Lupos correspond to the ninth mode by Optistruct, and vice versa. Moreover, the frequency of the ninth mode by Lupos is very near to the eighth mode one by Optistruct: this suggests that the two modes are found in the same way by the two softwares, while the mode at 280.0 Hz by Optistruct is found by Lupos at the lower frequency of 266.1 Hz.

7.2 Model with Rubber

The results obtained by the two solvers for the model with Rubber are compared in Table 7.2. A noticeable difference between the two series of values led to a deep analysis of the model, but any error has been found, so the discrepancy has been ascribed to the different methods in executing the calculation by the two softwares.

Table 7.2.1 – Model with Rubber, frequencies comparison.

Optistruct		**Lupos**	
Mode #	**Frequency [Hz]**	**Mode #**	**Frequency [Hz]**
1	45.45	1	49.60
2	47.11	2	56.59
3	69.96	3	72.65
4	73.30	4	80.99
5	110.0	5	117.6
6	115.3	6	122.1
-	142.9	-	142.3
7	149.7	7	151.8
-	214.1	-	219.6
-	226.7	-	229.3
-	231.2	-	233.0
-	249.0	-	256.5
-	252.4	-	259.7
8	272.9	-	277.0
9	280.4	8	277.5
-	281.0	-	285.3
-	285.5	-	290.3
10	289.3	9	292.4

From Figure 7.2.1 to Figure 7.2.10 the first ten modes representations are reported, for the two softwares solutions comparison.

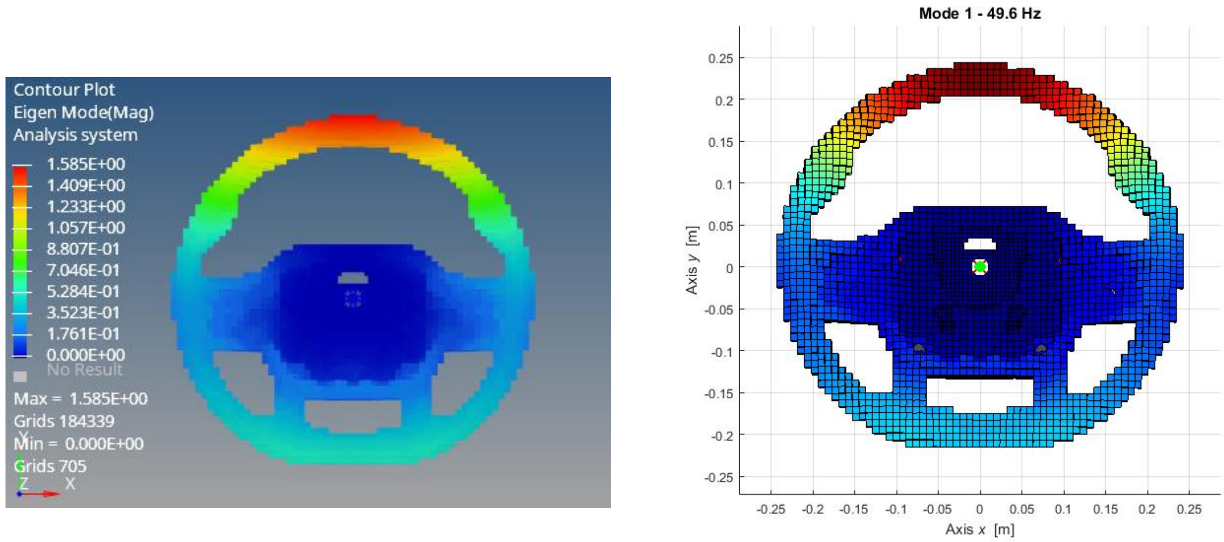

Figure 7.2.1 – Model with Rubber, first structural mode at 45.45 Hz and 49.60 Hz respectively.

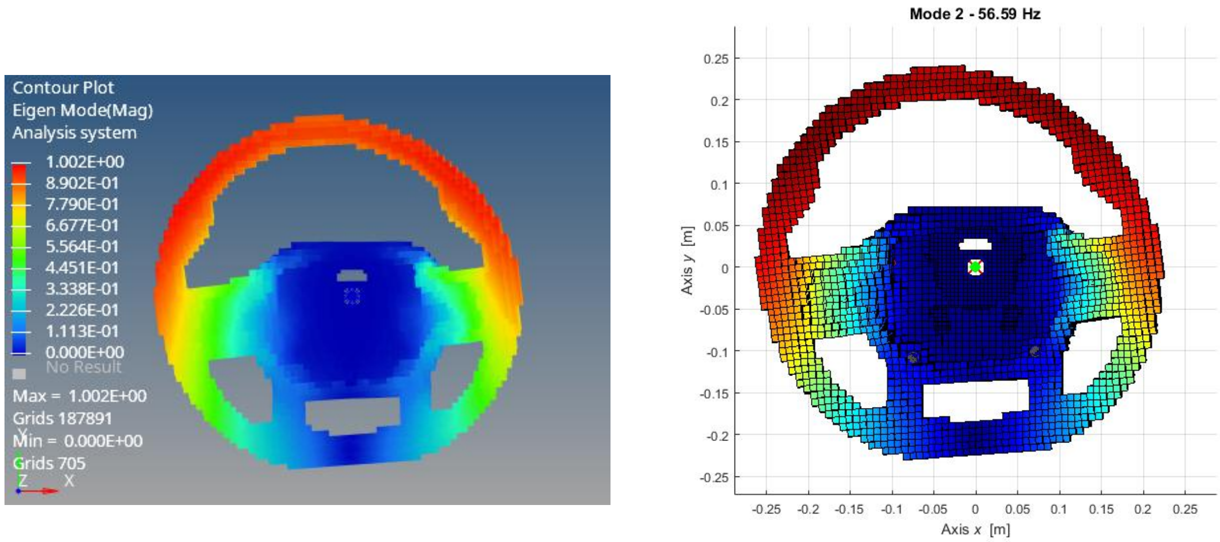

Figure 7.2.2 – Model with Rubber, second structural mode at 47.11 Hz and 56.59 Hz respectively.

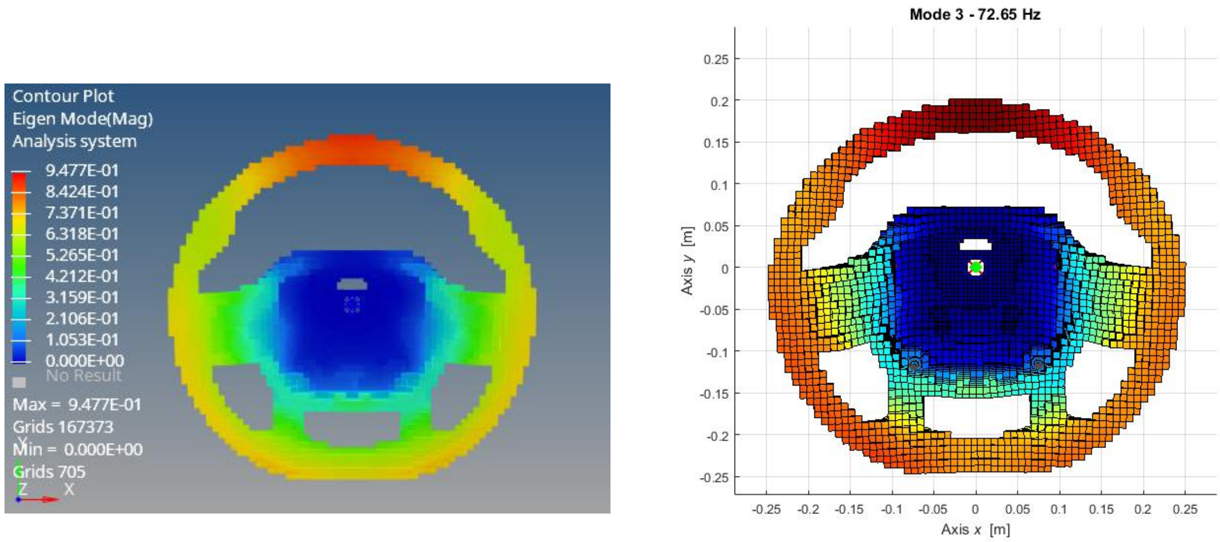

Figure 7.2.3 – Model with Rubber, third structural mode at 69.96 Hz and 72.65 Hz respectively.

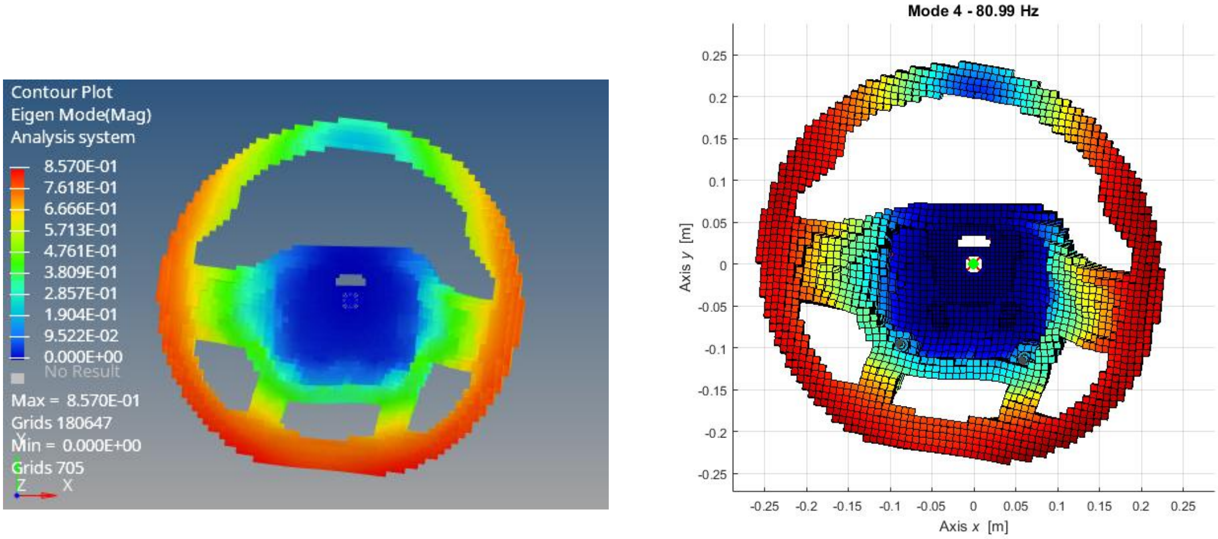

Figure 7.2.4 – Model with Rubber, fourth structural mode at 73.30 Hz and 80.99 Hz respectively.

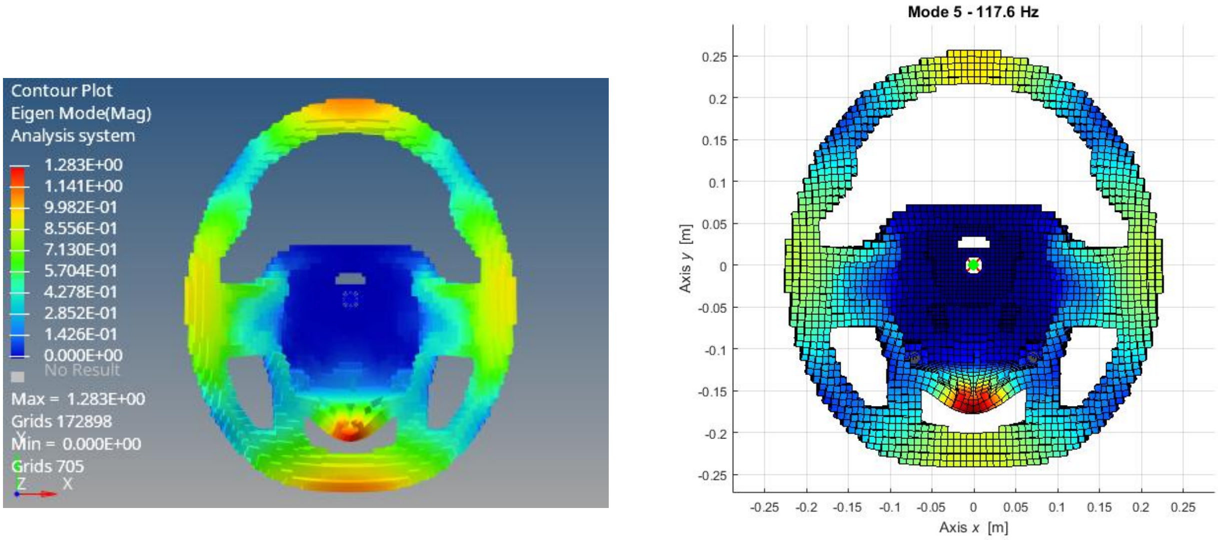

Figure 7.2.5 – Model with Rubber, fifth structural mode at 110.0 Hz and 117.6 Hz respectively.

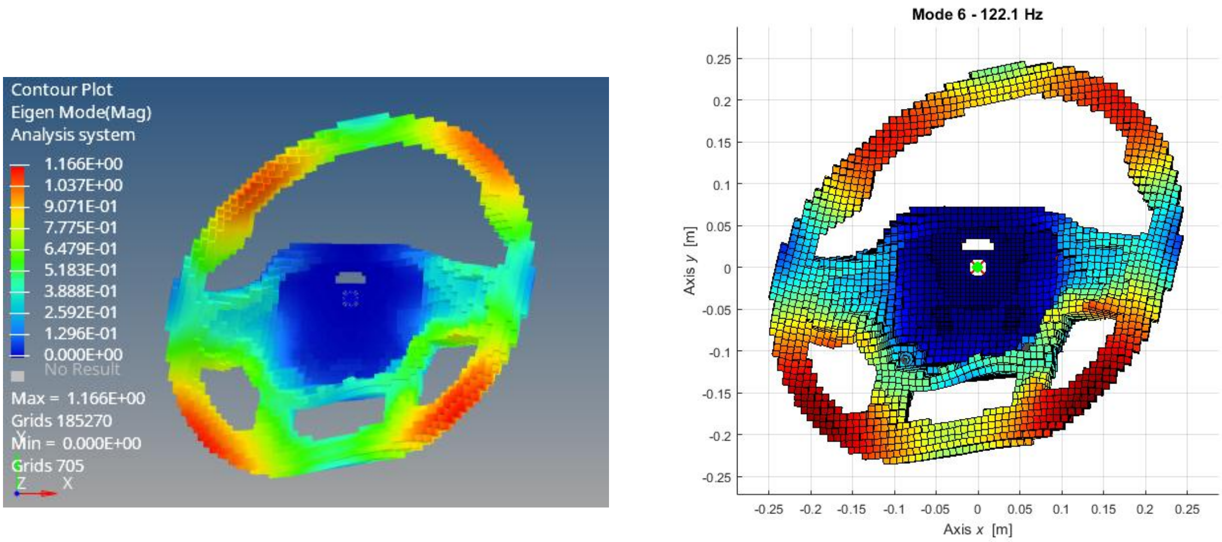

Figure 7.2.6 – Model with Rubber, sixth structural mode at 115.3 Hz and 122.1 Hz respectively.

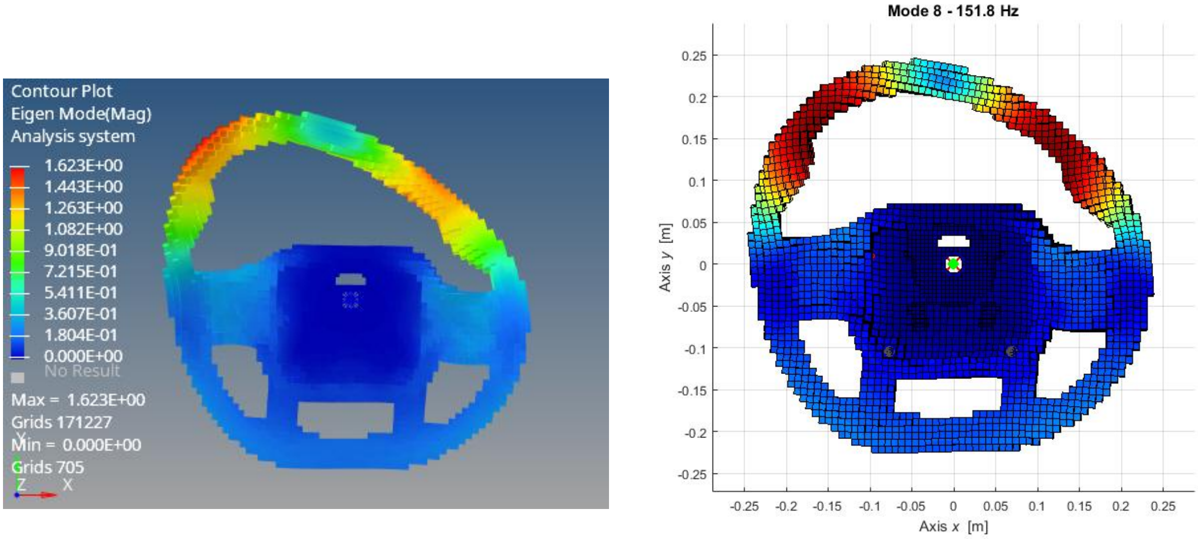

Figure 7.2.7 – Model with Rubber, seventh structural mode at 149.7 Hz and 151.8 Hz respectively.

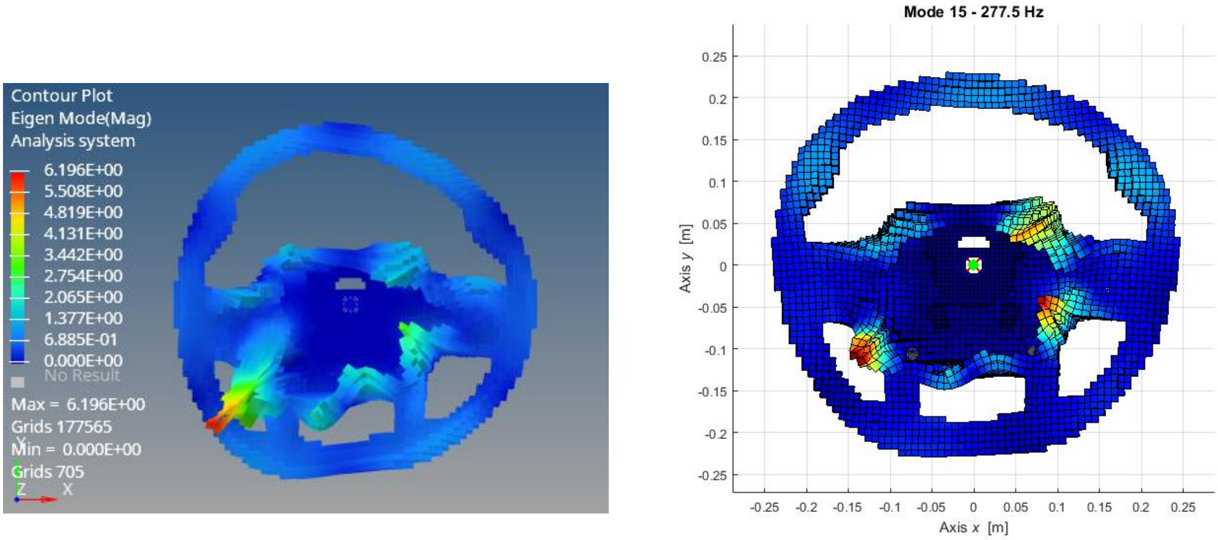

Figure 7.2.8 – Model with Rubber, eighth structural mode at 272.9 Hz and 277.5 Hz respectively.

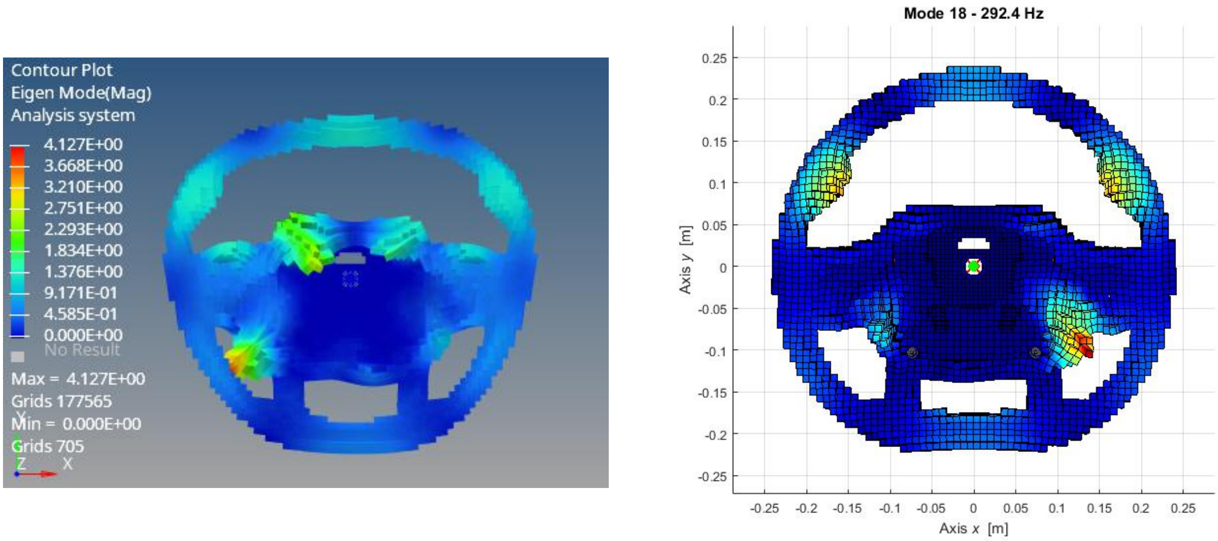

Figure 7.2.9 – Model with Rubber, ninth structural mode at 280.4 Hz and 292.4 Hz respectively.

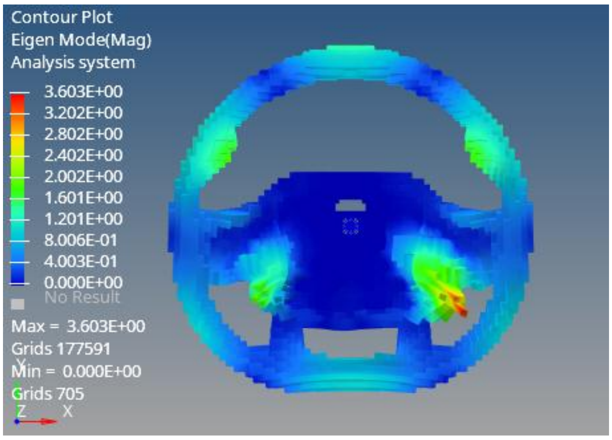

Figure 7.2.10 – Model with Rubber, tenth structural mode at 289.3 Hz.

As shown in Figure 7.2.8, Figure 7.2.9 and Figure 7.2.10 the differences between the solutions found by the two softwares involves the shapes too. It is noticeable that the ninth structural mode found by Lupos corresponds to the tenth structural mode found by Optistruct. By analyzing the frequencies in Table 7.2.1, this discrepancy seems less evident, as the frequencies are quite similar. An accurate observation of Figure 7.2.8 suggests that the structural mode by Lupos at 277.5 Hz has a different shape with respect to the one by Optistruct at 272.9 Hz: the first involves the central upper part of the frame and the thicker parts aside of that, while the second involves just the portion of frame between them. Moreover, the structural mode at 280.4 Hz by Optistruct in Figure 7.2.9 seems to involve the same parts of frame as the Lupos mode at 277.5 Hz; it seems that the two modes found by Optistruct result in just one by Lupos. Looking at the results obtained by the analysis of the models without Rubber, differences in eighth and ninth modes by the two softwares have been already pointed out, so probably those modes are the result of the different computational methods assumed by the two softwares. Anyway, experimental data will help to clarify the issue.

7.3 MAC

In order to have a quantitative comparison between the eigenvectors obtained by the two software, a Modal Assurance Criterion [2] has been evaluated. This tool compares two series of n eigenvectors, as reported by eq. (7.3.1), and returns a nxn matrix contained values from 0 to 100, as percentage of the correlation between the eigenvectors. The calculation has been implemented in Matlab, as a tool of Lupos, so the eigenvectors from Optistruct have been previously translated from the punch file format to three Lupos files, containing the list of nodes with their respective dofs, the list of eigenvalues and the list of eigenvectors.

$$MAC_{j,k} = \frac{[\mathbf{\Phi}_j^T \mathbf{\Phi}_k]^2}{[\mathbf{\Phi}_j^T \mathbf{\Phi}_j][\mathbf{\Phi}_k^T \mathbf{\Phi}_k]} \tag{7.3.1}$$

7.3.1 Lupos vs. Optistruct MAC

Figure 7.3.1.1 shows a representation of the MAC evaluated for the models without Rubber. As already qualitatively noticed, the correlation between the results of the two softwares is very high.

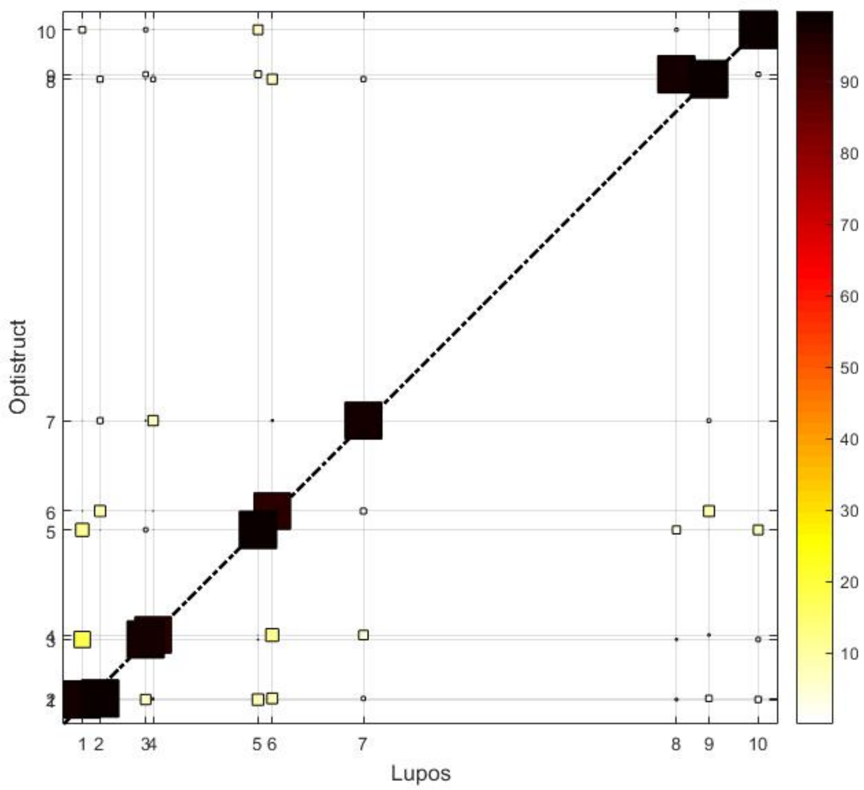

Figure 7.3.1.1 – Model without Rubber, MAC of Lupos and Optistruct eigenvectors.

The MAC has the mean value of 97.8%. As highlighted in Chapter 7.1, it is shown that the 8th Lupos mode corresponds to the 9th Optistruct one and vice versa. The black line is the isofrequency line.

Considering the model with the Rubber, the MAC has been evaluated for the first eighteen modes, as there are several non-structural modes, which are not physically sensible. Figure 7.3.1.2 reports a representation of the MAC: a good correlation is visible for the first twelve modes. The first modes in fact are structural, due to the steel and aluminium parts composing the frame; at higher frequencies, the presence of the rubber affects the vibrational behaviour. As already shown in Table 7.2.1 and in Figure 7.2.8 and Figure 7.2.9, there is a lower correlation for modes 14, 15 and 16, probably due to the strong influence of the Rubber. However, the mean value of the MAC is quite high, reaching 86.6%.

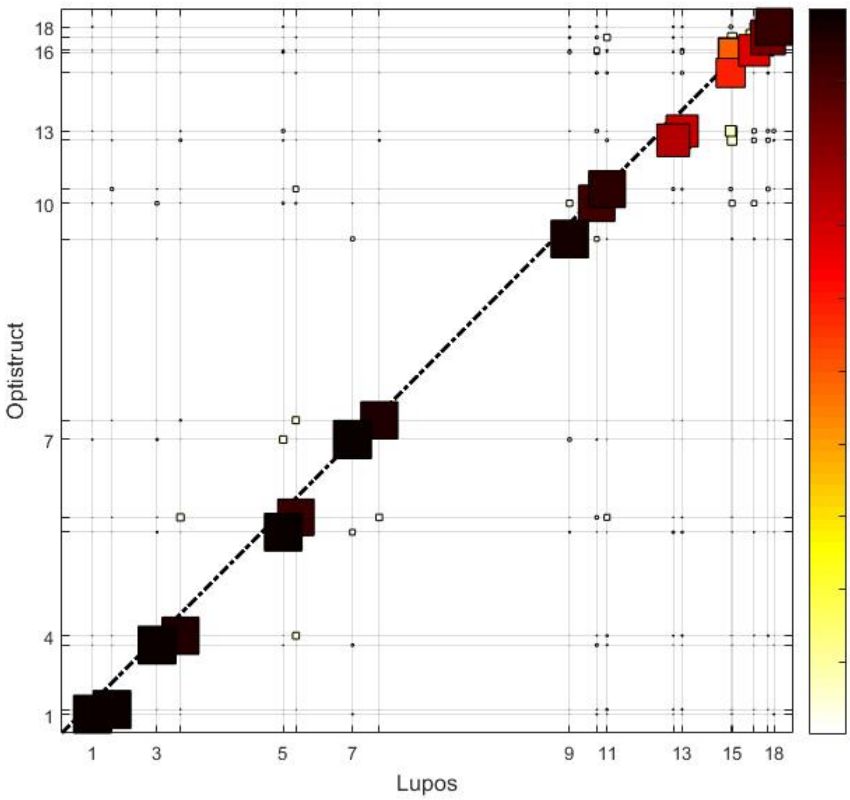

Figure 7.3.1.2 – Model with Rubber, MAC of Lupos and Optistruct eigenvectors.

7.3.2 The Minecraft Project MAC

In order to have a quantitative information about the reliability of the remeshing process from tetrahedrons into hexahedrons, a further analysis has been made considering the MAC of the two types of solid mesh models. Figure 7.3.2.1 reports the MAC evaluated for the Models without Rubber. The first twenty modes have been examined; the mean MAC value is very high, 95.3%, ensuring a good reliability of the process. Inversion is visible for modes from 15 to 18, but their frequency is quite high, over 500 Hz, so it is not so important. However, being the remeshed zone limited to the Central part, the Models with Rubber have been analysed too.

Figure 7.3.2.2 reports the MAC evaluated for the two Models with Rubber. The mean value is quite high, 91.1%, despite the miscorrelation of the 19th tetra-meshed Model mode and of the 20th hexa-meshed Model mode. Once again the reliability of the simplification technique introduced in the first chapter of this document is confirmed.

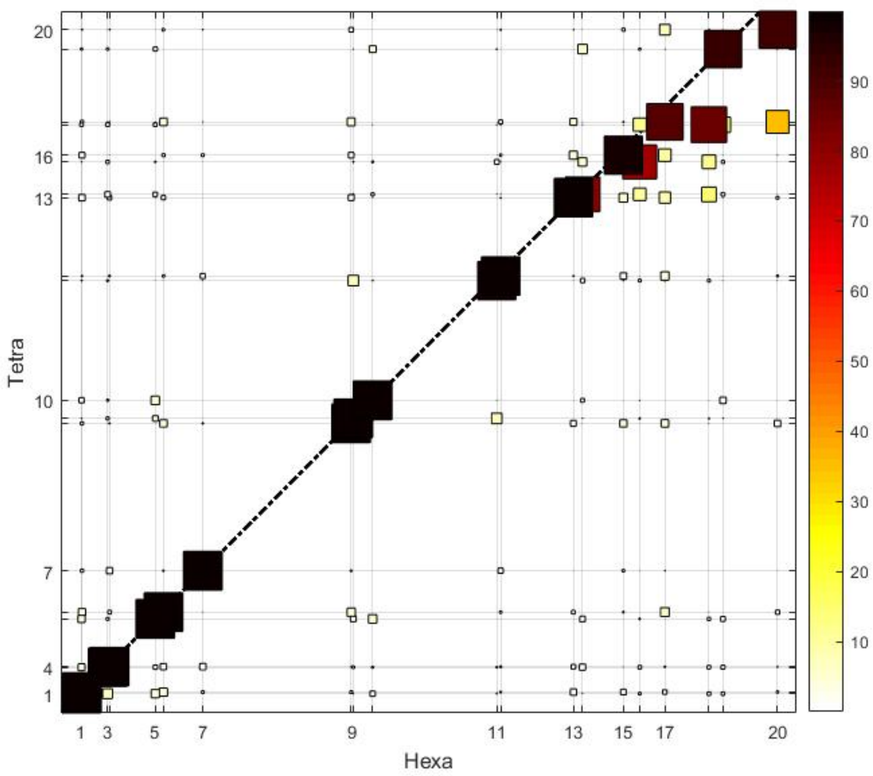

Figure 7.3.2.1 – Tetrahedral vs. hexahedral meshed Model without Rubber.

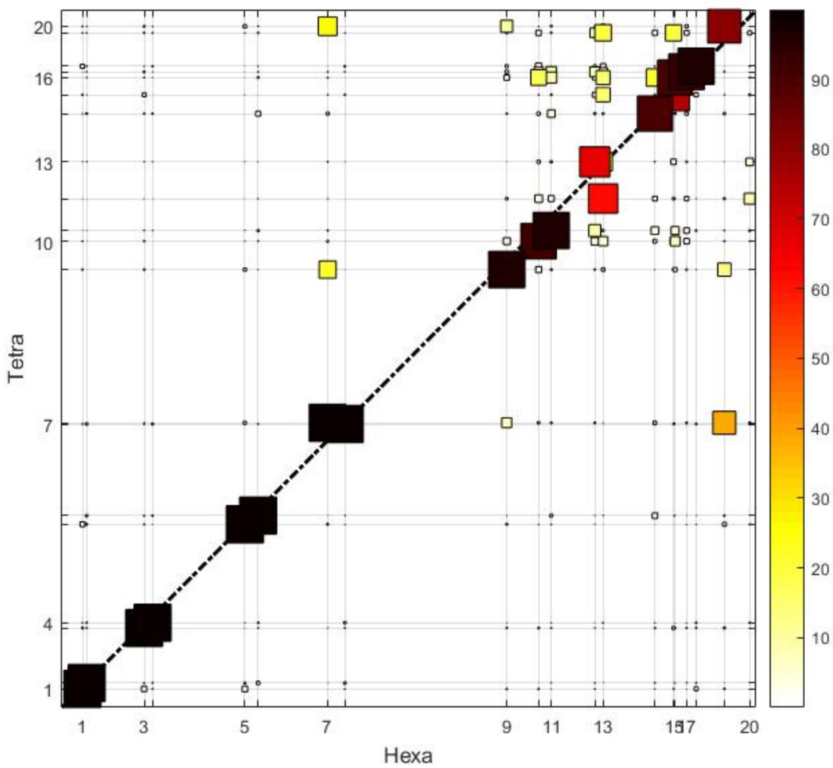

Figure 7.3.2.2 – Tetrahedral vs. hexahedral meshed Model with Rubber.

8. Experimental analysis test rig setup

The experimental analysis has to be prepared properly, studying the requested condition in order to run the acquisition at the best. It is fundamental, for this type of analysis, to have the possibility to constrain the object in exam as rigidly as possible, in order to ensure that the test rig natural vibrations do not affect the acquisition. The following paragraphs explain the solutions that have been adopted in this case.

8.1 FIAT Group Performance Standard

According to FIAT Group Performance Standard [3], the natural frequencies of steering systems are evaluated through an off vehicle test. The standard is applied for frequencies up to 200 Hz and it can provide an idea on how to execute the experimental analysis. The steering-column considered in this analysis is not actually from a car, but the document proposed could be a good starting point anyway. Analogies and differences will be underlined and will lead to the final design of the test rig.

8.1.1 Bench setup

The first issue is represented by how to organize an appropriate testing bench. The Standard [3] suggests to place the steering-column on an heavy steel block, in order to have the most rigid possible constraint. Then, the column has to be positioned as on vehicle, with the same inclination and through heavy links on the bench. In case of testing of the steering wheel only, it has to be linked to a very heavy mass by a shaft as it was on the column, even trying to reach the most rigid constraint. Figure 8.1.1.1 shows a clear example of a steering-column bench setup. The steering-column base in exam is not clamped horizontally, as described by the Standard, but vertically, so this solution is not feasible.

Figure 8.1.1.1 – FIAT Standard steering-column setup.

8.2. Design of test rigs

The FIAT Standard have suggested two good solutions, but they are not feasible because of practical issues. The two next paragraphs illustrate a possible alternative each.

8.2.1 Steering-column bench setup

The first issue is how to place the column on a heavy enough bench, which has a stiffness the highest possible. Figure 8.2.1.1 shows a bench in the Vehicle's Mechanics laboratory that might work. As the FIAT Standard suggests, the column is thought to be placed as on the vehicle, that means that the heavy base, as shown in Figure 8.2.1.2, will be placed vertically.

Figure 8.2.1.1 – Testrig for steering-column.

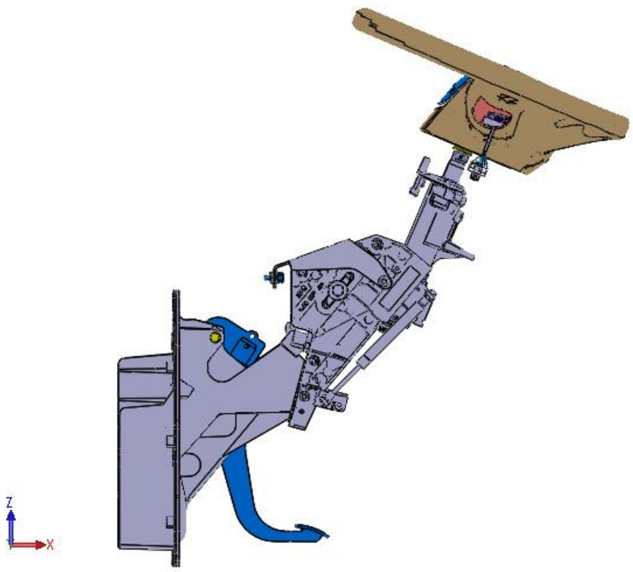

Figure 8.2.1.2 – Steering-column on-vehicle position.

In order to have a link with a good stiffness, a structure has been designed, using aluminium beams and steel plates. It has been thought in order to recycle old benches parts, so only the steel plates have been bought, because of their particular shape. Figure 8.2.1.3 shows a couple of views of the 3D design of the structure, including the base of the steering column.

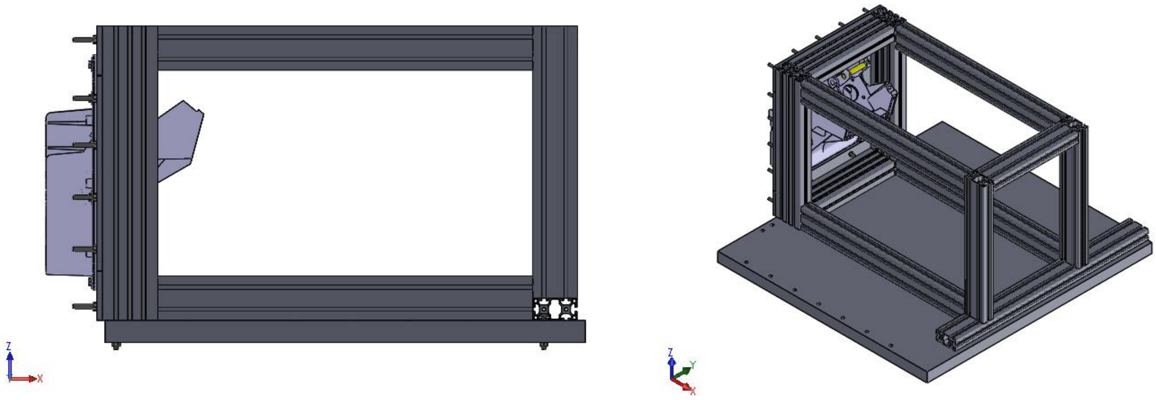

Figure 8.2.1.3 – Views of the structure.

This solution has been chosen because of the irregular patterns of holes of the bench, being reluctant to do new ones. Figure 8.2.1.4 reports a particular view of the connection between the structure and the column. The four steel plates are 10 mm thick and simulate the firewall where the column is usually placed on. They hold the column through a series of seven M8 bolts and are linked to the structure by eighteen M8 bolts with a particular shaped head which fits the grooves of the aluminium beams. Figure 8.2.1.5 shows a section of every beam employed. The whole structure is thought to have natural frequencies much higher than the column, in order to avoid interferences during the tests. A modal analysis should be run in order to have the certainty of having designed a structure stiff enough.

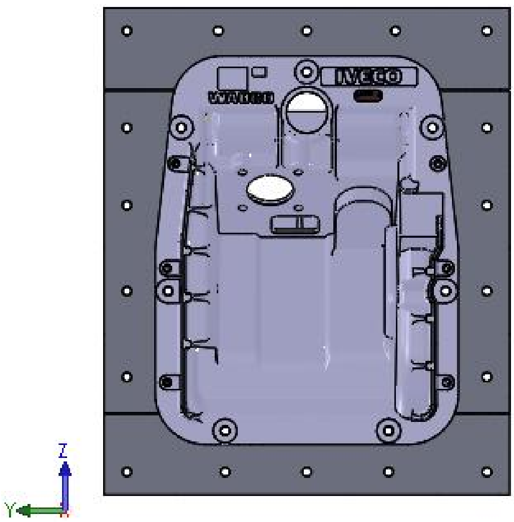

Figure 8.2.1.4 – View of base fixing on the structure.

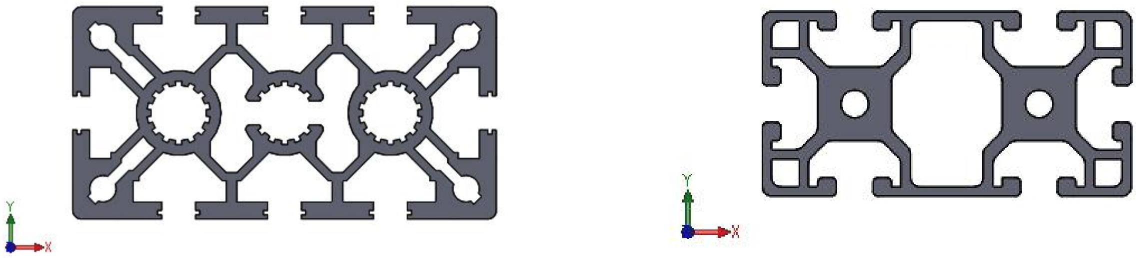

Figure 8.2.1.5 – Beams sections.

The left section beams, being the stiffest, have been used for holding the column, while the right section beams have been used for the back structure.

8.2.2 Wheel bench setup

The Wheel will be clamped on a huge mass of a materials testing machine, which has a very low natural frequency, being linked to ground by a series of big springs. The wheel will be clamped to the mass using a bolt that simulates the steering shaft. This solution is similar to the one proposed by the FIAT Standard, differing in the natural frequency of the bench (very low and very high respectively). Figure 8.2.2.1 shows the future test rig.

Figure 8.2.2.1 – Steering-wheel test rig.

9. Test rig modal analysis

In order to be ensured about the stiffness of the steering-column test rig, a modal analysis has been run by Optistruct. This check is necessary because the structure described in the previous chapter could not be actually suitable for supporting the column during the experimental test, being basically composed by aluminium beams.

9.1 Model building

The model has been thought as simple as possible, because it is not the object under investigation and its modal analysis is just an assurance of having natural frequencies high enough, in order to not influence the measurements on the steering-column. The numbers of nodes and elements have been kept as lower as possible, ensuring low computational time and effort. Table 9.1.1 resumes the main characteristics and properties of the model, while Table 9.1.2 resumes the materials properties.

Table 9.1.1 – Model characteristics.

Component	# of nodes	Type of elements	# of elements	Material
Bench	6762	Hexahedrons	4320	Steel
Beams	317	1D beams	305	Aluminium
Plates	1639	Quadrilateral shells	1440	Steel
Column base	16462	Tetrahedrons	50418	Steel
Steering-column	4	Concentrated mass	1	-
Total	27663	-	56484	-

Table 9.1.2 – Material properties.

Material	Density [kg/m^3]	Young module [GPa]	Poisson coefficient [-]
Steel	7800	210	0.33
Aluminium	2790	75	0.3

9.1.1 Bench

The base bench has been modelled by an hexahedral solid mesh. The holes have been neglected, as their dimensions are far too small with respect to the whole bench. The solid mesh has been constrained to ground by a series of RBE2s, simulating the two heavy H sectioned beams that are bolted along each side of the bench. Figure 9.1.1.1 shows the part.

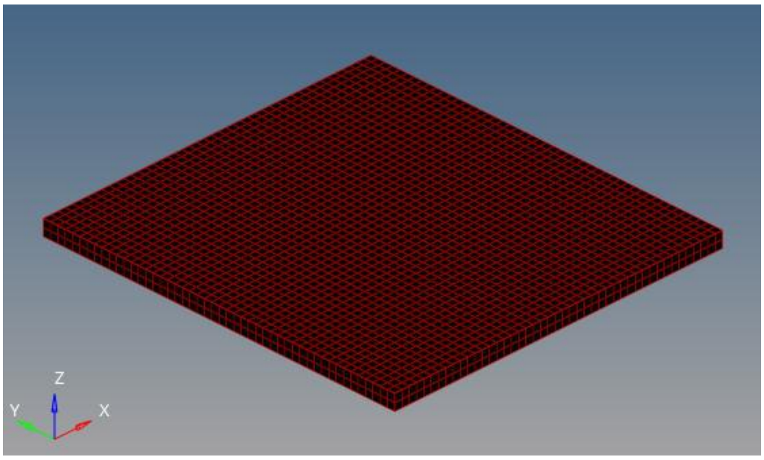

Figure 9.1.1.1 – Bench FE model.

9.1.2 Aluminium beams

The aluminium beams have been modelled by a series of 1D beam elements. The particular sections of the two types of beams have been imported in Hypermesh and then, using a tool, have been set as section of the 1D elements. This solution simplifies the model and the model building process in few passages. Figure 9.1.2.1 shows the parts. The connections have been modelled by RBE2s. The bolts that connect the beams to the bench have been modelled by three RBE2s each.

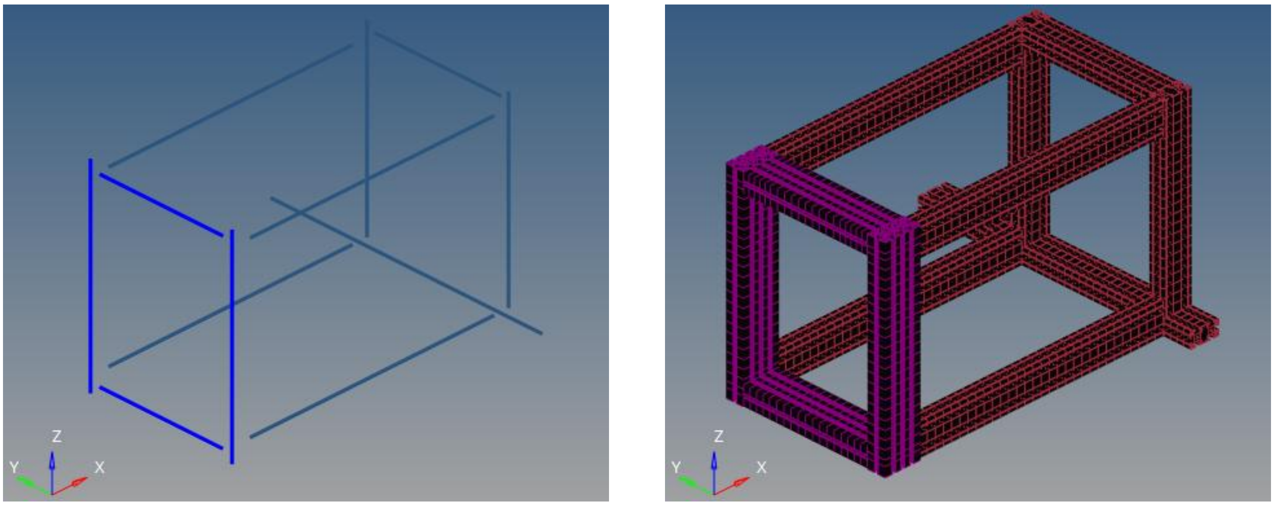

Figure 9.1.2.1 – Aluminium beams FE model, in both 1D and 3D visualization.

9.1.3 Steel plates

The steel plates supporting the column base have been modelled by quadrilateral shells. This solution is again a simple technique to keep the model as light as possible. The holes have been once again neglected. Figure 9.1.3.1 shows the parts. The links with the other parts are modelled by RBE2s, trying to simulate the bolts.

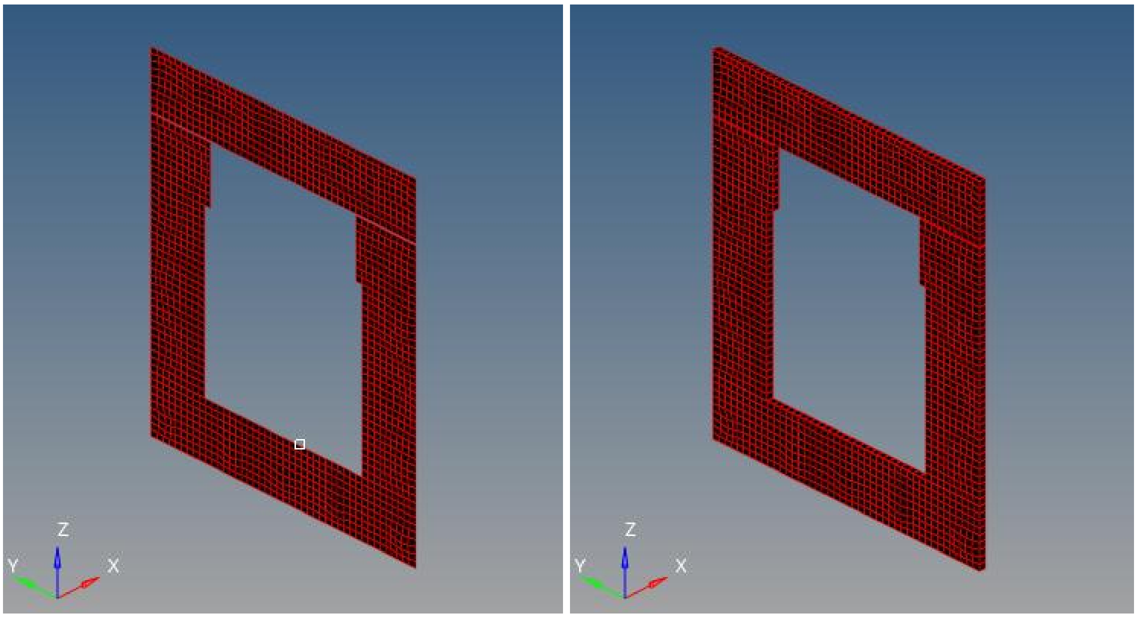

Figure 9.1.3.1 – Steel plates FE model, in both 2D and 3D visualization.

9.1.4 Steering-column

In order to have a proper representation of the vibrational behaviour of the structure, the whole steering-column has been modelled. The most important part is the base, as it is the interface with the structure, so it has been modelled by a tetrahedral mesh, while the other components have been just modelled as a lumped mass CONM2 of 12 kg in their overall centre of mass and linked to the base by RBE3s on proper nodes. Figure 9.1.4.1 shows the parts. The details on the base have been neglected as far as the dimension of the solid elements allowed. The complicated geometry do not let to use large elements, so the number of nodes is quite high.

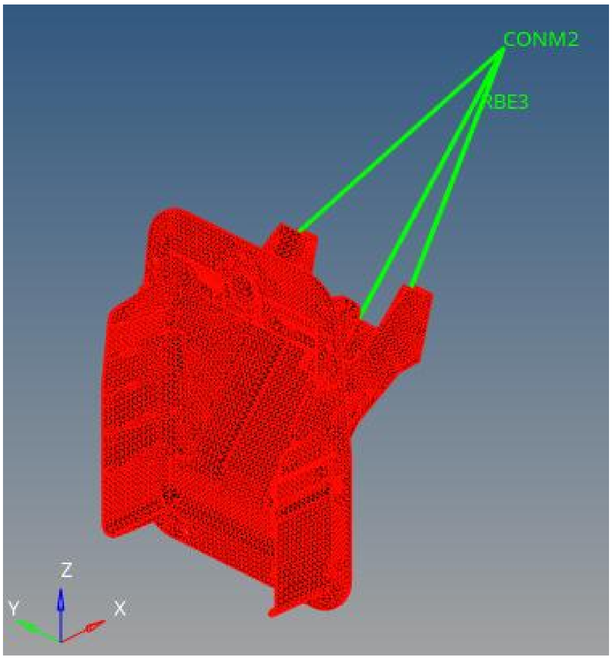

Figure 9.1.4.1 – Steering-column FE simplified model.

9.2 Contacts

A critical aspect in FE modelling is the correct representation of the contacts between the parts. In this model, this issue is crucial, as the parts involved are not all three-dimensional. The problem of interfacing a 1D element with 2D or 3D element shall be analysed carefully. The non-linear nature of a contact relationship is not compatible with modal analysis: a careful linearization could be done through the use of a proper number of Rigid Body Elements RBE2s, but too many of them would make the whole structure too stiff. Moreover, the rigid body behaviour that characterizes these elements is not compatible with the problem, in fact in order to lock properly the desired degree of freedom, more than one element should be used, involving multiple nodes and affecting the relationship with other degrees of freedom. In order to get over this issue, Multi-Point Constraints have been used. MPCs permit to manually define the equations between the degrees of freedom of the considered nodes, without involving any physical connection. This solution is still dangerous, because it stiffens the structure and leads to results that overestimate the actual natural frequencies. On the other hand, this kind of connections does not consider the friction between the parts, that obviously affects the real objects and increases the global stiffness. The following paragraphs analyse every contact case. Figure 9.2.1 shows the model, including the rigid elements simulating the contact relationships.

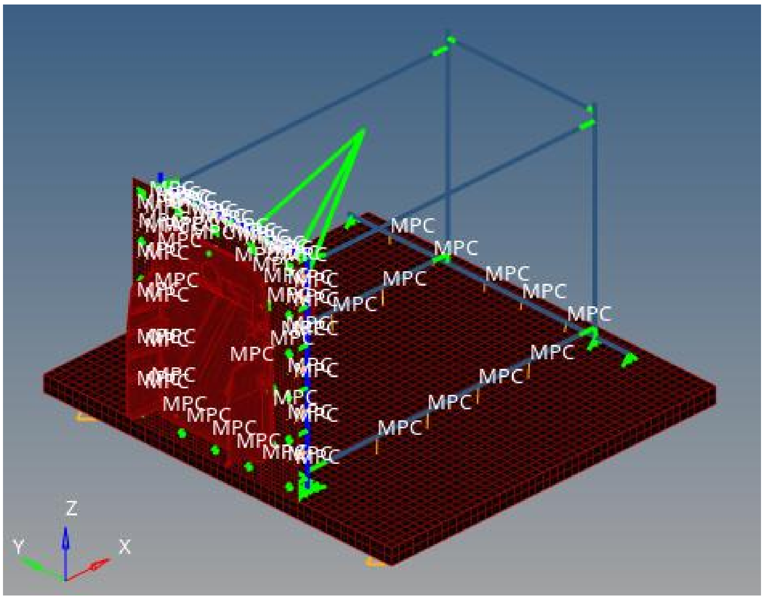

Figure 9.2.1 – Complete model view.

9.2.1 Contact between bench and beams

Figure 9.2.1.1 shows, on the left, how the parts appear without any contact relation, on the right, how they appear in reality. The number of bolts locking the structure to the bench is very limited, as there are very few suitable holes on the bench; the long beams that lie on the bench are not bolted to the bench, but only to the two vertical frames; so in order to avoid interpenetrations, four MPCs for each beam have been created, locking the vertical displacement of four beams nodes to the respective bench nodes. This solution is more actual than the use of RBE2s, because it does not involve any geometric parameter and limits the constraint to the z direction only. The vertical frame opposite to the column support is bolted to the bench in only three points. In order to model the contact, five MPCs have been created, locking the beam nodes z displacement to the respective bench nodes ones.

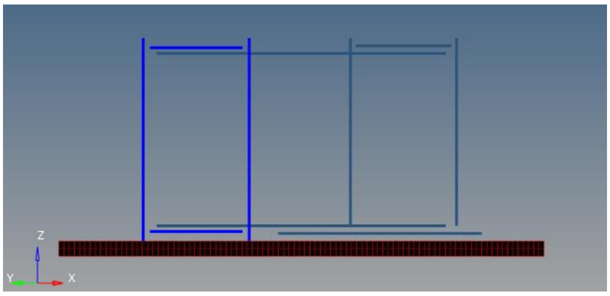
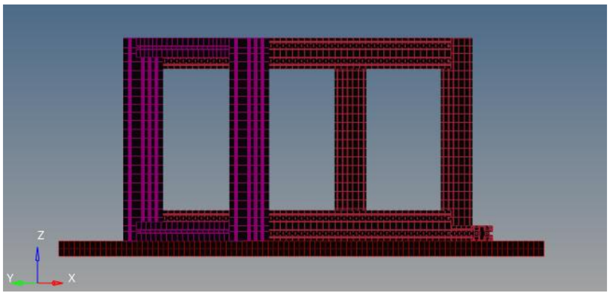

Figure 9.2.1.1 – Contact between bench and beams.

9.2.2 Contact between beams and plates

Another critical contact is between 2D steel plates and 1D aluminium beams: once again, the technique used for modelling the contact is not perfect and the stiffness of the structure could be overestimated. The influence of this contact relation has the highest importance, as it determines basically the whole vibrational behaviour, being the direct support for the steering-column. Figure 9.2.2.1 shows, on the left, how the parts appear without any contact relation, on the right, how they appear in reality. The bolts holding the plates against the beams have been modelled through a star of RBE2s (locking 6 dofs each) on the plates, connected to the respective nodes of the beams by a RBE2. This solution locks totally the plates nodes involved to the respective beams nodes as bolts would do. The contact has been emulated by couples of MPCs on *x* direction, that link a series of nodes aligned with the bolts. The contact between the vertical beams and the bench has been modelled by a star of RBE2s linking bench nodes to the first node of each beam.

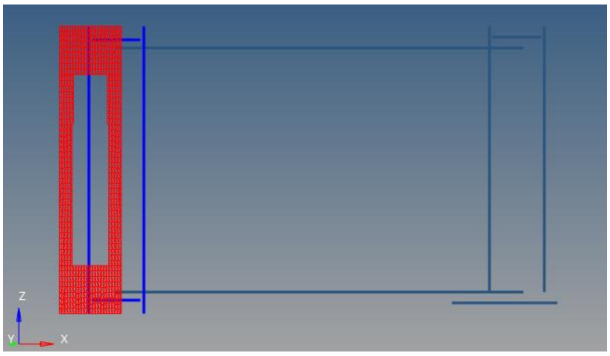
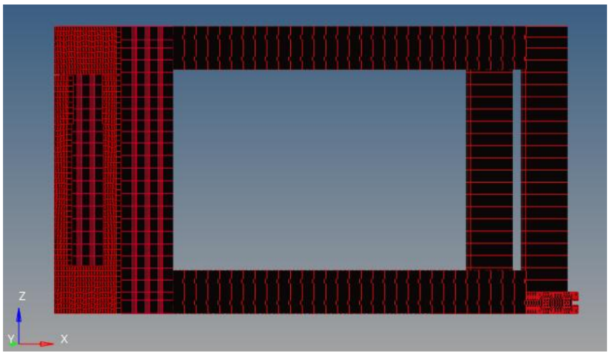

Figure 9.2.2.1 – Contact between beams and plates.

9.2.3 Contact between plates and column base

The column base is linked to the plates by seven bolts: they are too few to ensure an appropriate contact between the parts, so MPCs have been used to connect few nodes along the column base external rim to the plates, along the *x* direction. This solution is thought to not too much overestimate the stiffness, as the interface between the two parts is supposed to have a high friction, due to the presence of a rubber lining all around the rim.

9.3 Modal analysis

A modal analysis of the FE model has been run in Optistruct. The results are not completely physical, as already explained. The natural frequencies obtained by the modal analysis are reported in Table 9.3.1.

Table 9.3.1 – First ten natural frequencies from Optistruct modal analysis.

Mode #	Frequency [Hz]
1	111.8
2	115.1
3	138.7
4	143.7
5	201.3
6	215.3
7	269.6
8	331.1
9	448.1
10	450.3

These values of frequency are supposed to be high enough to allow the experimental modal analysis on the steering column, considering that the actual natural frequencies of the structure could be higher, because of the strong simplification that characterizes this model.
From Figure 9.3.1 to Figure 9.3.3 reports a representation of the first six modes from Optistruct modal analysis.

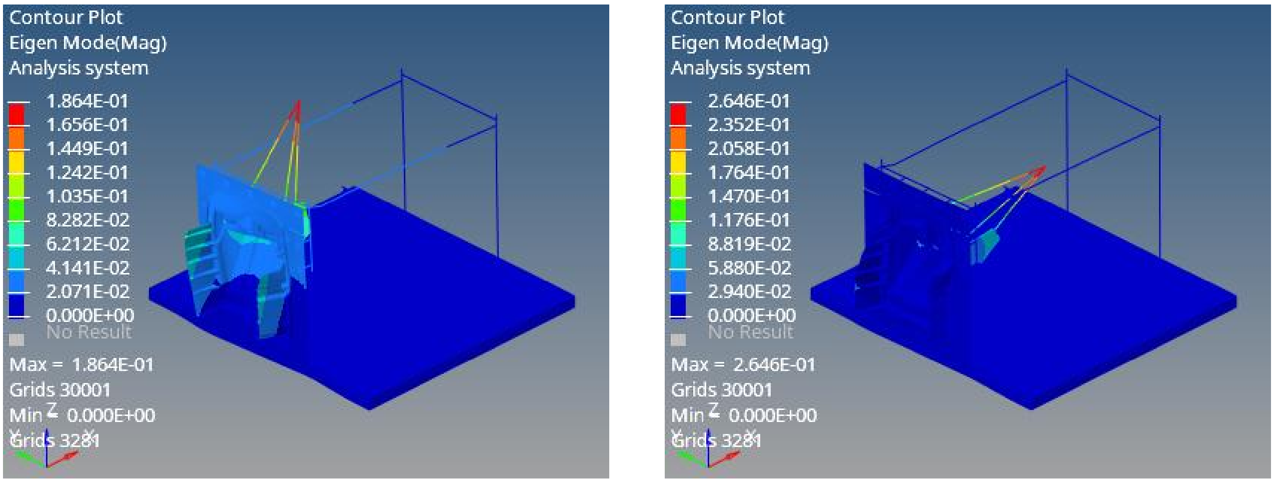

Figure 9.3.1 – First and second modes, at 111.8 Hz and 115.1 Hz respectively.

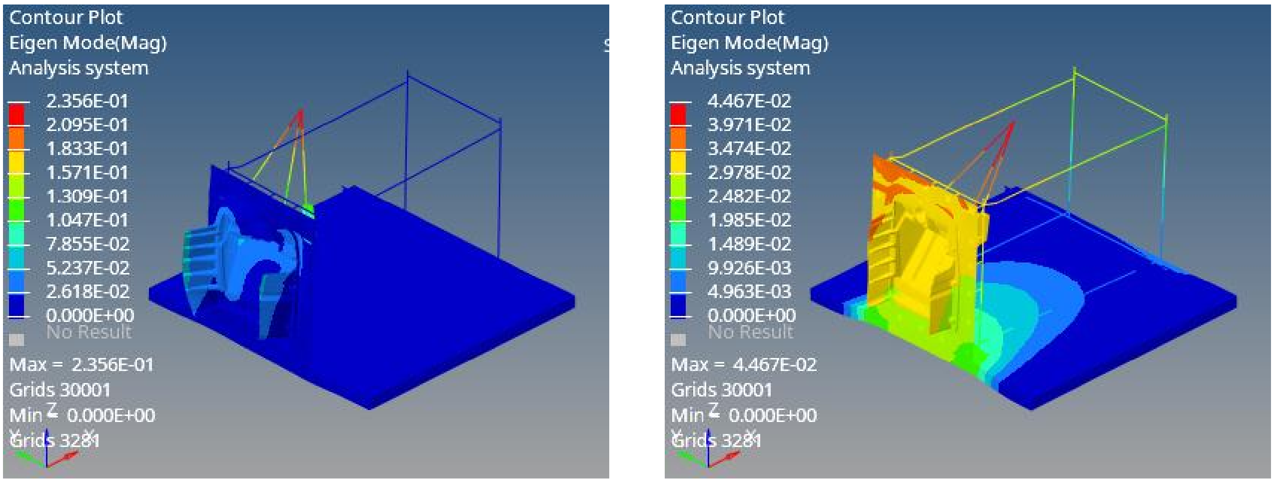

Figure 9.3.2 – Third and fourth modes, at 138.7 Hz and 143.7 Hz respectively.

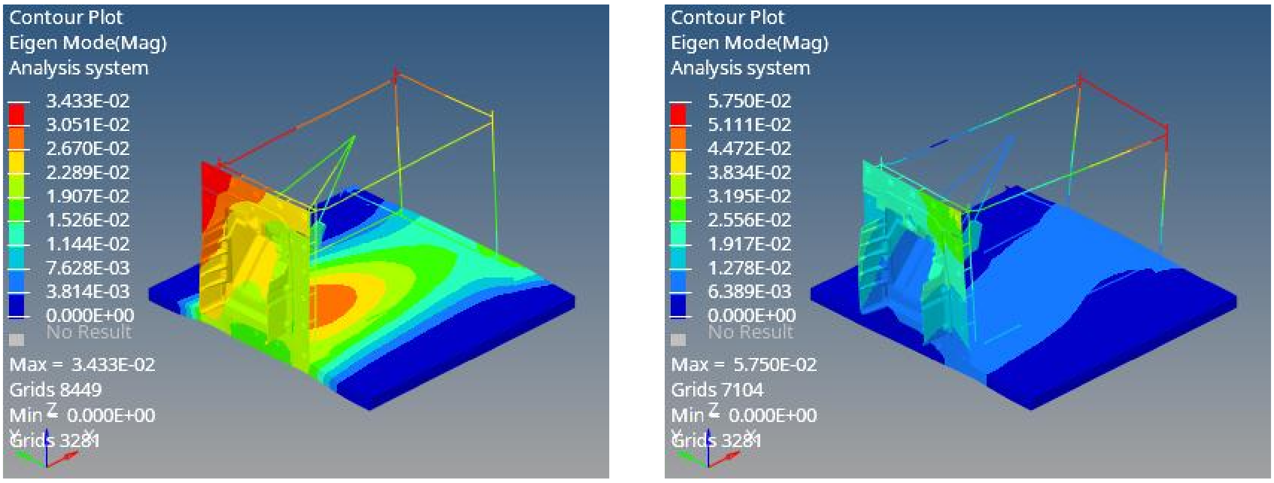

Figure 9.3.3 – Fifth and sixth modes, at 201.3 Hz and 215.3 Hz respectively.

10. Sensors positioning

The last stage before the experimental phase is the selection of sensors positions. This issue is crucial: a good pattern of nodes has to be formed in order to have a complete representation of the vibrational behaviour of the analysed object. Many techniques are available, based on different strategies and the following paragraphs report two of those.

10.1 FIAT Group Performance Standard

Once again, the FIAT Group Performance Standard [3] suggests a simple and efficient method, reported by Figure 10.1.1: four accelerometers are employed and placed in only two points: at 12 hours and 9 hours, two couples formed by a *z*-axis and a *y*-axis sensor each. As will be evidenced by the results in the next paragraphs, this solution is a good starting point. However, in order to have a better and more complete representation of the model behaviour, a larger number of nodes should be involved.

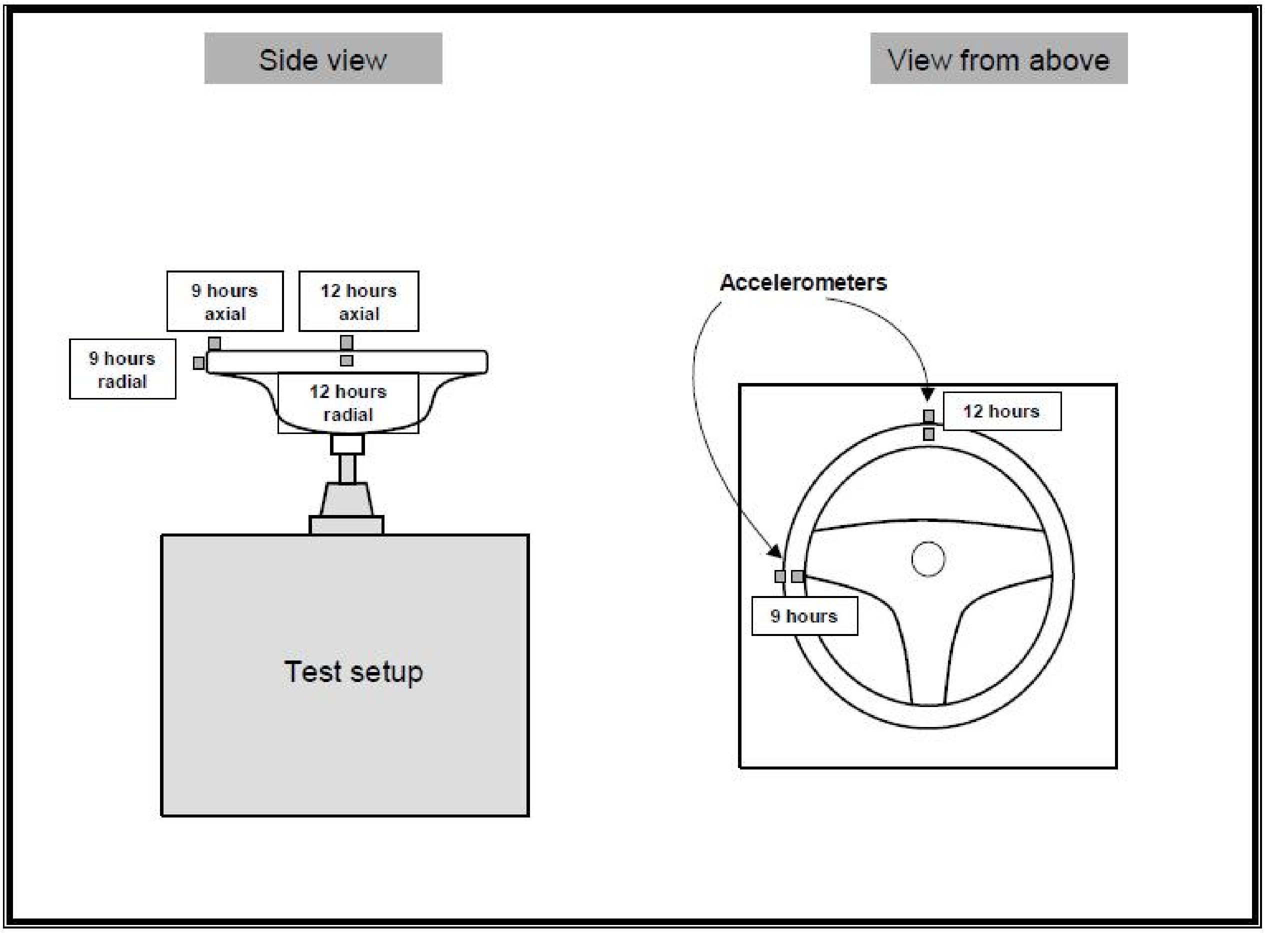

Figure 8.1.2.1 – FIAT Standard sensors placing.

10.2 Modal and Geometrical Selection Criterion

As already explained, a good data acquisition is based on the correct positioning of sensors on the structure. In addition to the method proposed in Paragraph 10.1, a more complex but complete technique is described as follows. Modal and Geometrical Selection Criterion, MoGeSeC [4], is an efficient tool, based on both geometry and modal properties of the system, obtained by a numerical modal analysis, for choosing the best representative nodes. The concept behind this technique is that the modal behaviour of a model can be represented by a list of nodes, whose eigenvectors resume the modal properties of the whole system. The progressive optimal location is based on both modal independence information and geometrical location to distribute accelerometers on the whole structure.

The Selection Criterion is based on the evaluation of the maximum value of the vector **w**:

$$\mathbf{w} = \mathbf{diag}(\mathbf{w}_g \mathbf{w}_m{}^T)$$

that represents the combination of the geometrical vector and the modal vector, calculated for each node, as follows:

$$\mathbf{w}_{g,\mathrm{p}} = \frac{1}{\max(\mathbf{w}_g)} \frac{1}{\sum_{i=1}^{r} \left[\frac{1}{(x_p - x_i)^2 + (y_p - y_i)^2 + (z_p - z_i)^2} \right]^{k_1}}$$

$$\mathbf{w}_{m,p} = \frac{1}{\max(\mathbf{w}_m)} \sum_{j=1}^{3(r+1)} \left[\mathbf{\Phi}_{p,x}^{(j)^2} + \mathbf{\Phi}_{p,\mathrm{y}}^{(j)^2} + \mathbf{\Phi}_{p,z}^{(j)^2} \right]^{k_2}$$

Coefficients k_1 and k_2 allow to weigh the influence of each component; start value are respectively 2 and 1.

The result of this selection is a list of nodes positioned as far as possible on the structure, with an homogeneous distribution, in order to have the best possible representation of the vibrational behaviour.

10.3 Application to the Wheel Models

The MoGeSeC has been applied to both the models, with and without the Rubber. The calculation has been implemented in Matlab. It requires, as geometrical property, the Lupos file containing the nodes coordinates and, as modal properties, the results in Lupos format. The solutions here reported include both Lupos and Optistruct modal results, representing a further comparison of the two softwares.

Figure 10.3.1 shows the selected nodes from the two softwares solutions. With X marks the software identifies the nodes where accelerometer in *x*-axis have to be placed; with triangles accelerometers in *y*-axis and circles in *z*-axis.

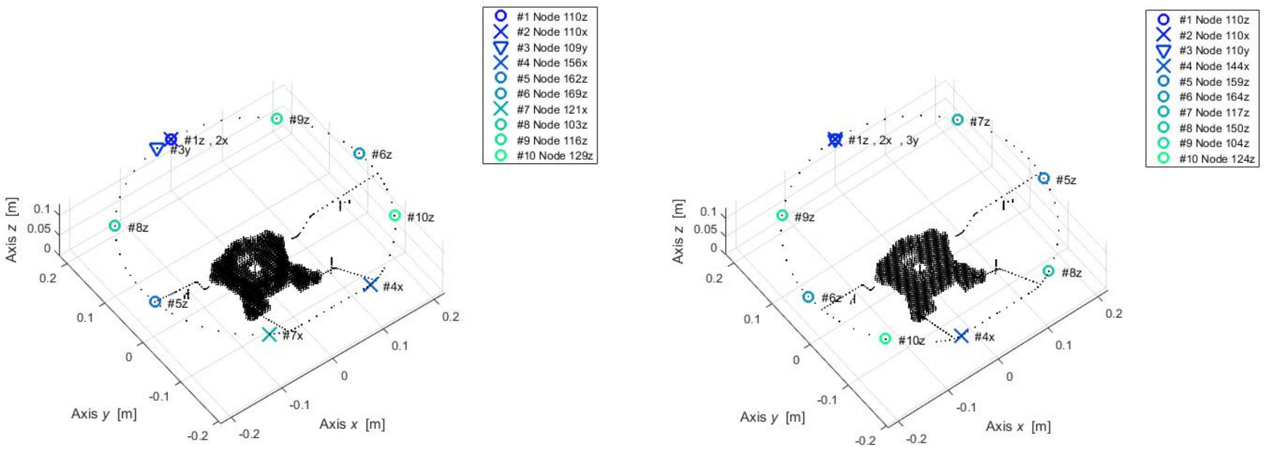

Figure 10.3.1 – Model without Rubber, MoGeSeC results
for Lupos and Optistruct eigenvectors respectively.

As expected, the selected nodes are nearly the same. The distribution is very similar and the difference in position of the two series is minimal, not important from a practical point of view. This result is a further validation of the reliability of Lupos.
Figure 10.3.2 reports the solution for the Model with Rubber. Only the first eighteen modes have been considered.

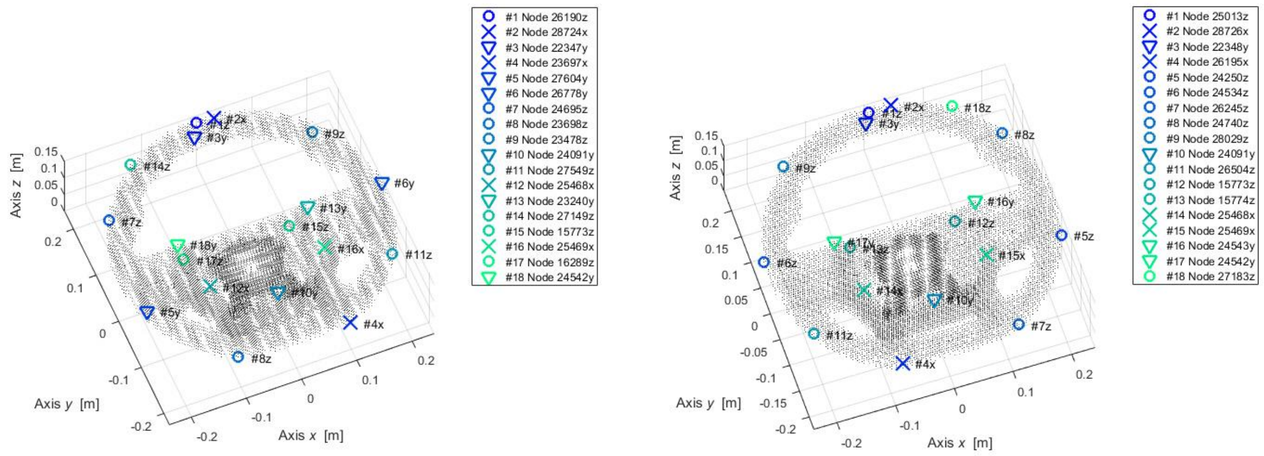

Figure 10.3.2 – Model with Rubber, MoGeSeC results
for Lupos and Optistruct eigenvectors respectively.

The software implemented in Matlab allows to impose a set of nodes as master and finds the remaining ones starting from them. A trial has been done imposing two nodes as suggested by the FIAT Standard; Figure 10.3.3 reports the result for the Model without Rubber, with imposed nodes in red marks.

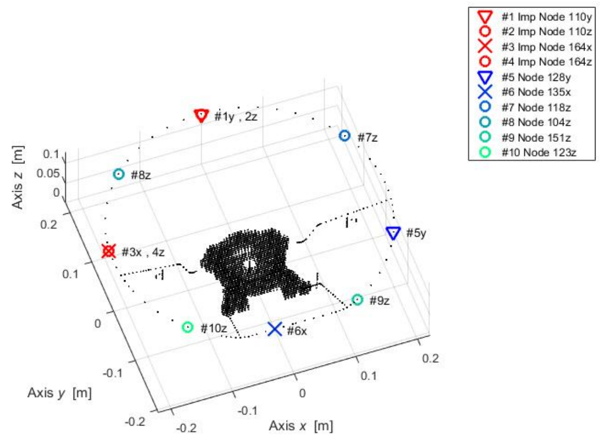

Figure 10.3.3 – Model without Rubber, MoGeSeC results
for Lupos and Optistruct eigenvectors respectively, with two master nodes imposed.

The differences from the previous results are minimal. Figure 10.3.4 shows the same evaluation for the Model with Rubber. These results confirm as the solution proposed by the FIAT Group Performance Standard [3] is a good starting point, but to be further improved with additional nodes for a better analysis.

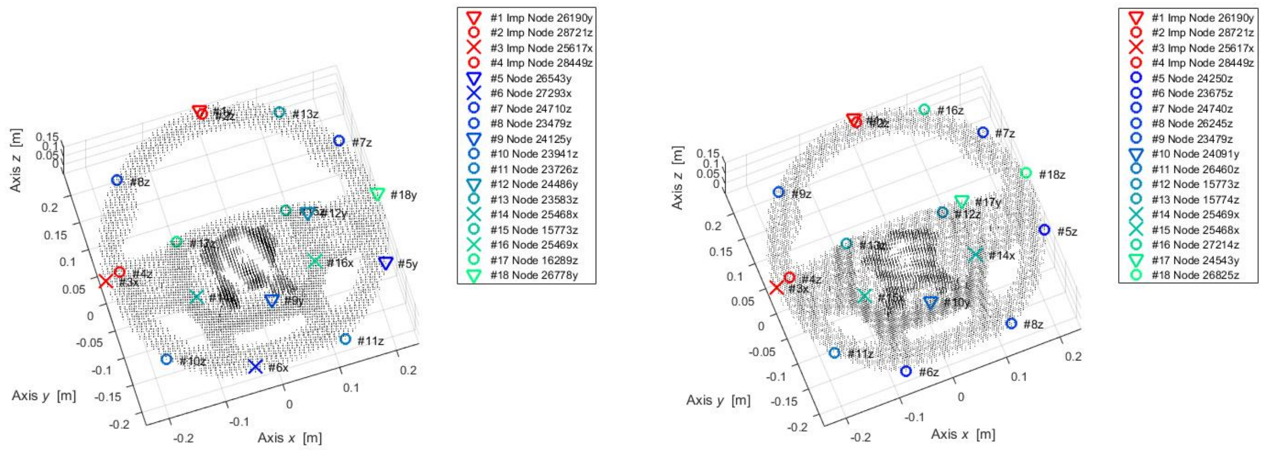

Figure 10.3.4 – Model with Rubber, MoGeSeC results
for Lupos and Optistruct eigenvectors respectively, with four master nodes imposed.

A further analysis has been done considering 3-axis sensors. Figure 10.3.5 reports the results for the Model with Rubber.

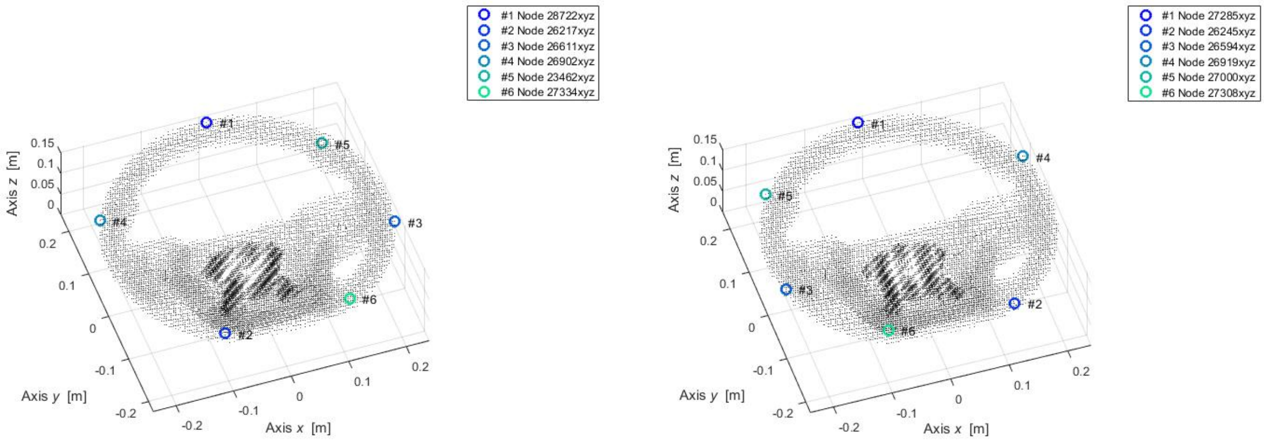

Figure 10.3.5 – Model with Rubber, MoGeSeC results
for Lupos and Optistruct eigenvectors respectively, for 3-axis sensors.

The result obtained for the two solutions is practically equivalent, remarking the substantial correlation between the two series of eigenvectors.
The experimental test is now prepared, the next step is the execution. The numerical phase is completed, at the moment; it will continue with the final adjusting, in order to make the finite elements models match the physical vibrational behaviour.

Conclusions

The numerical data, including both FEM models and their analysis results, are ready for being compared to the experimental data. An adjusting phase will be certainly needed, but the models have been built for that and the process will not be hard. Nevertheless, at the end of this master thesis much more than a couple of finite element models has been obtained. The deep analysis of different modelling techniques has given the necessary knowledge for efficiently building proper virtual prototypes, that means a good trade-off between number of nodes and accuracy, at least for modal analysis. The four models in fact have shown the possibility to progressively decrease their complexity, improving their manageability and strongly reducing the analysis time. Certainly the experimental data will be the tougher judge, but the numerical results are really optimistic.
A particular attention must be given to Chapter 5: the opportunity given by The Minecraft Project of strongly reducing the number of nodes of a solid meshed model, without obviously changing its physical properties, is very useful. CAD/CAE softwares often provides tools for automatically meshing a part, but do not allow the user to modify or adjust the result, usually turning into an heavy and inefficient model. Using the simple routine furnished by The Minecraft Project, the meshing process time is drastically reduced, making the user saving time. The new model can be easily further adjusted and completed even using softwares, like Lupos, that do not include any graphic interfaces for modifying.
Another relevant aspect is the huge range of tools provided by Lupos: this nearly home-made open source software has a long list of useful routines, that let the user to analyse a problem under any point of view. Moreover, being totally implemented in Matlab, the user can easily access every data and further manage them as Matlab allows to. An example is the MAC, reported in Chapter 7, that gives a numerical value to the correlation of two series of modal shapes, or MoGeSeC, that strongly accelerates the bench setup process providing a complete set of sensor positions.
Finally, the experimental test will evaluate the accuracy of this work, detecting the positive and negative aspects of the different techniques here exposed.

Appendix A – Tcl scripts for Hypermesh

Tcl is a simple software programming language, based on objects. The basic structure is the list and everything is read as a string, even numbers. Due to these characteristics, this language is very useful for managing large data, as a finite element model is supposed to be. A very important property is the possibility to interface codes in other languages without any difficulty and the presence of a proper GUI creation tool called Tk makes it a very powerful language. On the other hand, calculations are pretty complicated to program, requiring many commands, much more than simple languages as C. However, files and data can be easily imported and exported, so the calculations can be done in other softwares and then the results imported back.
Hypermesh has a very large Tcl library, with which the user can manage every aspect of the software, including graphics views and interfaces, modify and create entity and even evaluate properties and geometrical aspects, nearly as the GUI allows to. This characteristic is very useful as it allows to create powerful scripts that can include user interaction, making automatic process that could be impossible to be executed by the user.
The creation of the wheel models has been done with the support of three Tcl scripts, that simplified and quickened the job, reported in the following paragraphs.

A.1 Node clonator

The first script has been written for supplying a tool that duplicates nodes with the same degrees of freedom. The wheel frame is composed by the steel rods connected by tubular elements in aluminium. The nodes of rods and connectors were supposed to be coincident, modelling them through 1D beam elements, so the issue was to duplicate rods nodes, link every couple by RBE2s and create the new elements. Manually, it might be executed through the duplication of a node and then linking the two nodes by a RBE2. This process is pretty delicate, as using the graphic interface a node is not simply visible, moreover in case of duplicates. Another way could be the previous creation of the element desired, duplicate its nodes and then create the new element, but errors can be very common, and in case of large number of nodes it can take a very long time. In order to get over these issues, a script that does everything automatically has been created. It asks the user to indicate the nodes to duplicate, then it creates a new component, duplicates the nodes and links them to the originals. The degrees of freedom locked by the RBE2s can be set by easily modifying the script. The time taken is short and the result is good, making much faster the creation of duplicated and coincident nodes. This process can be useful every time there is the need of having two (or more) components with the same dofs, but maintaining their independence. In fact, in case of deleting a component from the model, the others would not be modified. The code is reported below.

```
# This script duplicates a list of nodes in a new comp and link to the original with a rbe2.
# The indipendent node is the original one.

*createmarkpanel nodes 1 "Select nodes to duplicate"

# Create new component:
*collectorcreateonly component Rigid_new {} 50
*currentcollector component Rigid_new

set nodesId1 [hm_getmark nodes 1]
```

```
*clearmarkall 1

# Evaluate the number of nodes:
set numb [llength $nodesId1]

# Create a rigid element for each couple of duplicate nodes:
set i 0
while {$i<$numb} {
      *clearmarkall 1
      *clearmarkall 2
      eval *createmark nodes 1 {"by id only"} [lindex $nodesId1 $i]
      *duplicateentities nodes 1 2
      set node2 [hm_getmark nodes 2]
      *rigid [lindex $nodesId1 $i] $node2 123456
      incr i
 }
```

A.2 Glue

The second script has been written for speeding up and making much more precise the creation of rigid links between two or more components. In particular, it has been thought for linking the rubber 3D mesh to the frame and the central part. Manually, this process would take tens of hours and the choice of which node to connect would be hard to do through the GUI. The solution was to write a script that asked the user the nodes to be set as masters, the nodes to be set as slaves, a distance within the masters constrain the slaves and then that did the job. For first it creates a new component, where the rigid elements will be stored; then, it evaluates the distance between the two series of nodes and links the nodes within the provided distance. In order to avoid multiple dependencies, it signs the nodes already linked as slaves and prevents from connecting them again. The process is not very quick, but compared to the manual procedure, it is far faster. This script has been used for connecting, in the hexahedral mesh models, even the central part to the frame. The dofs to be locked can be easily set by modifying the script. It can be used every time there is the need to connect, with a certain tolerance, two or more components through a large number of nodes. The code is reported below.

```
# This script creates a rigid link (6 dofs locked) between nodes of two components if their distance
      is less than a user defined tolerance.
# The indipendent node belongs to the first component selected.

*createmarkpanel nodes 1 "Select first component nodes (independent nodes)"
set nodesId1 [hm_getmark nodes 1]
*createmarkpanel nodes 2 "Select second component nodes (dependent nodes)"
set nodesId2 [hm_getmark nodes 2]

# Create new component:
*collectorcreateonly component Glue {} 50
*currentcollector component Glue
*clearmarkall 1
*clearmarkall 2

# Evaluate the number of nodes:
set numb1 [llength $nodesId1]
```

```
set numb2 [llength $nodesId2]

# Set the tolerance:
set tolerance [hm_getfloat "Tolerance=" "Please define the tolerance"]

# Create a rigid element for each couple of nodes:
set n 0
set m 0
set nodelinked 0
while {$n<$numb1} {
      set m 0
      set node1 [lindex $nodesId1 $n]
      while {$m<$numb2} {
        set node2 [lindex $nodesId2 $m]
        set distance [lindex [hm_getdistance nodes $node1 $node2 0] 0]
        if {$distance<$tolerance && [lsearch $nodelinked $node2]==-1} {
                *rigid $node1 $node2 123456
                lappend nodelinked $node2
                }
        incr m
        }
      incr n
}
```

A.3 HexToHm

The third script has been created during the building of models with hexahedral mesh. The process that converts the tetrahedrons in hexahedrons is executed in Matlab and returns a couple of file in Lupos format that contain the hexahedral mesh nodes and the geometrical and physical characteristics (Model.geo and Model.hex files). In order to re-import the data in Hypermesh, the script has to be used. It reads the two Lupos files; for first, it creates the nodes listed in the Model.geo file returned by Matlab, then it creates the new elements on these nodes, as indicated in the Model.hex file. The process is quick; manually, it would be very time consuming. It has been used several times, for importing the new meshed central part and rubber. The code is reported below.

```
#This program converts Lupos files .geo and .hex to an HyperMesh component.

#Select the .geo file:
set NodeFileName [open Model.geo]
set Nodes [read $NodeFileName]
close $NodeFileName;
set NodesLines [split $Nodes "\n"];

set n 0;
set Nodes_number [llength $NodesLines]

while {$n<$Nodes_number} {
      scan [lindex $NodesLines $n] %d%f%f%f Node_Id x y z
      *createnode $x $y $z 0 0 0
      *createmarklast nodes 1
```

```
      *renumber nodes 1 $Node_Id 1 0 0
      *clearmark nodes 1
      unset x
      unset y
      unset z
      unset Node_Id
      incr n
}
unset n
unset NodesLines
unset NodeFileName
unset Nodes


#Import .hex file:
set HexFileName [open Model.hex]
set Hexas [read $HexFileName]
close $HexFileName
set HexasLines [split $Hexas "\n"]

set n 0
set Hexas_number [llength $HexasLines]

while {$n<$Hexas_number} {
      scan [lindex $HexasLines $n] %d%d%d%d%d%d%d%d Node_1 Node_2 Node_3 Node_4 Node_5 Node_6 Node_7
      Node_8
      *createlist nodes 1 $Node_1 $Node_2 $Node_3 $Node_4 $Node_5 $Node_6 $Node_7 $Node_8
      *createelement 208 1 1 1
      *clearlist nodes 1
      incr n
}
```

Appendix B – Plates drawings

The steel plates drawings are reported. They have been resized in order to fit A4 format, so are not scaled as reported in the box.

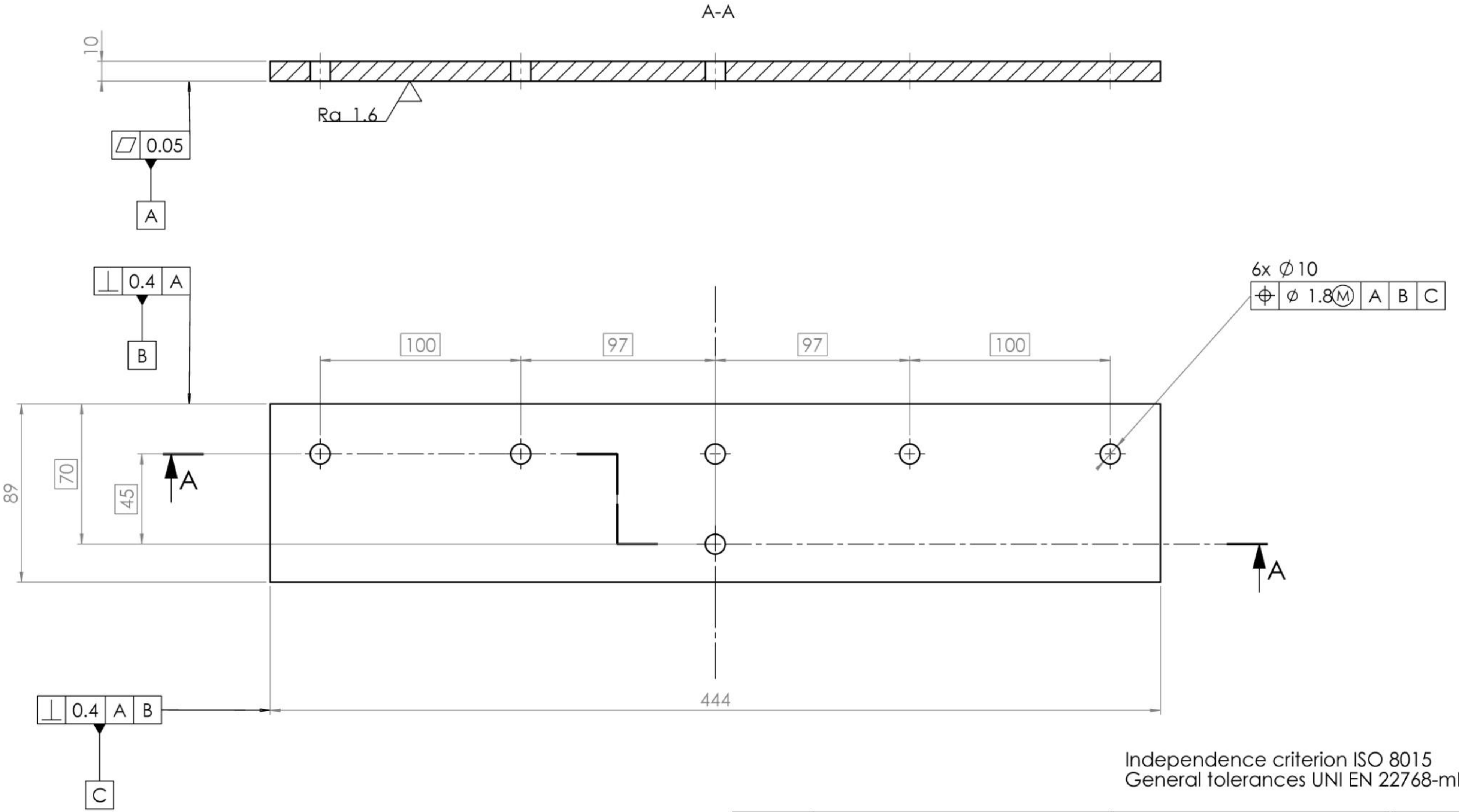

Independence criterion ISO 8015
General tolerances UNI EN 22768-mK

#	MATERIAL	STUDENT	Build
-		Stefano Averame	22/01/2020 17.59.21
SUBJECT		COURSE	SCALE 1:2
DESCRIPTION Top_plate			DATE 25/02/2020
Politecnico di Torino		SURFACE TEXTURE Ra 3.2	WEIGHT (Kg)
		PAPER A3 1/1	Drawing N.

Politecnico di Torino - Corso Duca degli Abruzzi, 24 - 10129 TORINO

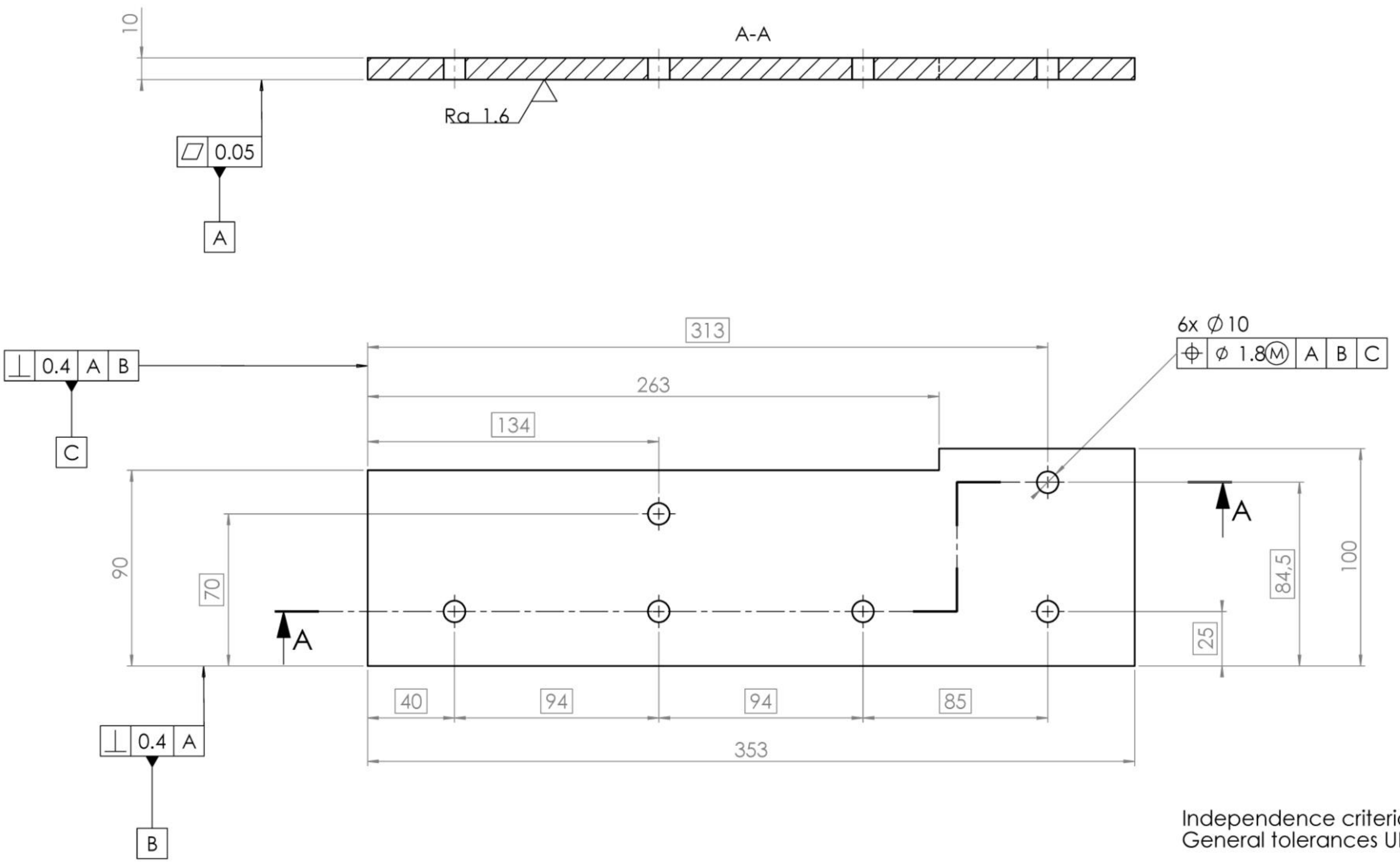

Independence criterion ISO 8015
General tolerances UNI EN 22768-mK

# -	MATERIAL	STUDENT Stefano Averame	Build 22/01/2020 17.59.21
SUBJECT		COURSE	SCALE 1:2
DESCRIPTION Side_plate			DATE 25/02/2020
Politecnico di Torino	SURFACE TEXTURE Ra 3.2	WEIGHT (Kg)	
Politecnico di Torino - Corso Duca degli Abruzzi, 24 - 10129 TORINO	PAPER A3 1/1	Drawing N.	

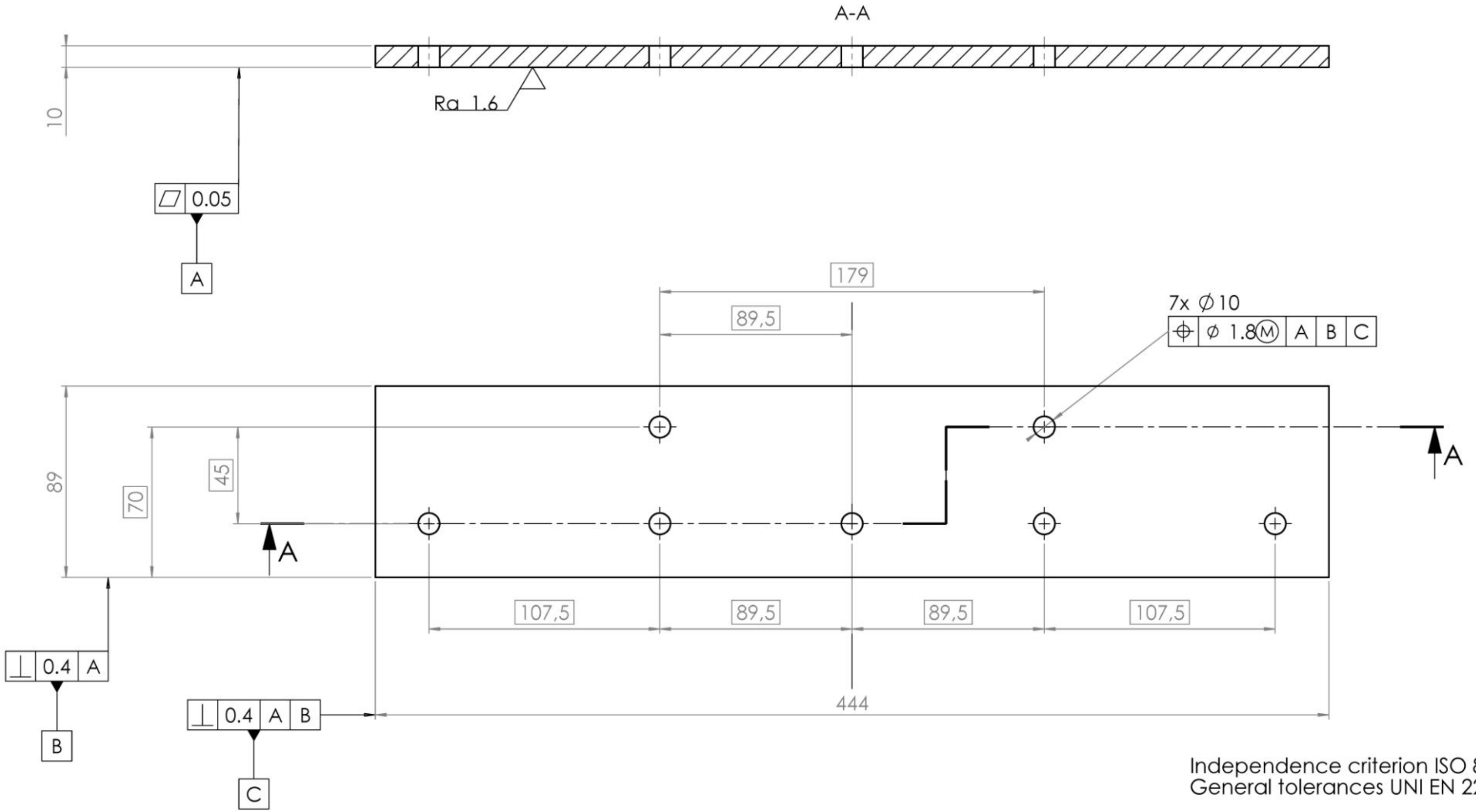

Independence criterion ISO 8015
General tolerances UNI EN 22768-mK

#	MATERIAL	STUDENT	Build
-		Stefano Averame	22/01/2020 17.59.21
SUBJECT		COURSE	SCALE 1:2
DESCRIPTION	Bottom_plate		DATE 25/02/2020
Politecnico di Torino		SURFACE TEXTURE Ra 3.2	WEIGHT (Kg)
		PAPER A3 1/1	Drawing N.

Politecnico di Torino - Corso Duca degli Abruzzi, 24 - 10129 TORINO

Reference

[1] Bonisoli E., *LUPOS, LUmped Parameters Open Source FEM code*, 2020.
LUPOS_Tutorial_2020-03-16.pdf

[2] Allemang R.J., "The modal assurance criterion (MAC): Twenty years of use and abuse", *Proc. 20th IMAC*, 2002, Los Angeles, California, February 4-7, 2002, pp. 1-9.
Allemang_The modal assurance criterion (MAC)_Twenty years of use and abuse_IMAC2002.pdf

[3] FIAT Group automobiles, "Performance Standard 7-R0158", 2008.
FIAT Standard 7-R0158.pdf

[4] Bonisoli E., Delprete C., Rosso C., "Proposal of a modal-geometrical-based master nodes selection criterion in modal analysis", *Mechanical Systems and Signal Processing*, 23(3), April 2009, ISSN: 0888-3270, DOI: 10.1016/j.ymssp.2008.05.012, pp. 606-620.
Bonisoli,Delprete,Rosso_Proposal of a modal-geometrical based master nodes selection criterion in modal analysis_MSSP2009.pdf